Defining Protein Motions that Comprise the Reaction Barrier in Human Epithelial 15-Lipoxygenase-2

by

Amanda Ohler

May 2022

Director of Thesis: Adam R. Offenbacher

Major Department: Chemistry

Proteins are dynamic in nature, with these motions playing a role in substrate binding and product release. Protein thermal motions have emerged as participating in the bond making/breaking steps of catalysis and by extension the rate enhancement observed in enzymes. A family of enzymes, known as lipoxygenases (LOXs), play a large role in growth and pathogenic defense in plants and homeostasis, cell signaling, and inflammation in humans. The regulation of LOX pro- and anti-inflammatory properties is thought to be controlled through allosteric interactions with small molecules, proteins, and membranes. For all organisms, LOXs oxidize polyunsaturated fatty acids through an often rate-limiting C-H activation step that proceeds through a tunneling mechanism. The activation energy barrier for this LOX reaction is expected to be related to the thermal fluctuations of the protein-substrate complex. How protein motions transfer heat from the surface to buried active sites remains an open question. Furthermore, the connection between thermal motions mediating allostery and the chemical step(s) are not well resolved. Recent studies on the model plant LOX, soybean lipoxygenase (SLO), have identified a solvent-exposed loop that is linked to the origins of a defined network for thermal activation that is distinct from the defined allosteric network. The human counterpart, human epithelial 15-lipoxygenase-2 (15-LOX-2), exhibits similar function but lacks some of these structural features found in SLO, thereby raising

the question as to the evolution of structure and protein motions in these enzymes. In this thesis, biophysical methods, including temperature-dependent hydrogen deuterium exchange-mass spectrometry, X-ray crystallography, and differential scanning calorimetry, as well as enzyme kinetics are used to regionally define catalytically linked dynamics related to both allostery and chemical bond breaking step(s) of 15-LOX-2 to further understand how thermal motions regulate lipoxygenase function.

Defining Protein Motions the Comprise the Reaction Barrier in Human Epithelial 15-Lipoxygenase-2

A Thesis

Presented to the Faculty of the Department of Chemistry

East Carolina University

In Partial Fulfillment of the Requirements for the Degree

Master of Science in Chemistry

by

Amanda Ohler

May 2022

©Amanda Ohler, 2022

Defining Protein Motions that Comprise the Reaction Barrier in Human Epithelial 15-Lipoxygenase-2

by

Amanda Ohler

APPROVED BY:

DIRECTOR OF THESIS: ____

Adam R. Offenbacher, Ph.D.

COMMITTEE MEMBER: ____

Sambuddha Banerjee, Ph.D.

COMMITTEE MEMBER: ____

Yumin Li, Ph.D.

COMMITTEE MEMBER: ____

Patrick J. Horn, Ph.D.

CHAIR OF THE
DEPARTMENT OF CHEMISTRY: ____________________________________

Andrew T. Morehead, Jr., Ph.D.

DEAN OF THE
GRADUATE SCHOOL: ____

Paul Gemperline, Ph.D.

ACKNOWLEDGEMENTS

I would like to start by thanking my thesis advisor and mentor, Dr. Adam Offenbacher. Thank you for being a great mentor, both in my education and in my life. Thank you for every opportunity you have given me to help me succeed. And thank you for believing in me, even when I didn't believe in myself. You have been so influential in making me into the scientist and person that I am today.

Thank you to the Offenbacher Lab for finding a way to make me laugh every day and giving me a family here at ECU. And a special shout out to Ethan Patel, who helped me achieve everything I set out to at the beginning of my degree here at ECU.

A huge thank you to fellow Masters' students Daniella Roberts and Rachel Signorelli. I know that I would not have made it through these past two years without your friendship and support throughout my time here in North Carolina. You helped me find the best in each day, even the hard ones, and I am so grateful for all of the memories we have made together.

Finally, I would like to thank my family and friends back in Ohio. I would not have taken this opportunity to follow my dreams without your unwavering support and I am so grateful for all of the love you show me, no matter how far apart we are.

TABLE OF CONTENTS

TITLE PAGE……i

COPYRIGHT PAGE……ii

SIGNATURE PAGE……iii

ACKNOWLEDGEMENTS……iv

LIST OF TABLES……vii

LIST OF FIGURES……viii

LIST OF ABBREVIATIONS……ix

CHAPTER 1 INTRODUCTION……1

- Enzymes, Catalysis, and CH Activation……1
- The Lipoxygenase Family……5
- Human Lipoxygenases……8
- Biological Implications of 15-LOX-2……11
- References……14

CHAPTER 2 ALLOSTERIC REGULATION OF HUMAN EPITHELIAL 15-LIPOXYGENASE-2 BY NATURAL EFFECTOR, 13*S*-HODE……17

- Introduction……17
- Materials and Methods……24
- Results and Discussion……27
- Conclusion……39
- References……40

CHAPTER 3 INVESTIGATIONS INTO THE THERMAL ACTIVATION NETWORK OF HUMAN 15-LIPOXYGENASE-2……43

Introduction……………………………………………………………………………43

Materials and Methods…………………………………………………………...46

Results and Discussion…………………………………………………………...50

Conclusion………………………………………………………………………….61

References……………………………………………………………………….63

APPENDIX A HDX-MS TRACES FOR WT, V427L, AND V426A 15-LOX-2…………......66

LIST OF TABLES

CHAPTER 1

Table 1.1: Human LOXs and Expression Locations……………………………………………….9

CHAPTER 2

Table 2.1: 15-LOX-2 Kinetics With 13*S*-HODE for Various Substrates…………………………19

Table 2.2: Substrate Specificity Kinetics for 15-LOX-2 With 13*S*-HODE……………………….29

Table 2.3: pH Dependence on Substrate Specificity With 13*S*-HODE…………………………...31

CHAPTER 3

Table 3.1: Catalytic Parameters for WT 15-LOX-2 and Variants………………………………...53

Table 3.2: Catalytic Parameters for 15-LOX-2 with Various Substrates…………………………56

Table 3.3: KIE of 15-LOX-2 and V427 Series Mutants…………………………………………..56

LIST OF FIGURES

CHAPTER 1

Figure 1.1: Michaelis-Menten Curve and Reaction Coordinate Diagram for LOXs……………...3

Figure 1.2: Hydrogen and Deuterium Arrhenius Plots…………………………………………4

Scheme 1.1: LOX Reaction………………………………………………………………………5

Figure 1.3: Organismal LOX Comparison……………………………………………………..6

Figure 1.4: Hydrogen and Deuterium Exchange Within a Protein……………………………..8

Figure 1.5: HDX-MS Methodology………………………………………………………………8

Figure 1.6: 15-LOX-2 Structure…………………………………………………………………10

Figure 1.7: LOX vs. COX Pathways…………………………………………………………...13

CHAPTER 2

Figure 2.1: PUFA Substrates and Allosteric Effectors for LOXs…………………………………18

Figure 2.2: KIE Data Comparing OA and OS with SLO…………………………………………20

Figure 2.3: Biosynthetic Pathways for AA and DHA with LOXs……………………………...22

Figure 2.4: Docking Model of 15-LOX-2 and 13*S*-HODE………………………………………23

Figure 2.5: SDS-PAGE of 15-LOX-2 Purification………………………………………………28

Figure 2.6: DSC Thermograms of 15-LOX-2 With and Without 13*S*-HODE……………………33

Figure 2.7: SEC Chromatogram of 15-LOX-2 With and Without 13*S*-HODE…………………...34

Figure 2.8: HDX-MS of 15-LOX-2 With and Without 13*S*-HODE………………………………35

Figure 2.9: HDX-MS With Competitive Inhibitor……………………………………………..37

Figure 2.10: ITC Thermogram for 15-LOX-2 and 13*S*-HODE Binding…………………………38

CHAPTER 3

Figure 3.1: Solvent Water Layers And Thermal Energy Transfer for a Protein…………………..44

Figure 3.2: Thermal Activation Network for SLO……………………………………………………..45

Figure 3.3: Confirmation of WT 15-LOX-2 and Variants Purification and Stability……………..51

Figure 3.4: Hydrophobic Active Site Residues of 15-LOX-2……………………………………….52

Figure 3.5: E_a Analysis of V427X Series……………………………………………………………54

Figure 3.6: TDHDX-MS Comparison of WT 15-LOX-2, V426A and V427L…………………...58

Figure 3.7: X-Ray Crystal Structure Overlay of 15-LOX-2 V427L and WT……………………..59

Figure 3.8: Trehalose Effects on the Catalytic Parameters of 15-LOX-2…………………………60

Figure 3.9: ILV Islands in SLO and 15-LOX-2………………………………………………………..62

LIST OF ABBREVIATIONS

13*S*-HODE	13-(*S*)-hydroxyoctadecadienoic acid	17
15-LOX-2	Human epithelial 15-lipoxygenase-2	9
AA	Arachidonic acid	5
C8E4	Tetraethylene glycol monooctyl ether	49
DAD	Donor-acceptor distance	1
DHA	Docosahexaenoic acid	21
E_a	Activation energy	1
GLA	γ-linolenic acid	18
HDX-MS	Hydrogen deuterium exchange-mass spectroscopy	7
KIE	Kinetic isotope effect	3
LA	Linoleic acid	5
LOX	Lipoxygenase	5
OS	Oleyl sulfate	19
PUFA	Polyunsaturated fatty acid	5
SDS-PAGE	Sodium dodecyl-sulfate polyacrylamide gel electrophoresis	25
s.e.m.	Standard error of the mean	25
SLO	Soybean lipoxygenase	7
TRS	Tunneling ready state	1
ZPE	Zero point energy	3

CHAPTER 1

INTRODUCTION

Enzymes, Catalysis, and C-H Activation

Many reactions in the world occur with the help of enzymes to act as a catalyst. An enzyme is a protein that functions as a biological catalyst by lowering the activation energy (E_a) required for the reaction to proceed and accelerating the reaction. The E_a is the energy required to reach the highest energy transition state when moving from the ground state of the reactants to the products.[1] In this semi-classical behavior of enzymes, the enzyme (E) and substrate (S) will form a complex (ES) together that helps to progress the conversion to the product (P). Once the substrate is converted to the product, an enzyme-product complex (EP) is formed, which is dissolved when the product is released. The enzyme passes through the transition state of the reaction when the ES complex is converted to the EP complex. By lowering the energy barrier, the overall reaction can occur at a much faster rate. But the mechanism that enzymes are able to do this is still under much study.

One example of a reaction that occurs with the help of an enzyme is C-H activation. C-H activation (or C-H functionalization) occurs when the carbon-hydrogen bond is cleaved and replaced with a new bond to an oxygen, carbon, or nitrogen atom.[2,3] In some cases of C-H activation, the enzyme uses a redox-active metallocofactor, such as iron or manganese, or an organic centered radical that aids in the reaction.[2,3] C-H activation appears to follow a non-classical behavior, known as tunneling. In this scenario, the enzyme and substrate face a barrier of a different nature. In tunneling, the transfer of a hydrogen atom is considered as a wave rather than a particle. For C-H activation to occur, the acceptor molecule and carbon-hydrogen donor must be within the accepted donor-acceptor distance (DAD) of ~2.7 Å to be in the tunneling ready state

(TRS).[2] This distance allows for wavefunction overlap to occur by increasing the probability for the hydrogen atom to appear on the atom on either side as a reactant or a product. When the probabilities of the hydrogen occurring in the reactant and product are equal, wavefunction overlap will occur, which is barrier-less. The barrier then arises from the protein and its interactions with the solvent that help to promote reactive configurations with the appropriate geometrics and electrostatics for efficient wavefunction overlap.[4] This enables the hydrogen to travel through the barrier. For example, lipoxygenases, which are a family of enzymes that oxidize polyunsaturated fatty acids through C-H activation, the oxygen atom must be within the DAD of the selected C-H bond of the fatty acid.[2] At this distance, the probability that the hydrogen atom is on the oxygen or carbon atom is equal and the DADs help to dictate the compaction that is required within the active site.

Enzyme catalysis can be quantified through kinetics, which relates the rate of the reaction to a given substrate concentration. In the cases in which enzymes follow Michaelis-Menten kinetics, their reactions are expressed through Eq. 1.

$$v = \frac{k_{cat}[S]}{K_M+[S]} \tag{1}$$

In this equation, v is the velocity, or rate of the reaction, and $[S]$ is the substrate concentration. Using this equation, an enzymatic reaction will create a hyperbolic curve with which the first order rate constant (k_{cat}) and the second order rate constant ($k_{\text{cat}}/\text{K}_{\text{M}}$) can be extrapolated from the plot (Figure 1.1A). The first order rate constant reports on the maximum rate of the reaction under saturating substrate concentrations. This provides information about the efficiency and product release of the enzyme. The second order rate constant reports on the proficiency of the enzyme. By taking both the maximum rate of the reaction and the K_{M}, which provides information into substrate binding and configuration, into consideration, the k_{cat}/K_M is able to provide information about the substrate capture of the enzyme.

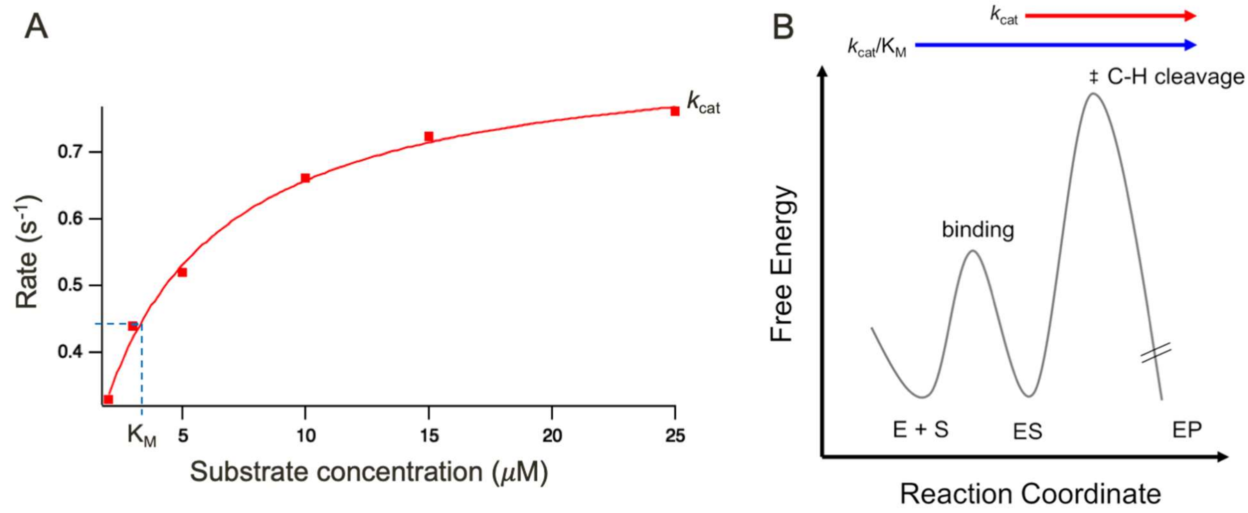

Figure 1.1. *Representative Michaelis-Menten curve and reaction coordinate diagram for the C-H bond cleavage of lipoxygenases. (A) The Michaelis-Menten curve shows the extrapolated* k_{cat} *and* K_M *values from a kinetic data set. (B) A representative reaction coordinate diagram for the C-H bond cleavage of lipoxygenases shows how* k_{cat} *and* K_M *quantify the reaction.*

The barriers of a kinetic analysis can further be shown visually through the reaction coordinate diagram for the C-H activation of the example enzyme, lipoxygenases (Figure 1.1B).[2] In this diagram, we see that k_{cat} is only representative of one part of the reaction, or the C-H cleavage step, which is also the irreversible and predominantly rate limiting step of the reaction. However, k_{cat}/K_M is able to provide us with a better understanding of the whole reaction by representing both the binding of the enzyme-substrate complex and the C-H bond cleavage steps.

Isotopes can also be used to study the rate-limiting steps of a reaction, such as the C-H bond cleavage. A kinetic isotope effect (KIE) is a temperature independent effect observed because of the difference in the zero-point energies (ZPE) in the ground states of two isotopes, such as hydrogen and deuterium.[2] In the case of C-H activation, the hydrogen that is being cleaved can be replaced with its heavier isotope, deuterium, resulting in a KIE that is higher than the semi-classical limit of 7.[2] This is based on the difference in the ZPE for a classical ‘over the barrier’ reaction. A kinetic analysis can also determine the E_a values for the cleavage of H and D. The E_a of an enzyme is related to the temperature dependent rate of the reaction, which is expressed through the Arrhenius equation (Eq. 2).[1] In this equation, k is the rate constant, A is the Arrhenius pre-factor, R is the gas constant, and T is the temperature.

$$k = A \times e^{\frac{-E_a}{RT}} \tag{2}$$

The difference between these values (ΔE_a) is indicative of a semi-classical or tunneling model of catalysis. When the Arrhenius plots of hydrogen and deuterium converge at the y-axis, the semi-classical model of catalysis is suggested. This produces a ΔE_a that is greater than 0. But, parallel hydrogen and deuterium Arrhenius plots are indicative of a tunneling model (Figure 1.2).[1,2] While

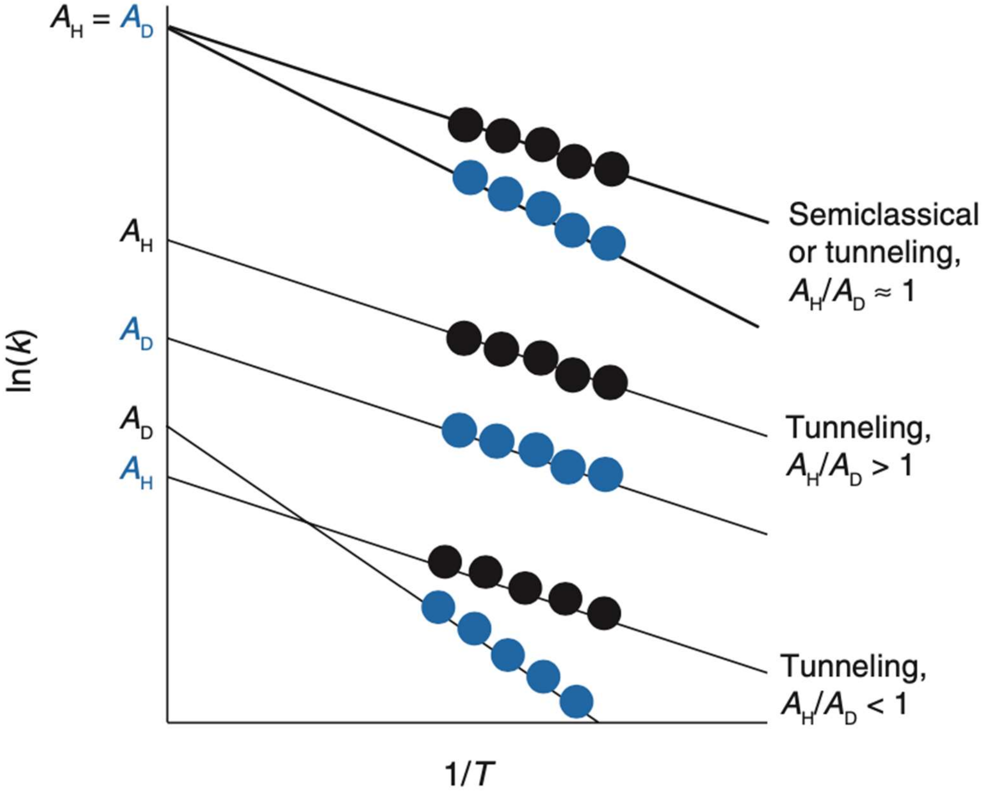

Figure 1.2. *Comparison of Arrhenius plots for hydrogen and deuterium representing semi-classical and tunneling behaviors of enzymes. Figure reproduced from reference (1).*

the E_a for these reactions is greater than 0, a ΔE_a that is equal to 0 is indicative of tunneling for natively evolved C-H activation enzymes. From the analytical rate expression that explains tunneling, based on Marcus theory of electron transfer, wavefunction overlap is inherently temperature independent. Thus, the observed E_a values of > 0 reflect the role for the enzyme-substrate motions related to bringing about the catalytically conducive configurations. This offers C-H activation enzymes as model systems to understand the origins of thermal activation of bond cleavage reactions in enzymes.

The Lipoxygenase (LOX) Family

Lipoxygenases (LOXs) are a family of non-heme iron-containing enzymes that regulate fatty acid oxidation. These enzymes help to insert molecular oxygen into polyunsaturated fatty acids (PUFAs), such as arachidonic acid (AA) and linoleic acid (LA), in a regio- and stereoselective manner to produce hydroperoxide compounds (Scheme 1.1).[2] This reaction occurs

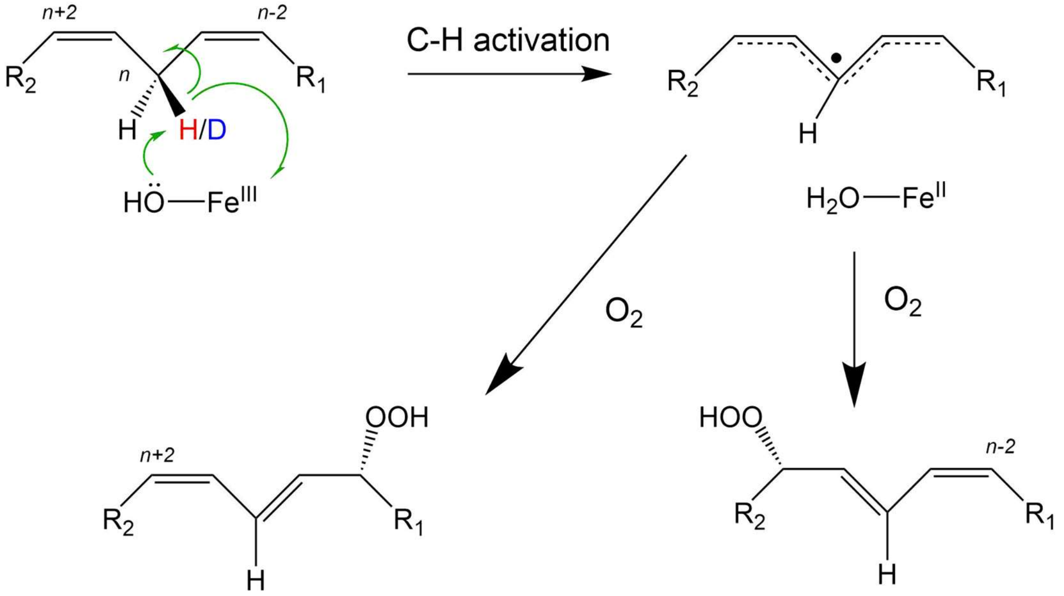

Scheme 1.1. *Oxidation of PUFAs through C-H activation catalyzed by LOXs to produce hydroperoxides. Figure reproduced from reference (2).*

when a hydrogen is abstracted from the bisallylic methylene of the fatty acid substrate. The oxygen of the iron ligand accepts the hydrogen as a proton while the iron accepts the resulting electron, reducing it from a ferric iron to a ferrous iron. Once this C-H activation is complete, a radical is created on the fatty acid. The radical undergoes rearrangement so that the electron is in the (n+2) or (n-2) position, moving towards the methyl end or towards the carboxylate group of the fatty acid, respectively. This position is specific depending on the LOX involved in the reaction. Molecular oxygen can then be inserted into the delocalized radical and the peroxy anion is protonated to produce the hydroperoxide product.[5] The products from this reaction are used as cell-signaling molecules or can go on to produce other compounds that can further be used as mediators in other various biological functions, such as inflammation.

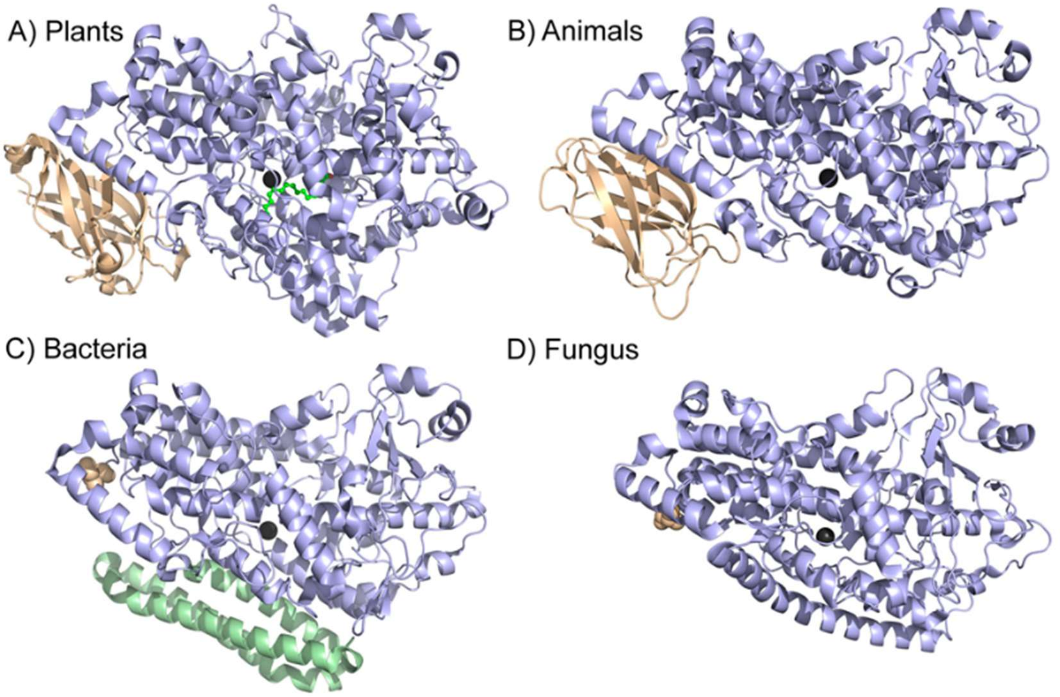

Figure 1.3. *Comparison of LOXs from various organisms. The catalytic domain (light blue) is present in all organisms, while the PLAT domain (wheat) is only present in plants and animal LOXs. Additional helices (pale green) that are present in the catalytic domain of bacterial LOXs are also shown. Figure reproduced from reference (6).*

LOXs can be found in many different organisms, such as bacteria, fungi, plants, and mammals, but there is a low sequence identity between the LOXs of each organism (Figure 1.3). Plant LOXs play a role in seed germination, growth, and pathogenic defense, animal LOXs play a role in homeostasis, cell signaling, and inflammation, and fungal LOXs aid in host pathogenesis.[2] LOXs from plants and mammals are much larger, being composed of two different domains, with plant LOXs being the largest of the family, while LOXs from bacteria and fungi consist of only a single domain.[7] But all of these LOXs, with the exception of fungal LOXs, share a similar catalytic domain that consists of an iron atom surrounded by many alpha helices. Fungal LOXs share the helices but have a manganese center rather than an iron center.[7]

LOXs have anomalously high KIEs and ΔE_a values of zero, which establishes them as model systems for studying tunneling.[2] The plant model LOX, soybean lipoxygenase (SLO), is a more commonly studied LOX due to the accessibility and stability of this enzyme.[2] The allosteric regulation of SLO was shown with the fatty acid mimic, oleyl sulfate, using hydrogen deuterium exchange-mass spectrometry (HDX-MS) to track changes in the enzyme upon effector binding.[8] Comparisons of HDX-MS with active site mutations in SLO have provided insight into the roles of protein 'thermal networks' for effective substrate positioning relating to the origins of catalysis, as well.[6]

HDX-MS is a bioanalytical technique that quantifies the flexibility or dynamics of a protein. Proteins are naturally dynamic structures that exist in equilibrium between a closed state and an open state, in which the hydrogens are protected and exposed, respectively.[9] Once in the open state, the protein is able to exchange backbone amide hydrogens when incubated with deuterium (Figure 1.4).[9] The observed rate of exchange is dependent on the rate constants for the opening (k_{op}) and closing (k_{cl}) motions of the protein, as well as the rate of exchange (k_{exch}). Under native conditions, hydrogen exchange occurs under the EX2 regime, in which $k_{cl} >> k_{exch}$. EX2 conditions can be controlled by pH and validated by the MS isotopic envelope.[9,10]

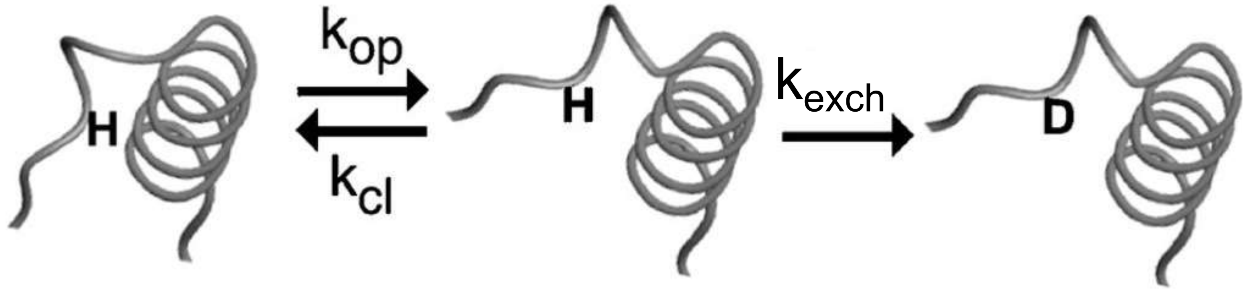
H
k_{op}
k_{cl}
H
k_{exch}
D

Figure 1.4. *Mechanism of hydrogen and deuterium exchange within a protein. Figure reproduced from reference (9).*

To initiate this exchange, protein samples are incubated with D_2O solvent for varying lengths of time, where the amide hydrogens are able to exchange with deuterium. The protein is then quenched at a lower temperature and pH/pD to eliminate back exchange before undergoing proteolytic digest. The resulting peptides are separated using HPLC and analyzed through mass spectrometry (Figure 1.5).[10] Changes in the protein's environment, such as the addition of small molecules or mutations can lead to local or regional changes throughout the protein. This technique under EX2 exchange conditions can also describe differences due to changes in temperature, allowing for comparison with temperature dependent kinetic values.

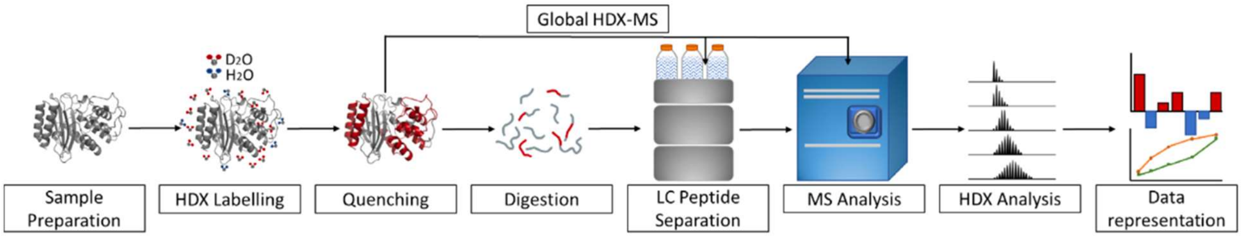
Global HDX-MS
D2O
H2O
Sample Preparation
HDX Labelling
Quenching
Digestion
LC Peptide Separation
MS Analysis
HDX Analysis
Data representation

Figure 1.5. *HDX-MS methodology. Figure reproduced from reference (10).*

Human Lipoxygenases

One subgroup of mammalian LOXs are present in humans. There are six different LOXs expressed in humans, all of which are encoded by a different gene (Table 1.1).[11] Each human LOX receives its name based on the position on AA where molecular oxygen is inserted. Human LOXs are being studied because of the role they play in producing cell signaling molecules that can be linked to homeostasis and diseases of inflammation, such as cancer, asthma, and cardiovascular disease (CVD). With as many as 30 known PUFAs in the body, there are many pathways that the various human LOXs can participate in.[2] A large substrate pool also leads to a wide variety of products that can be synthesized with a diverse range of physiological functions. While some of these products have been linked to the progression of inflammation, others serve as anti-inflammatory or pro-resolution compounds or as precursors to those compounds. With a family of enzymes that have a dual effect of synthesizing compounds that are both harmful and beneficial based on the substrate converted, there is much to be learned about their mechanisms of action.

Table 1.1. *Known Lipoxygenases in Humans and their Locations for Expression.*[a]

Human gene	Encoded LOX	Major Expression
ALOX15	12/15-LOX	eosinophils, bronchial epithelium
ALOX15B	15-LOX-2	hair roots, skin, prostate
ALOX12	pl12-LOX	thrombocytes, skin
ALOX12B	12*R*-LOX	skin
ALOXE3	eLOX3	skin
ALOX5	5-LOX	leukocytes, macrophages, dendritic cells

[a]*Table reproduced from reference (11).*

One of the six human LOX isozymes that is currently being studied is human epithelial 15-lipoxygenase-2 (15-LOX-2). When compared to other human LOXs, including its other human 15-LOX counterpart, 15-LOX-1, 15-LOX-2 shares a resemblance in structure, but the sequence identity displays only a 40% similarity (44% for 5-LOX and 38-39% for 12-LOX and 15-LOX-1).[12] 15-LOX-2 also differs from 15-LOX-1 in substrate specificity and product formation. The preferred substrate for 15-LOX-2 is AA to exclusively produce 15-HETE, while the preferred substrate for 15-LOX-1 is LA with a product distribution consisting of both 12- and 15-HETE.[12]

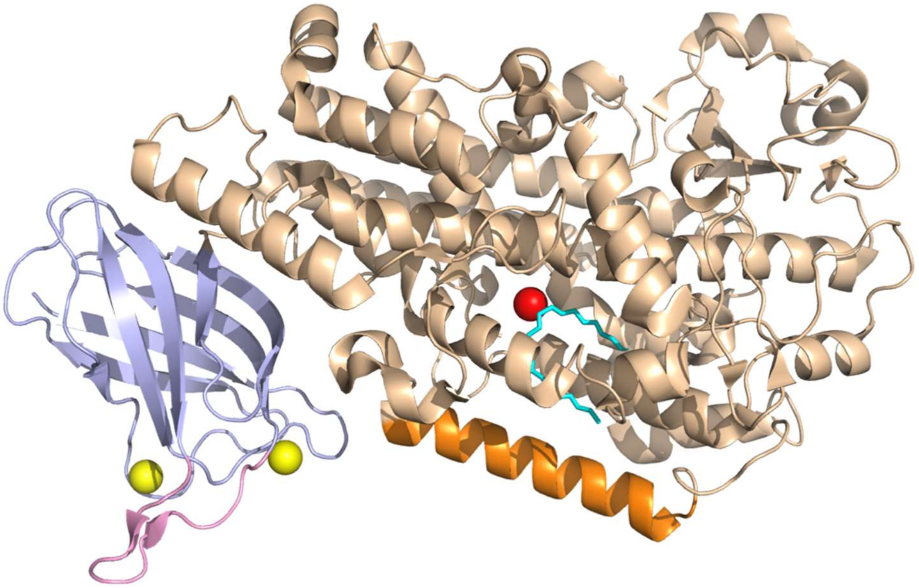

Figure 1.6. *Structure of 15-LOX-2. The catalytic domain (wheat) is shown with the non-heme iron (red) and the substrate mimic (cyan), tetraethylene glycol monooctyl ether (C8E4), in the active site. Helix α2 (orange), which gates the substrate entrance for the enzyme is also highlighted above. The PLAT domain (light blue) is shown with the membrane binding loop (pink) and its associated calcium ions (yellow). Figure modified from reference (13).*

15-LOX-2 has two domains – the polycystin-1, lipoxygenase, α-toxin (PLAT) domain and the catalytic domain (Figure 1.6). The PLAT domain (residues 1-118) is the smaller of the two domains that is unique to plant and mammalian LOXs. It is located at the N-terminus of the protein and is composed mostly of beta sheets. The PLAT domain contains a loop (residues 73-85) that extends out into the solvent that is thought to influence calcium-mediated membrane binding and association. The PLAT domain has also been found to influence the enzyme's substrate specificity. The catalytic domain (residues 119-676) is located at the C-terminus of the protein and is composed mainly of alpha helices. It contains the active site of the enzyme, which binds the substrate. One of the helices within the catalytic domain, helix α2 (residues 178-199), is also said to gate the substrate entrance into the active site of the enzyme.[2,7]

15-LOX-2 is analogous to the plant 15-LOX, soybean lipoxygenase (SLO). SLO can also be considered a 15-LOX because it inserts molecular oxygen into the 13-carbon position on LA, which is equivalent to the 15-position on AA. SLO now serves as a model system for the study of 15-LOX-2 because of its similarity in structure and enzymatic function, but the two enzymes only share a 28% sequence identity.[2]

Biological Implications of 15-LOX-2

The products of 15-LOX-2 form a group of fatty acids known as eicosanoids. Eicosanoids, such as prostaglandins and lipoxins, are bioactive cell signaling lipids that are the product of the oxidation of PUFAs through LOX, cyclooxygenase (COX), or cytochrome P450 enzyme pathways.[14] These molecules are most commonly associated with homeostasis and inflammation. The human body has the ability to produce eicosanoids that lead to inflammation (prostaglandins and leukotrienes), but also inflammation resolution (lipoxins and protectins) depending on the pathway that each PUFA takes. This mechanism of regulation plays a large role in several different diseases, such as atherosclerosis and arthritis.

15-LOX-2 has been implicated in the CVD, atherosclerosis. Atherosclerosis begins when low-density lipoproteins (LDLs) become oxidized. Macrophages identify the oxidized LDLs and absorb them. The accumulation of cholesterol then converts the oxidized LDLs to lipid foam cells, which builds up to form plaques.[15] The vascular wall becomes inflamed due to the buildup of these atherosclerotic plaques and blood is prevented from flowing smoothly through the artery. 15-LOX-2 is highly and continually expressed in the macrophages and carotid lesions that are attributed to atherosclerosis. While the products of both human 15-LOXs are present in atherosclerotic plaques, *in vivo* animal studies suggest 15-LOX-2 rather than 15-LOX-1 as the antagonist in this disease. According to the Center for Disease Control and Prevention, atherosclerosis is the second leading cause of death in the United States and in North Carolina. This disease is especially prevalent in eastern North Carolina, which includes Pitt County, making it even more imperative to investigate the biological role of 15-LOX-2.

15-LOX-2 has also been implicated in the inflammation associated with arthritis. Human synovial fluid is necessary to provide nutrition and lubrication to the articular cartilage, but the accumulation of this fluid in the joints will lead to arthritis. This fluid contains cytokines and immune cells that lead to inflammation in patients with arthritis, but also PUFA lipid mediators.[16] The products of 15-LOX-2 are implicated in the resolution of this inflammatory disease by synthesizing SPMs.

While the preferred substrate for 15-LOX-2 is AA, COXs are considered the key enzyme in converting AA to eicosanoids. While the LOX and COX pathways do share some similarities, they diverge past the same substrate pools. The COX pathways appear to be more straight-forward, with COX-1 keeping the body at homeostasis and COX-2 being the main contributor to inflammation, disease, and pain.[17] Medications, such as nonsteroidal anti-inflammatory drugs (NSAIDs) like aspirin and ibuprofen, have been created to inhibit the COX pathway (Figure 1.7). But the less commonly studied LOX pathway lacks the therapeutics that the COX pathway has. The only drug known to target LOXs is Zileuton for the treatment of asthma (Figure 1.7). But this drug only inhibits 5-LOX, has relatively poor selectivity, and has since been banned in the United States. Other drugs, such as Montelukast, which is a leukotriene inhibitor for asthma patients, are still used today, but they only inhibit the eicosanoid after it has been produced. With the LOX pathways being less commonly studied and more intricate, as well as serving just as important of a role in biological functions, we work to gain insight into the structure and function of 15-LOX-2 in hopes of providing new possibilities for therapeutics.

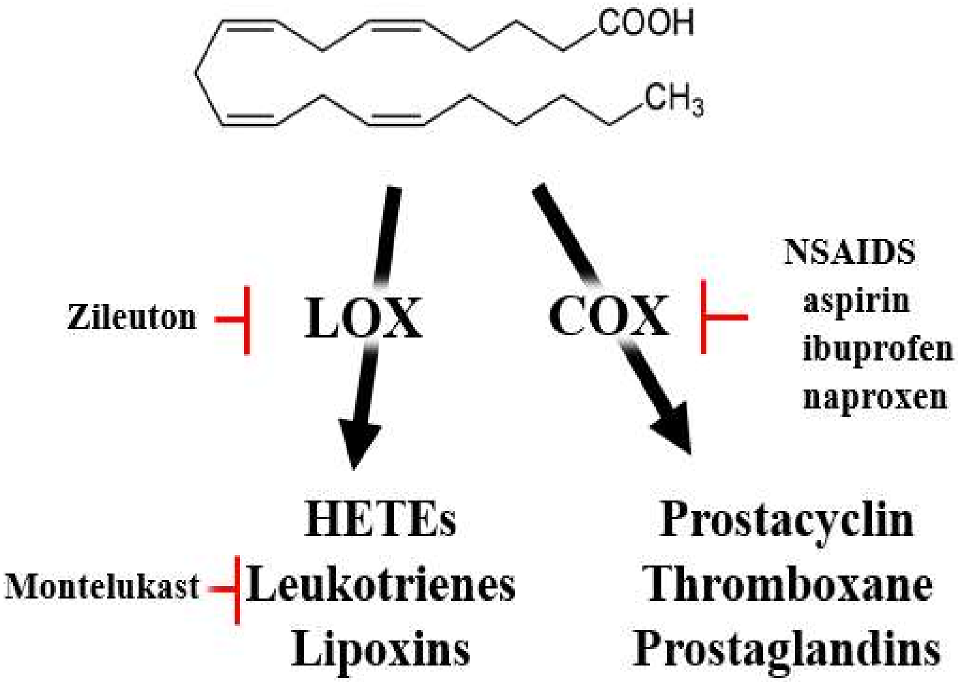
COOH
CH3
Zileuton
LOX
COX
NSAIDS
aspirin
ibuprofen
naproxen
HETEs
Montelukast
Leukotrienes
Lipoxins
Prostacyclin
Thromboxane
Prostaglandins

Figure 1.7. *Oxidation of AA through the LOX and COX pathways with current therapeutics for each pathway. While there are many NSAIDs that can be used to inhibit the production of eicosanoids through the COX pathway, fewer options exist as inhibitors to the LOX pathway.*

References

(1) Nagel, Z. D.; Klinman, J. P. A 21st Century Revisionist's View at a Turning Point in Enzymology. *Nat. Chem. Biol.* **2009**, *5* (8), 543–550. https://doi.org/10.1038/nchembio.204.

(2) Offenbacher, A. R.; Holman, T. R. Fatty Acid Allosteric Regulation of C-H Activation in Plant and Animal Lipoxygenases. *Molecules*. 2020. https://doi.org/10.3390/molecules25153374.

(3) Whittington, C.; Latham, J.; Offenbacher, A. R. Tunneling through the Barriers: Resolving the Origins of the Activation of C-H Bonds Catalyzed by Enzymes. In *ACS Symposium Series*; 2020; Vol. 1357. https://doi.org/10.1021/bk-2020-1357.ch007.

(4) Klinman, J. P.; Offenbacher, A. R.; Hu, S. Origins of Enzyme Catalysis: Experimental Findings for C-H Activation, New Models, and Their Relevance to Prevailing Theoretical Constructs. *Journal of the American Chemical Society*. 2017. https://doi.org/10.1021/jacs.7b08418.

(5) Ivanov, I.; Heydeck, D.; Hofheinz, K.; Roffeis, J.; O'Donnell, V. B.; Kuhn, H.; Walther, M. Molecular Enzymology of Lipoxygenases. *Archives of Biochemistry and Biophysics*. 2010, pp 161–174. https://doi.org/10.1016/j.abb.2010.08.016.

(6) Offenbacher, A. R.; Hu, S.; Poss, E. M.; Carr, C. A. M.; Scouras, A. D.; Prigozhin, D. M.; Iavarone, A. T.; Palla, A.; Alber, T.; Fraser, J. S.; et al. Hydrogen-Deuterium Exchange of Lipoxygenase Uncovers a Relationship between Distal, Solvent Exposed Protein Motions and the Thermal Activation Barrier for Catalytic Proton-Coupled Electron Tunneling. *ACS Cent. Sci.* **2017**, *3* (6). https://doi.org/10.1021/acscentsci.7b00142.

(7) Newcomer, M. E.; Brash, A. R. The Structural Basis for Specificity in Lipoxygenase

Catalysis. *Protein Sci.* **2015**, *24* (3), 298–309. https://doi.org/10.1002/pro.2626.

(8) Offenbacher, A. R.; Iavarone, A. T.; Klinman, J. P. Hydrogen-Deuterium Exchange Reveals Long-Range Dynamical Allostery in Soybean Lipoxygenase. *J. Biol. Chem.* **2018**, *293* (4), 1138–1148. https://doi.org/10.1074/jbc.M117.817197.

(9) Hoofnagle, A. N.; Resing, K. A.; Ahn, N. G. Protein Analysis by Hydrogen Exchange Mass Spectrometry. *Annual Review of Biophysics and Biomolecular Structure*. 2003. https://doi.org/10.1146/annurev.biophys.32.110601.142417.

(10) Oganesyan, I.; Lento, C.; Wilson, D. J. Contemporary Hydrogen Deuterium Exchange Mass Spectrometry. *Methods* **2018**, *144* (February 2018), 27–42. https://doi.org/10.1016/j.ymeth.2018.04.023.

(11) Kuhn, H.; Banthiya, S.; Van Leyen, K. Mammalian Lipoxygenases and Their Biological Relevance. *Biochimica et Biophysica Acta - Molecular and Cell Biology of Lipids*. 2015. https://doi.org/10.1016/j.bbalip.2014.10.002.

(12) Brash, A. R.; Boeglin, W. E.; Chang, M. S. Discovery of a Second 15S-Lipoxygenase in Humans. *Proc. Natl. Acad. Sci. U. S. A.* **1997**, *94* (12). https://doi.org/10.1073/pnas.94.12.6148.

(13) Kobe, M. J.; Neau, D. B.; Mitchell, C. E.; Bartlett, S. G.; Newcomer, M. E. The Structure of Human 15-Lipoxygenase-2 with a Substrate Mimic. *J. Biol. Chem.* **2014**. https://doi.org/10.1074/jbc.M113.543777.

(14) Dennis, E. A.; Norris, P. C. Eicosanoid Storm in Infection and Inflammation. *Nature Reviews Immunology*. 2015. https://doi.org/10.1038/nri3859.

(15) Snodgrass, R. G.; Brüne, B. Regulation and Functions of 15-Lipoxygenases in Human Macrophages. *Front. Pharmacol.* **2019**, *10* (July), 1–12.

https://doi.org/10.3389/fphar.2019.00719.

(16) Giera, M.; Ioan-Facsinay, A.; Toes, R.; Gao, F.; Dalli, J.; Deelder, A. M.; Serhan, C. N.; Mayboroda, O. A. Lipid and Lipid Mediator Profiling of Human Synovial Fluid in Rheumatoid Arthritis Patients by Means of LC-MS/MS. *Biochim. Biophys. Acta - Mol. Cell Biol. Lipids* **2012**, *1821* (11), 1415–1424. https://doi.org/10.1016/j.bbalip.2012.07.011.

(17) DuBois, R. N.; Abramson, S. B.; Crofford, L.; Gupta, R. A.; Simon, L. S.; Putte, L. B. A.; Lipsky, P. E. Cyclooxygenase in Biology and Disease. *FASEB J.* **1998**, *12* (12), 1063–1073. https://doi.org/10.1096/fasebj.12.12.1063.

CHAPTER 2

ALLOSTERIC REGULATION OF HUMAN EPITHELIAL 15-LIPOXYGENASE-2 BY NATURAL EFFECTOR, 13*S*-HODE

Introduction

Enzymes can be controlled using regulatory mechanisms, such as allostery. For allosteric regulation to occur, a molecule, macromolecule, or membrane, known as an allosteric effector, must bind at a site in the protein that is different from the active site, resulting in a change in the protein's function, structure, or flexibility.[1] Most models of allostery are determined through static X-ray structural models, but more dynamic views of allostery are emerging.[2] In the past, allosteric effects were only associated with conformational changes. Since then, more protein models have emerged that show a dynamical change in the protein, with only a subtle change in the structure.[3] Allostery can be either activating or inhibiting, but it differs from competitive activation or inhibition.[1] With competitive regulation, the molecule binds directly at the active site rather than elsewhere in the protein. But in both cases, the rate of the reaction will be affected by these mechanisms of regulation.

Lipoxygenases are an example of a family of enzymes that use allostery to regulate their various functions. Allosteric regulation has been implicated in both plant and mammalian LOXs, including human LOX pathways.[4] It has been suggested through a series of *in vitro* kinetic assays that the human LOX, 15-LOX-2, is allosterically regulated by 13-(*S*)-hydroxyoctadecadienoic acid (13*S*-HODE) (Figure 2.1).[5] 13*S*-HODE is a physiologically relevant effector, being the product of the oxidation of LA with human reticulocyte 15-LOX-1.

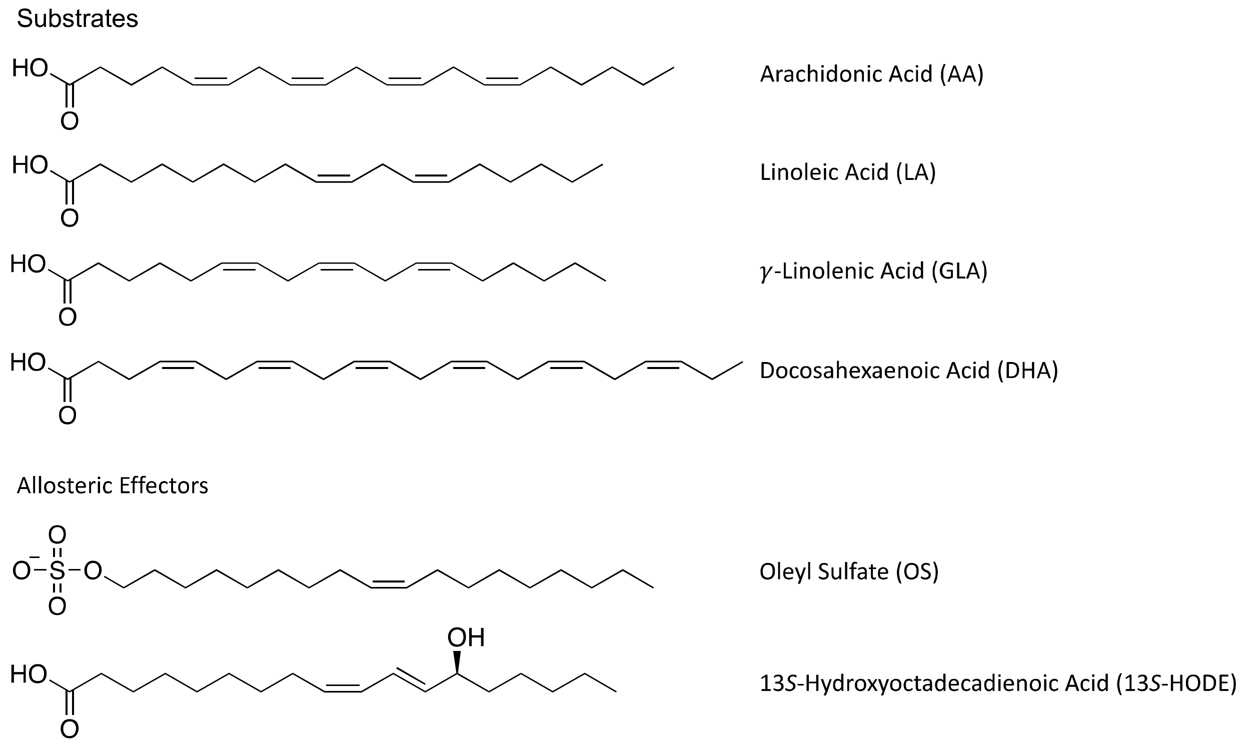
Substrates
Arachidonic Acid (AA)
Linoleic Acid (LA)
γ-Linolenic Acid (GLA)
Docosahexaenoic Acid (DHA)
Allosteric Effectors
Oleyl Sulfate (OS)
13S-Hydroxyoctadecadienoic Acid (13S-HODE)
HO
O
OH
S

Figure 2.1. *Relevant PUFA substrates and allosteric effectors for LOX allostery. Figure modified from reference (4).*

The preferred substrate for 15-LOX-2 is AA, but in previous *in vitro* kinetic studies comparing AA and LA, AA became a poorer substrate while LA became a better substrate for 15-LOX-2 with the addition of 13*S*-HODE (Table 2.1).[5] In another study 15-LOX-2 shows a preference for γ-linolenic acid (GLA) over AA, but its substrate specificity changes with the addition of 13*S*-HODE so that its preferred substrate is AA (Table 2.1).[6]

Table 2.1. *Comparison of Steady-State Kinetic Data for 15-LOX-2 with Various Substrates With and Without the Allosteric Effector, 13S-HODE*[a]

	k_{cat}/K_M (μM^{-1} s^{-1})		k_{cat} (s^{-1})	
	No Product	13*S*-HODE	No Product	13*S*-HODE
AA[b]	0.10 ± 0.01	0.08 ± 0.02	0.74 ± 0.03	0.59 ± 0.08
LA[b]	0.013 ± 0.001	0.022 ± 0.008	0.14 ± 0.01	0.14 ± 0.02
AA/LA[b]	8.0 ± 1.0	3.9 ± 0.9	5.3 ± 0.5	5.3 ± 0.4
AA[c]	0.40 ± 0.02	0.66 ± 0.07	1.5 ± 0.03	1.3 ± 0.02
GLA[c]	0.64 ± 0.02	0.29 ± 0.02	1.8 ± 0.03	2.0 ± 0.06
AA/GLA[c]	0.63 ± 0.04	2.3 ± 0.3	0.83 ± 0.02	0.65 ± 0.02

[a]Table modified from references (5, 6). [b]The reaction was run in 25 mM Hepes, pH 7.5 at 22°C with and without 10 μM 13*S*-HODE. [c]The reaction was run in 25 mM Hepes, pH 7.5 at 22°C with and without 15 μM 13*S*-HODE.

Interestingly, the substrate preference is different between the model 15-LOXs in plants and animals. The plant 15-LOX, SLO, catalyzes both AA and LA at nearly the same rate with a slight preference for AA, while the preferred substrates for human 15-LOX-1 and 15-LOX-2 are LA and AA, respectively. This result is much different than expected because AA is not a fatty acid that is naturally available in most plants and the substrate preference between the two human 15-LOXs is different as well.[4] Because of the flexibility in the acceptance of PUFAs in the active site, both substrates are able to be catalyzed.

Allostery is commonly used by proteins to regulate their activity, but in some cases, such as with ribonucleotide reductase and LOXs, the substrate specificity of the enzyme is regulated instead.[7] The addition of oleyl sulfate (OS) has shown a change in the substrate specificity of SLO and the addition of 13*S*-HODE has shown the same control of substrate specificity in 15-LOX-2.[5,6,8] The active site of human 15-LOXs appears to be able to adapt to different lengths of PUFAs through dynamic motions in the enzyme or positioning changes to the substrate.[5] Human LOXs contain a large pool of PUFAs that can be used as substrates and with the ability for 15-LOX-2 to accept a variety of different fatty acids, the product distribution can also be very diverse.

Allosteric regulation in LOXs was initially shown with SLO and its allosteric effector, OS.[8] OS was predicted to be a competitive inhibitor to SLO because it mimics the non-reactive oleic acid (OA) fatty acid. However, the KIE data did not fit the typical model of competitive inhibition that was shown with OA (Figure 2.2A). Instead, the KIE increases very rapidly when very low concentrations of OS are present (Figure 2.2B). The increase in KIE values instead fit to a sharp hyperbolic curve, which is a strong indication of allostery.

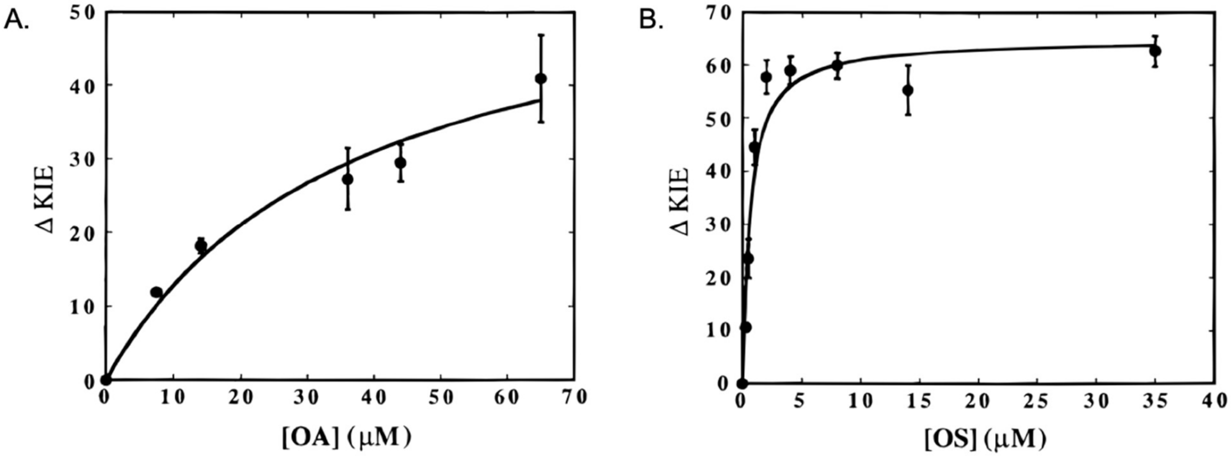

Figure 2.2. *KIE data for competitive inhibitor, oleic acid (OA) and allosteric effector, OS. Reactions were run in 100 mM borate, pH 9.2 at 5 °C with 5 μM H/D. The difference in these curves signifies OS as an allosteric effector. Figure reproduced from reference (8).*

Along with kinetic studies, other biophysical methods of characterization have been used to determine the mechanism of allostery of SLO chemistry by OS. For example, previous temperature-dependent hydrogen deuterium exchange-mass spectroscopy (TDHDX-MS) studies of SLO have shown an altered flexibility in the presence of OS at helix $\alpha 2$, which gates the substrate entrance in the catalytic domain, consistent with dynamic driven allostery.[9] More recently, isothermal titration calorimetry (ITC) studies demonstrated that OS binds to SLO (K_d = 1.0 ± 0.1 μM) and is dominated by an enthalpic contribution, suggesting an electrostatic interaction.[10] In both the absence and presence of OS, SLO has also been shown to exist as a monomer based on dynamic light scattering (DLS) and size exclusion chromatography (SEC) studies.[10] This behavior contrasts previous SAXS studies of the mammalian (rabbit) 12/15 LOX which indicated fatty acid induced dimerization.[11] Taken together with a docking model, the emerging data support that OS binds at the PLAT-catalytic domain interface, and elicits enhanced protein flexibility along helix $\alpha 2$ that may in turn control substrate acquisition.[10]

The LOX biosynthetic pathway is very intricate, with a wide range of nearly 30 PUFAs that are present in the human body as potential substrates. LOXs can also react with their own primary products in their mechanisms, such as the case with 13*S*-HODE acting as an allosteric effector, or even as substrates for subsequent reactions.[5] Together, these can create a diverse product distribution. This reasoning is also why the substrate specificity of 15-LOX-2 plays a large role in the progression and resolution of diseases of inflammation. 15-LOX-2 is highly expressed in the macrophages found in atherosclerotic plaques and in the specialized pro-resolving mediators (SPMs) found in the synovial fluid of arthritic diseases.[12,13]

The substrate preferences of 15-LOX-2 have only been determined between AA, LA, and GLA. 15-LOX-2 shows a preference for GLA *in vitro*, although it is unlikely the physiologically utilized substrate because it is found at much lower concentrations in the body.[6] It has recently been shown that docosahexaenoic acid (DHA) can be oxidized by 15-LOX-2 to produce the pro-resolving molecule, RvD5 (Figure 2.3).[14] The D-series resolvin, RvD5, has been shown to play an important protective role against inflammation. In our joints, for example, the buildup of synovial fluid can lead to joint damage and arthritis. RvD5 has been found in the synovial fluid of rheumatoid arthritis patients, indicating that pro-resolving mediators are present in instances of chronic inflammation.[12]

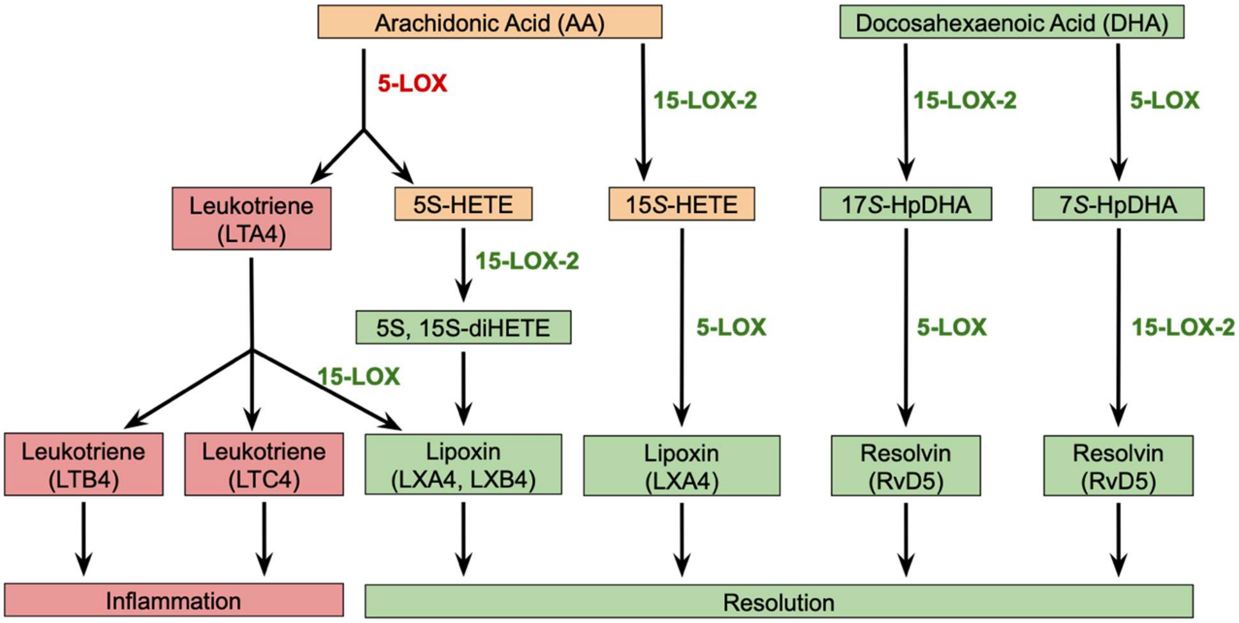
Arachidonic Acid (AA)
Docosahexaenoic Acid (DHA)
5-LOX
15-LOX-2
15-LOX-2
5-LOX
Leukotriene (LTA4)
5S-HETE
15S-HETE
17S-HpDHA
7S-HpDHA
15-LOX-2
5S, 15S-diHETE
5-LOX
5-LOX
15-LOX-2
15-LOX
Leukotriene (LTB4)
Leukotriene (LTC4)
Lipoxin (LXA4, LXB4)
Lipoxin (LXA4)
Resolvin (RvD5)
Resolvin (RvD5)
Inflammation
Resolution

Figure 2.3. *Biosynthetic pathways for various pro-inflammatory and pro-resolution molecules through AA and DHA with LOXs. Figure modified from reference (15).*

Allosteric effectors could serve as a good approach for therapeutics due to the ability to control the enzyme reactivity, rather than inhibiting the enzyme completely. There are a few known potent and selective competitive inhibitors for 15-LOX-2, but these eliminate any activity from the enzyme, including any anti-inflammatory or pro-resolution pathways the enzyme may participate in.[16,17] The influences of 13*S*-HODE on the regulation of AA versus DHA oxidation by 15-LOX-2 still remain unresolved. We can expand our knowledge of the allosteric regulation of 15-LOX-2 by looking at the preferred substrate versus another physiologically relevant substrate. With a deeper understanding of the mechanisms of allostery of 15-LOX-2 for substrates with more studied pathways, we can begin to work towards gaining control of the enzyme and isolating its substrate specificity towards pro-resolution products.

While there is a solved X-ray crystal structure of 15-LOX-2, the co-crystal structure with 13*S*-HODE has not been solved. Thus, the location of the allosteric site is also unresolved. Previous docking models suggest that the allosteric site lies between the PLAT and catalytic domains (Figure 2.4). The removal of the PLAT domain also supports the location of the allosteric site in between the two domains.[6] When the PLAT domain was removed from 15-LOX-2, the enzyme was able to retain its unique allosteric regulation abilities. An increase in the $(k_{cat}/K_M)^{AA/GLA}$ ratio with the removal of the PLAT domain indicates the influence of the domain in the substrate specificity.[6] However, the presence of the PLAT domain tunes the magnitude of the allosteric effects. These two findings combined indicate that the allosteric site includes the catalytic domain, but the PLAT domain is involved in the communication between the two domains of 15-LOX-2. The PLAT domain and helix $\alpha 2$ are both thought to play a role in substrate acquisition and regulation, which provides support for the predicted location of the allosteric site.[18]

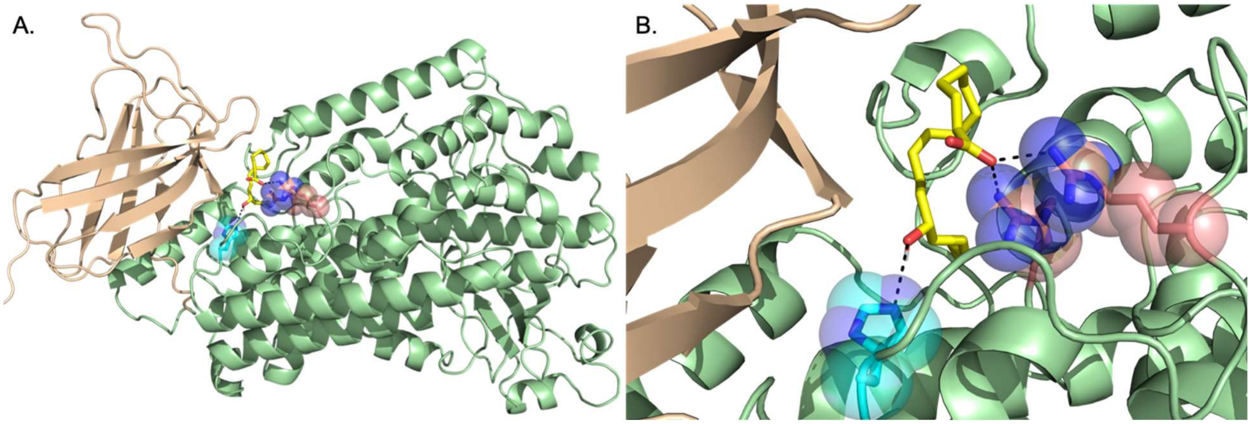

Figure 2.4. *Docking model of 13S-HODE in the predicted allosteric site between the two domains of 15-LOX-2. (A)13S-HODE docked in the predicted allosteric site shown in relation to the whole protein. (B) The predicted residue interactions between 15-LOX-2 and 13S-HODE. A histidine residue (blue) and two arginine residues (salmon) are predicted to bind with 13S-HODE.*[7]

There are still many questions about the impact that 13*S*-HODE has on the structure and function of 15-LOX-2. In this study, steady-state kinetics of WT 15-LOX-2 have been used to further probe the residues involved in the interaction with 13*S*-HODE and determine the impact the effector molecule has on the substrate specificity between AA and DHA. Because allostery is thermodynamically driven, we will use ITC to determine ΔH, ΔS, and the dissociation constant (K_d) of 13*S*-HODE to 15-LOX-2.[2] Hydrogen-deuterium exchange mass spectrometry (HDX-MS) also provided insight into the protein dynamics and flexibility that are linked to allostery within 15-LOX-2.

Materials and Methods

Materials

AA and DHA were purchased from Cayman Chemical Company (Ann Arbor, MI) while LA was purchased from Acros Organic, TCI (Palo Alto, CA). 13*S*-HODE was synthesized in collaborator, Dr. Theodore Holman's lab (University of California, Santa Cruz). Deuterium oxide (D_2O, 99% D), NaOD (99% D), and DCl (99% D) were purchased from Cambridge Isotopes (Tewksbury, MA). All bacterial cells, media, salts, and buffers were purchased from Fisher Scientific, Sigma-Aldrich, or VWR at the highest grade available.

Protein Expression and Purification

Wild type 15-LOX-2 encoded in the pET Duet-1 plasmid was transformed into *E.coli* Rosetta 2 cells for protein expression. The cells were transferred into an ampicillin-containing LB media and allowed to shake at 37°C overnight. This overnight starter culture was incubated in large scale (1L) 2xYT media and ampicillin and expressed using the leaky T7 promoter by incubation at 18°C overnight once the optical density, OD_{600}, reached ~1.0. The cells were harvested in 200 mL fractions in 5-minute intervals at 10000 g and flash frozen in liquid nitrogen until further use. The protein was purified as described, using a Ni-NTA column to capture the His-tagged protein.[19] The cell pellet was resuspended in lysis buffer (50 mM $NaPO_4$, 100 mM

NaCl, pH 7.9, 8% glycerol, and 2 mM magnesium sulfate supplemented with lysozyme, DNAse I, and 4-(2-aminoethyl)-benzenesulfonyl fluoride hydrochloride (AEBSF)) before lysis was performed by sonication. The lysed cells were then centrifuged at 18000 g for 25 minutes. The protein was purified over a linear gradient from buffer A (20 mM Tris-HCl, 20 mM imidazole, 500 mM NaCl, pH 8.0) to buffer B (20 mM Tris-HCl, 200 mM imidazole, 500 mM NaCl, pH 8.0) using a Ni-NTA column. The presence of protein was confirmed using UV-Vis spectroscopy (280 nm) and SDS-PAGE. The protein was further purified using size exclusion chromatography (SEC) with a Superdex^{TM} 200 increase 10/300 GL column on an ÄKTA^{TM} Prime fast-protein liquid chromatography (FPLC). The protein was eluted with the storage buffer (25 mM Tris, 150 mM NaCl, pH 7.5). The purified protein fractions were collected and concentrated. Pure protein was flash frozen in liquid nitrogen and stored at -80°C until needed.

Steady State Kinetic Measurements

A UV1800 Shimadzu UV-Vis spectrophotometer was used for steady-state kinetic analysis. The enzyme and substrate concentrations were determined enzymatically before being used in the reaction. The reactions were run in 50 mM Hepes buffer, 150 mM NaCl, pH 7.0 or 50 mM Hepes, 150 mM NaCl, pH 8.5 at 25°C or 37°C over the specified substrate concentrations (5-6 concentrations for each temperature) ranging from 2 μM to 25 μM to ensure that k_{cat} had been reached. The total reaction volume was 1.0 mL. The enzyme concentration varied for each enzyme-substrate combination, ranging from 10 μM-30 μM. Each substrate concentration at each temperature was collected and averaged through 3 replicates and reported as the mean ± s.e.m. The substrates used for the substrate specificity studies were AA, DHA, and LA. Experiments were run with and without the addition of 13*S*-HODE.

Hydrogen-Deuterium Exchange (HDX) Sample Preparation

HDX samples were prepared as previously described.[20] Aliquots of 110 μM wild-type 15-LOX-2 stocks were incubated at the desired temperatures (10, 20, 30°C) for 30-60 seconds before diluting 10-fold in D_2O buffer (10 mM Hepes, 250 mM NaCl, pD 7.47). When included, the 13*S*-HODE concentration was held at 10 μM. The samples were incubated for 9 time points (10, 20, 45, 60, 180, 600, 1800, 3600, 7200 seconds) at each temperature. After incubation for the desired time, the samples were cold-quenched (-20°C) and then acid-quenched (to pH 2.4 with 0.32 M citric acid stock solution and 19.6 mM DTT at 0°C) to minimize back-exchange. Guanidine HCl (in citric acid, pH 2.4) was added to the sample to a final concentration of 0.5 M to get the best sequence coverage. Samples were digested with immobilized pepsin for 2.5 minutes. The pepsin was filtered through centrifugation at 7000 g for 10 seconds before being flash-frozen in liquid nitrogen. Samples were stored at -80°C until data collection. The time points were randomly collected over two days for each temperature to reduce error.

Differential Scanning Calorimetry (DSC)

A NanoDSC microcalorimeter from TA Instruments was used to determine the thermodynamics for the stability of wild-type 15-LOX-2 with and without the addition of 13*S*-HODE. Protein samples were diluted to be about 30 μM using 25 mM Tris, 150 mM NaCl, pH 7.5. The system was pressurized up to 3 atm and the run was started when the heat was below 75 μW. The temperature range for the run was 30°C-90°C. An equimolar concentration of 14 μM was used for 13*S*-HODE and 15-LOX-2. The raw data was analyzed using NanoAnalyze software from TA instruments. The data was converted to the molar heat capacity using the molecular weight of the protein, the volume of the sample cell, and the concentration (mg/mL). The baseline is integrated using a 4th order polynomial to get a melting temperature (T_m) and ΔH. After integrating the baseline, the data was fit to the Gaussian model.

Isothermal Titration Calorimetry (ITC)

The thermodynamics of 13*S*-HODE binding to 15-LOX-2 was determined using a TA Instruments Nano-ITC. 13*S*-HODE stock solution (50 mM in 100% dimethyl sulfoxide, DMSO) was diluted in either 50 mM Tris, 150 mM NaCl, pH 7.5, 50 mM Tris, 150 mM NaCl, pH 8.5, or 50 mM phosphate, 150 mM NaCl, pH 7.5. 15-LOX-2 that was previously prepared in the desired buffer was thawed and DMSO was added to a concentration of 0.3% to prevent buffer mismatch between the protein and allosteric effector. The experiment was set up so that 2.02 µL (50 µL total) of 250 µM 13*S*-HODE was titrated into 65 µM 15-LOX-2 over 24 injections. Temperatures of 10°C and 20°C were tested and the reaction was stirred at 320 rpm.

Results and Discussion

Protein Expression and Purification

15-LOX-2 was expressed and purified as previously described with typical yields of 20-30 mg/L. SDS-PAGE was used to confirm that the protein had been fully purified. The SDS-PAGE showed a single spot around 75 kDa, indicating that the protein was pure with a migration pattern similar to what was expected for the size of the protein. Purification of 15-LOX-2 with the SEC was further completed for HDX-MS and ITC experiments to ensure the stability of the protein.

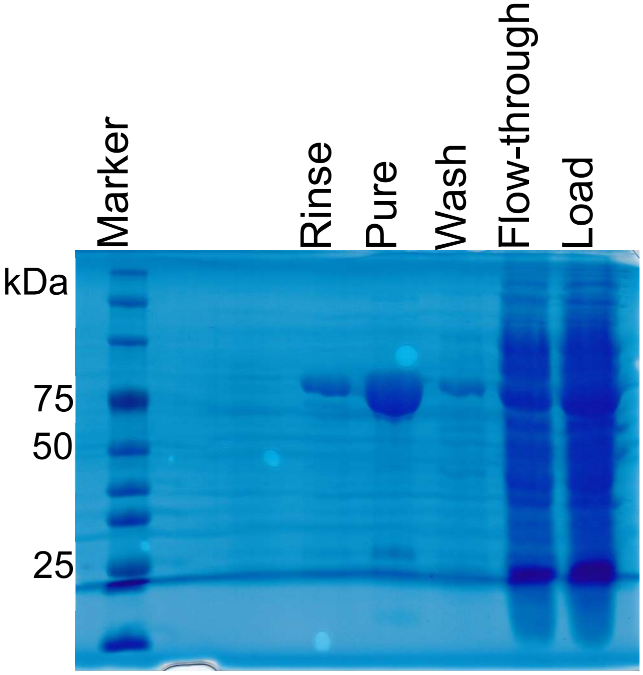

Figure 2.5. *SDS-PAGE of purification steps for 15-LOX-2 shows that the protein has been isolated using the Ni-NTA column and is fully purified.*

Steady State Kinetics Provide Insight into Allosteric Regulation with 13S-HODE

Steady state kinetics were used to determine the first order (k_{cat}) and second order (k_{cat}/K_M) rate constants to probe the substrate specificity of 15-LOX-2 with the addition of the allosteric effector, 13*S*-HODE. AA, the preferred substrate for 15-LOX-2, was compared against previously studied substrates, such as LA and GLA, along with the newly questioned physiologically relevant substrate, DHA. GLA was originally chosen as the substrate of study over LA because it is a better substrate catalytically for 15-LOX-2, although not as commonly found in the body.[6] The kinetic parameters have more recently been determined for DHA, but the effect of 13*S*-HODE on these parameters has not yet been resolved.[14]

Table 2.2. *Catalytic Parameters of 15-LOX-2 with Various Substrates With and Without the Addition of 13S-HODE at pH 7.0 and 37 ℃*[a]

	k_{cat}/K_M ($\mu M^{-1}s^{-1}$)		$(k_{cat}/K_M)^{AA}/(k_{cat}/K_M)^X$		k_{cat} (s^{-1})		k_{cat}^{AA}/k_{cat}^X	
	No Product	13*S*-HODE	No Product	13*S*-HODE	No Product	13*S*-HODE	No Product	13*S*-HODE
AA	0.77 ± 0.13	0.65 ± 0.08	-	-	1.41 ± 0.05	1.35 ± 0.04	-	-
DHA	1.34 ± 0.26	0.99 ± 0.14	0.57 ± 0.15	0.65 ± 0.12	1.95 ± 0.08	1.99 ± 0.06	0.72 ± 0.04	0.68 ± 0.03
LA	0.14 ± 0.03	0.19 ± 0.04	5.34 ± 1.48	3.45 ± 0.83	0.62 ± 0.04	0.59 ± 0.03	2.27 ± 0.17	2.29 ± 0.13
GLA	0.55 ± 0.16	0.37 ± 0.11	1.41 ± 0.49	1.74 ± 0.55	2.11 ± 0.19	2.19 ± 0.22	0.67 ± 0.06	0.62 ± 0.06

[a] The data is averaged from 3 replicates and reported as the mean ± s.e.m. The reaction was run in the prepared buffer with 50 mM Hepes, 150 mM NaCl at pH 7.0.

The substrate with the greatest k_{cat}/K_M in the absence and presence of 13*S*-HODE was DHA (1.34 ± 0.26 $\mu M^{-1}s^{-1}$ and 0.99 ± 0.14 $\mu M^{-1}s^{-1}$, respectively), which indicates that DHA had the greatest rate of substrate capture. LA presented as a poor substrate for 15-LOX-2, which was expected based on previous kinetic studies (0.14 ± 0.03 $\mu M^{-1}s^{-1}$ without 13*S*-HODE, 0.19 ± 0.04 $\mu M^{-1}s^{-1}$ with 13*S*-HODE) (Table 2.2). AA and GLA were observed to have a large increase in their second order rate constants when compared to LA (5.5-fold and 3.9-fold increases, respectively), but both fell short to the substrate capture abilities of DHA (Table 2.2). The second order rate constants between the substrates followed the same trend as previously shown, with decreasing k_{cat}/K_M values being DHA > AA > GLA > LA.[5,6,14] All of the PUFAs, with the exception of LA, showed a decrease in their k_{cat}/K_M with the addition of 13*S*-HODE. The values with the addition of 13*S*-HODE lied within the error for the k_{cat}/K_M values for 15-LOX-2 without 13*S*-HODE, but the errors were larger than expected. These results showed the same trend in the k_{cat}/K_M that was previously shown upon the addition of 13*S*-HODE, but to a much smaller magnitude than what was originally expected. This was not indicative of a change in substrate preference but did suggest a change in the substrate acquisition of the enzyme.

GLA had shown that it was a better substrate in regard to the production of hydroperoxide with the greatest first order rate constant (k_{cat}) of the fatty acids (2.11 ± 0.19 s^{-1} without 13*S*-HODE,

$2.19 \pm 0.22\ s^{-1}$ with 13*S*-HODE) (Table 2.2). Although DHA had the greatest k_{cat}/K_M, a slight decrease in the k_{cat} compared to GLA was observed ($1.95 \pm 0.08\ s^{-1}$ without 13*S*-HODE, $1.99 \pm 0.06\ s^{-1}$ with 13*S*-HODE) (Table 2.2). The kinetic analysis again suggested that LA is a poor substrate for 15-LOX-2 ($0.62 \pm 0.04\ s^{-1}$ without 13*S*-HODE, $0.59 \pm 0.03\ s^{-1}$ with 13*S*-HODE) (Table 2.2). There was little change observed in the k_{cat} values upon the addition of 13*S*-HODE for all of the substrates studied, meaning that the catalytic efficiency of the enzyme was unaffected by the binding of effector. This lack in change was previously observed through the kinetic studies with AA and GLA.[6] This also signified that the change that was observed through the k_{cat}/K_M values could be attributed to a change in the K_M, which would again suggest a change in the substrate acquisition of the enzyme.

DHA had a slightly greater k_{cat} and k_{cat}/K_M than AA, indicating that it was the preferred substrate (Table 2.2). The similarities in kinetic values between the two substrates and the role of DHA in the biosynthetic pathways of 15-LOX-2 showed that DHA is a physiologically relevant substrate for 15-LOX-2 and slightly more preferred over LA and GLA, respectively. DHA remained the preferred substrate with the addition of 13*S*-HODE, but the $(k_{cat}/K_M)^{AA/DHA}$ ratio trends upward, indicating an increase in the preference for AA (Table 2.2). Its ability to act as a good PUFA substrate for 15-LOX-2, but not as the preferred substrate for the active site cavity led to questions of the role of 15-LOX-2, as well as DHA, in the pathways of inflammation and resolution in the body that we are still working to resolve.

The ratio of the kinetic parameters for each of the substrates relative to AA can be used to determine the preference for each substrate. Previously, the $k_{cat}/K_M^{AA/GLA}$ ratio increased 3.7-fold, indicating a change in the substrate preference from GLA to AA (Table 2.2). The $k_{cat}/K_M^{AA/GLA}$ and $k_{cat}/K_M^{AA/DHA}$ ratios increased and the $k_{cat}/K_M^{AA/LA}$ ratio decreased with 13*S*-HODE as previously observed.[6,7] Each of the k_{cat} ratios with the given substrates followed the same trend as the k_{cat}/K_M ratios (Table 2.2). While these kinetic substrate ratios somewhat followed the same trends as previously shown on k_{cat}/K_M, our kinetic data are not consistent with a change in the substrate preference for 15-LOX-2 in the presence of 13*S*-HODE.

Investigating pH Dependence Through Steady State Kinetics

Previous studies have suggested that there is also a pH dependence associated with the addition of 13*S*-HODE, thus we decided to probe this further between AA and LA.[7] Without 13*S*-HODE, the k_{cat} value for LA decreased significantly while k_{cat}/K_M stayed the same with the increase in pH (Table 2.3). Both k_{cat} and k_{cat}/K_M for AA decreased with the increase in pH in the absence of 13*S*-HODE (Table 2.3). In the presence of 13*S*-HODE, k_{cat} and k_{cat}/K_M decreased for both AA and LA with the increase in pH, indicating that AA and LA became poorer substrates for 15-LOX-2.

Table 2.3. *pH Dependence on the Catalytic Parameters of 15-LOX-2 with AA and LA With and Without 13S-HODE*

	k_{cat}/K_M ($\mu M^{-1}s^{-1}$)		k_{cat} (s^{-1})		
	No Product[b]	13*S*-HODE[c]	No Product[b]	13*S*-HODE[c]	
AA	0.77 ± 0.13	0.65 ± 0.08	1.41 ± 0.05	1.35 ± 0.04	pH 7.0
LA	0.14 ± 0.03	0.19 ± 0.04	0.62 ± 0.04	0.59 ± 0.03	
AA	0.46 ± 0.16	0.39 ± 0.07	1.15 ± 0.10	0.78 ± 0.03	pH 8.5
LA	0.14 ± 0.07	0.080 ± 0.028	0.082 ± 0.005	0.078 ± 0.004	

[a]The data is averaged from 3 replicates and reported as the mean ± s.e.m. [b]The reaction was run at 25°C in the prepared buffer with 50 mM Hepes, 150 mM NaCl at the given pH. [c]The reaction was run at 37°C in the prepared buffer with 50 mM Hepes, 150 mM NaCl at the given pH.

The docking model predicts two histidine residues to be involved in the binding of the allosteric effector at the intersection of the catalytic and PLAT domains. In this case, the histidine residues would be positively charged at pH 7.5 and neutral at pH 8.5. When charged, the histidine would be able to hydrogen bond with the negatively charged carboxylate tail of 13*S*-HODE, thus suggesting a tighter binding affinity between the enzyme and effector at pH 7.5 than pH 8.5. Previous kinetic studies support this pH dependence, as shown through an decrease in the k_{cat} and k_{cat}/K_M of GLA and an increase in the k_{cat} and k_{cat}/K_M of AA as the pH increased.[6] The trend that was observed between AA and LA was the opposite of the pH dependence previously reported between AA and GLA. While the steady state kinetics provided further insight into LA as a substrate, comparing the data of AA did not follow the trend as expected.

The pH dependence of the allosteric site, as well as its effect on substrate specificity can be further probed with mutations at the residues predicted to bind the allosteric effector as determined through the docking model.[6] Some of the kinetic data collected here was completed at 37°C to be closer to physiological temperature. This is 15°C warmer than the temperature at which previous kinetics were collected.[6] While there was a temperature dependence of the enzyme, the trends with pH and substrate specificity had been shown to stay the same. This difference in kinetic data leads to questions of the extent of the role of the allosteric effector.

Impact of 13S-HODE on the Structure of 15-LOX-2

The impact of 13*S*-HODE on the structure of 15-LOX-2 was determined using differential scanning calorimetry (DSC) and size exclusion chromatography (SEC). DSC was able to show if the addition of 13*S*-HODE affected the stability of 15-LOX-2 through a comparison of the T_m values. The DSC thermogram of 15-LOX-2 was represented through a single peak modeled from two Gaussian curves (Figure 2.6A). When the DSC thermogram without the addition of effector was compared to that with the addition of 13*S*-HODE, the two peaks were seen to align to each other, signifying that there was no change in the stability of the enzyme in the presence of 13*S*-

HODE (Figure 2.6B). The T_m values of 15-LOX-2 without and with the addition of the allosteric effector were 57.1°C and 56.6°C, respectively, also indicating that 13*S*-HODE did not significantly impact the stability of 15-LOX-2.

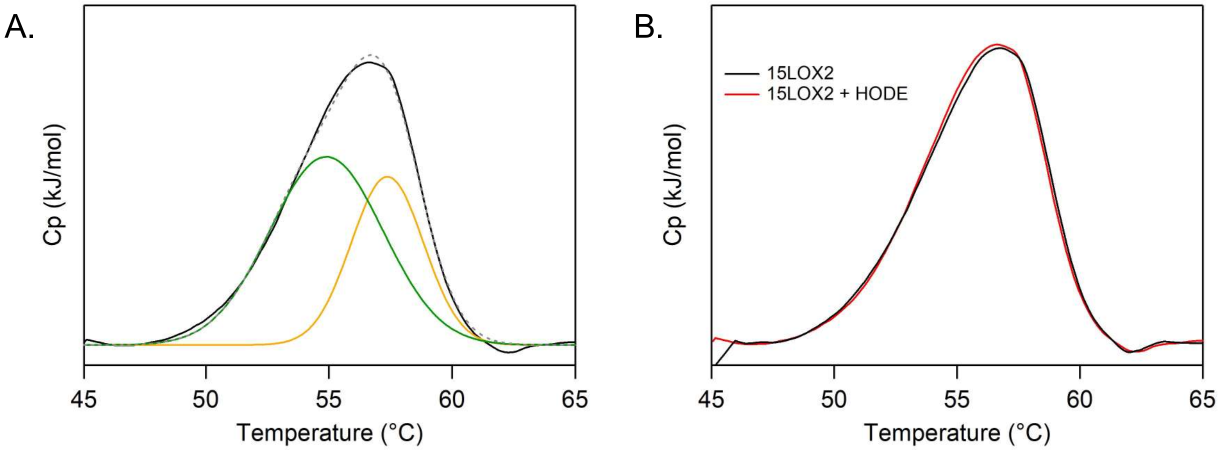

Figure 2.6. *Modeled DSC thermograms of 15-LOX-2 in the absence and presence of 13S-HODE. (A)Gaussian modeling of DSC data shows that two separate Gaussians (green and yellow) make up the single peak that represents the* T_m*. (B)Overlay of DSC thermograms with (red) and without (black) the addition of 13S-HODE show almost identical* T_m *values. The scans were collected from 30℃-90℃ under 3 atm pressure and each fit with two Gaussian models.*

SEC data were also collected with and without the addition of 13*S*-HODE. Like the DSC data, the overlay of the SEC chromatograms showed that 13*S*-HODE did not shift the elution volume of 15-LOX-2 (Figure 2.7). This further supported that 13*S*-HODE did not cause dimerization of 15-LOX-2.

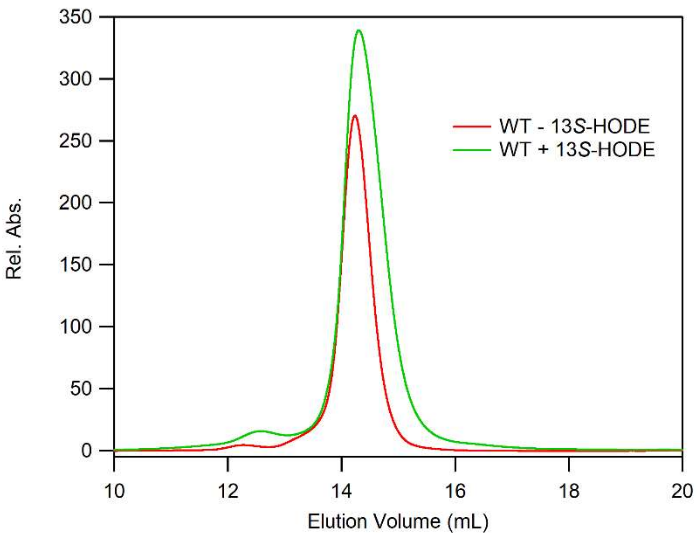

Figure 2.7. *SEC chromatograms of 15-LOX-2 with (green) and without (red) the addition of 13S-HODE show a similar elution volume for the enzyme.*

Hydrogen-Deuterium Exchange Suggests Dynamically Driven Allostery

The dynamic allostery of 15-LOX-2 can be further studied through the flexibility in the structure of the protein. HDX-MS allowed for the comparison of the regional flexibility of 15-LOX-2 with and without the addition of 13*S*-HODE. HDX-MS traces of WT 15-LOX-2 showed high percentages of flexibility throughout the PLAT domain, helix $\alpha 2$, and the linker shown at the intersection of the catalytic and PLAT domains (Figure 2.8A). With the addition of 13*S*-HODE, the linker between the catalytic and PLAT domains, as well as helix $\alpha 2$ experienced a decrease in exchange, which indicated a rigidification or structuring of these peptides (Figure 2.8B-C). Rigidity of the linker between the two domains suggested a conformational change of the protein to clamp down on the allosteric effector. The membrane loop, which helps to anchor 15-LOX-2 to the membrane in the presence of calcium ions and is not present in SLO, also showed a decrease in exchange in the presence of 13*S*-HODE (Figure 2.8B-C). This regional flexibility suggested conformational control.

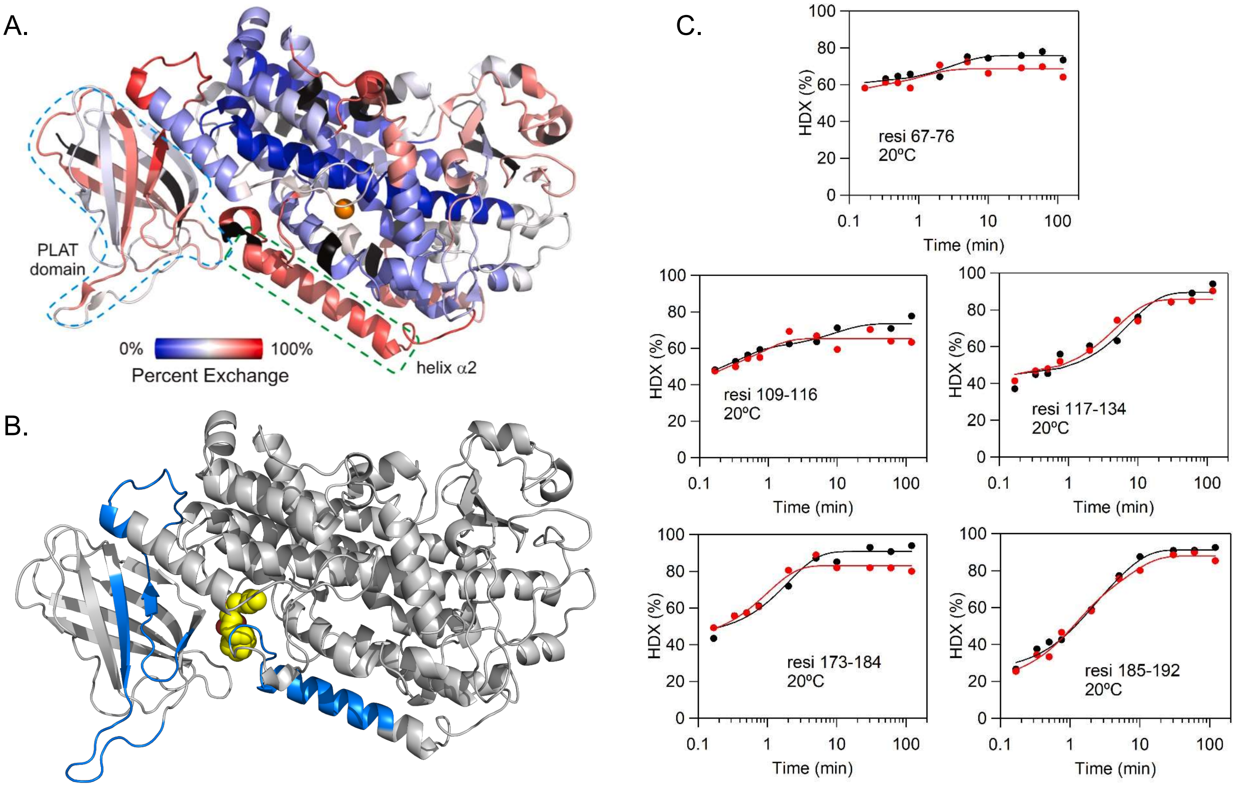

Figure 2.8. *HDX-MS of 15-LOX-2 in the absence and presence of 13S-HODE. (A) HDX-MS of WT 15-LOX-2 without 13S-HODE at 2 h and 25°C highlighting the PLAT domain (blue dotted line) and helix α2 (green dotted line). The exchange percentage is shown as a spectrum with black representing the uncovered regions.*[17] *(B) Rigidified regions of 15-LOX-2 (blue) with the addition of 13S-HODE (yellow), as determined through HDX-MS. (C) Comparison of HDX-MS traces between 15-LOX-2 in the absence (black) and presence (red) of 13S-HODE shows decreased exchange with the effector.*

The HDX-MS traces for 13*S*-HODE and 15-LOX-2 were different than those for SLO and OS. SLO and OS show a conformational change in the PLAT domain in the presence of OS, like 13*S*-HODE. But SLO and OS display an increase in exchange at the N-terminal rather than a rigidification within the domain.[9] SLO also shows an increase in rate of exchange at the C-terminal with the addition of OS, which also differed from the exchange patterns observed between 15-LOX-2 and 13*S*-HODE.[9] In contrast to 15-LOX-2, SLO exhibits an enhanced flexibility of helix $\alpha 2$ in the presence of OS, which shows the influence of the allosteric effector on substrate specificity of the enzyme.[9] This HDX-MS behavior tracks the trends in the k_{cat}/K_M. In the case of SLO, the presence of OS increases the k_{cat}/K_M values for substrate and is associated with an enhanced flexibility of helix $\alpha2$. In contrast as shown here for 15-LOX-2, 13*S*-HODE caused a decrease in the k_{cat}/K_M values for almost all substrates under all conditions explored and this behavior is associated with a rigidified or restructured helix $\alpha2$.

This HDX-MS data with the addition of the allosteric effector can be compared to the exchange data with the addition of a competitive inhibitor.[17] When compared to the HDX with the addition of a competitive inhibitor, different patterns of rigidity were observed. The addition of two different competitive inhibitors showed a decrease in exchange at only helix $\alpha2$ (Figure 2.9A).[17] This indicates that a compound that is bound at the active site leads to a localized rigidification of 15-LOX-2. The observed behavior further supports that the additional rigidity observed upon binding 13*S*-HODE is indicative of an allosteric effect.

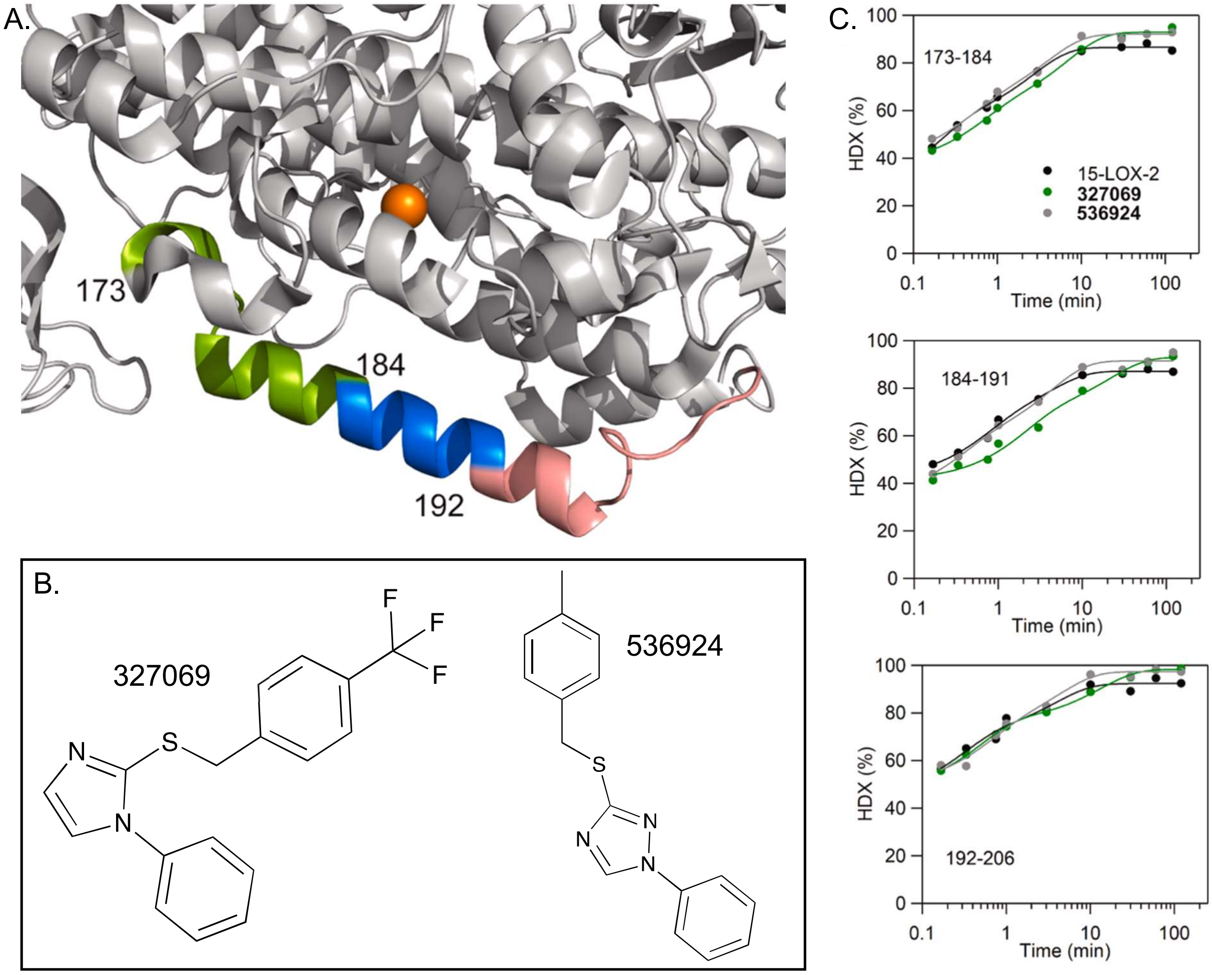

Figure 2.9. *HDX-MS with the addition of competitive inhibitor. (A)The peptides affected by the addition of competitive inhibitors are mapped onto helix α2. (B)HDX-MS traces for the peptides of helix α2 show a decrease in percent exchange in the presence of competitive inhibitors.*[17]

Optimization of Thermodynamic Measurements

The role of entropy in the thermodynamics of allostery has been termed dynamic allostery and can also add to the support of dynamically driven allostery. ITC has previously been used to probe the thermodynamics of the allosteric binding event between SLO and OS.[10] Previous ITC studies have shown that the ideal system for SLO and OS is 250 µM and 65 µM SLO and OS, respectively, in 50 mM pyrophosphate buffer, pH 9.0 with 0.3% DMSO at 20°C.[10] While the ITC conditions have been optimized for the SLO and OS system, the conditions for 15-LOX-2 and

13*S*-HODE have yet to be determined. We started the optimization for the conditions of 15-LOX-2 and 13*S*-HODE by comparing 50 mM phosphate buffer, pH 7.5 and 50 mM Tris buffer, pH 7.5 at 20°C. Because of the large background noise observed with titrating 13*S*-HODE into buffer, as well as the temperature dependence that had been observed with SLO and OS, we chose to test the two buffer systems at 10°C as well. Between temperatures and buffers, the Tris buffer system, pH 7.5 worked the best at 20°C. We then compared the pH of the system by testing 50 mM Tris buffer, pH 8.5. This showed better results than pH 7.5, although no binding data could be extrapolated from the plot. While the thermogram has some shape to it to designate binding, the corrected and integrated data was not able to be fit to a model, indicating that the heats generated upon the binding of 13*S*-HODE were not significant enough to extrapolate a K_d (Figure 2.10). Our other data collected supports an interaction between 15-LOX-2 and 13*S*-HODE. Thus, further optimization is ongoing to eliminate the large heats associated with the buffer and provide sufficient thermodynamic binding data.

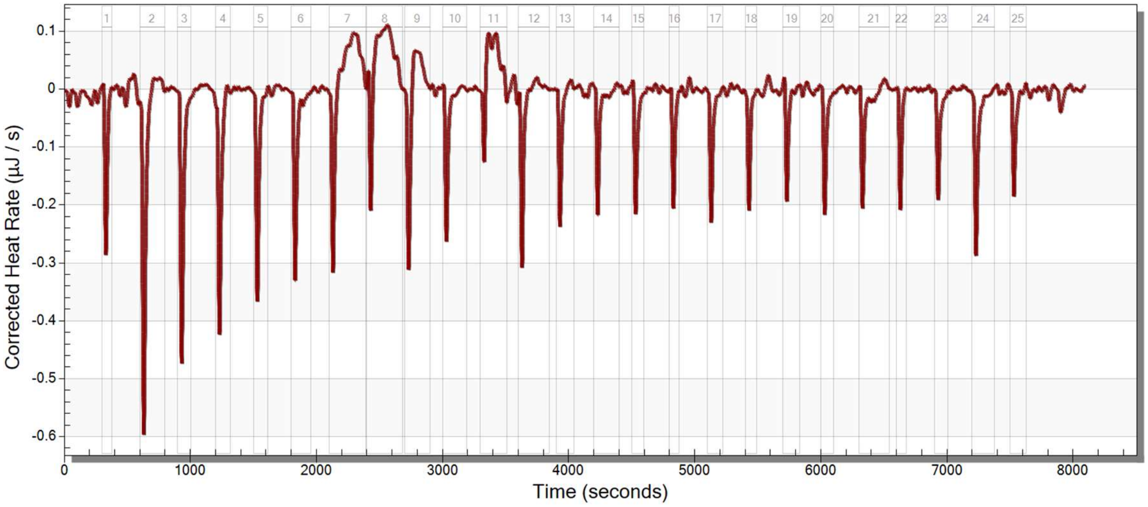

Figure 2.10. *Preliminary ITC thermogram with 50 mM Tris, 150 mM NaCl, pH 8.5 represents a weak binding interaction between 15-LOX-2 and 13S-HODE. This signifies that while binding is present between the enzyme and effector, there is still much optimization to be done.*

Conclusion

15-LOX-2 is allosterically regulated by 13*S*-HODE, as shown through the conformational control with HDX-MS, but the full extent of this is still currently being studied. The difference in kinetic data has led to further questions about the mechanism of allosteric regulation for 15-LOX-2. Further kinetics will have to be completed to determine the substrate specificity of 15-LOX-2 with and without the addition of 13*S*-HODE. Mutants for 15-LOX-2 have been created through site-directed mutagenesis and kinetic experiments will be used to test their substrate specificity and pH dependence with 13*S*-HODE. This can further test our hypothesis on the allosteric role of 13*S*-HODE, as well as the location of the allosteric site. ITC experiments need to be further optimized to quantify the thermodynamics of 13*S*-HODE and 15-LOX-2 binding. By determining the K_d and providing insight into the enthalpic and entropic contributions to the binding, we can provide support for the docking model without a co-crystal structure. 13*S*-HODE does not induce any structural changes to 15-LOX-2, though there are significant influences on the dynamics of the enzyme. The regional rigidification of the membrane binding loop and PLAT domain, in particular, have led to questions about the role of the physiological allosteric effector on membrane association and chemistry at the membrane-protein interface that we hope to investigate in the future.

References

(1) Goodey, N. M.; Benkovic, S. J. Allosteric Regulation and Catalysis Emerge via a Common Route. *Nature Chemical Biology*. 2008. https://doi.org/10.1038/nchembio.98.

(2) Motlagh, H. N.; Wrabl, J. O.; Li, J.; Hilser, V. J. The Ensemble Nature of Allostery. *Nature* **2014**, *508* (7496), 331–339. https://doi.org/10.1038/nature13001.

(3) Guo, J.; Zhou, H. X. Protein Allostery and Conformational Dynamics. *Chem. Rev.* **2016**, *116* (11), 6503–6515. https://doi.org/10.1021/acs.chemrev.5b00590.

(4) Offenbacher, A. R.; Holman, T. R. Fatty Acid Allosteric Regulation of C-H Activation in Plant and Animal Lipoxygenases. *Molecules*. 2020. https://doi.org/10.3390/molecules25153374.

(5) Wecksler, A. T.; Kenyon, V.; Deschamps, J. D.; Holman, T. R. Substrate Specificity Changes for Human Reticulocyte and Epithelial 15-Lipoxygenases Reveal Allosteric Product Regulation. *Biochemistry* **2008**, *47* (28). https://doi.org/10.1021/bi800550n.

(6) Joshi, N.; Hoobler, E. K.; Perry, S.; Diaz, G.; Fox, B.; Holman, T. R. Kinetic and Structural Investigations into the Allosteric and PH Effect on the Substrate Specificity of Human Epithelial 15-Lipoxygenase-2. *Biochemistry* **2013**. https://doi.org/10.1021/bi4010649.

(7) Wecksler, A. T.; Kenyon, V.; Garcia, N. K.; Deschamps, J. D.; Van Der Donk, W. A.; Holman, T. R. Kinetic and Structural Investigations of the Allosteric Site in Human Epithelial 15-Lipoxygenase-2. *Biochemistry* **2009**, *48* (36). https://doi.org/10.1021/bi9009242.

(8) Mogul, R.; Johansen, E.; Holman, T. R. Oleyl Sulfate Reveals Allosteric Inhibition of Soybean Lipoxygenase-1 and Human 15-Lipoxygenase. *Biochemistry* **2000**, *39* (16). https://doi.org/10.1021/bi992805t.

(9) Offenbacher, A. R.; Iavarone, A. T.; Klinman, J. P. Hydrogen-Deuterium Exchange Reveals Long-Range Dynamical Allostery in Soybean Lipoxygenase. *J. Biol. Chem.* **2018**, *293* (4), 1138–1148. https://doi.org/10.1074/jbc.M117.817197.

(10) Roberts, D. E.; Benton, A. M.; Fabian-Bayola, C.; Spuches, A. M.; Offenbacher, A. R. Thermodynamic and Biophysical Study of Fatty Acid Effector Binding to Soybean Lipoxygenase: Implications for Allostery Driven by Helix A2 Dynamics. *FEBS Lett.* **2022**, 1–10. https://doi.org/10.1002/1873-3468.14275.

(11) Ivanov, I.; Shang, W.; Toledo, L.; Masgrau, L.; Svergun, D. I.; Stehling, S.; Gómez, H.; Di Venere, A.; Mei, G.; Lluch, J. M.; et al. Ligand-Induced Formation of Transient Dimers of Mammalian 12/15-Lipoxygenase: A Key to Allosteric Behavior of This Class of Enzymes? *Proteins Struct. Funct. Bioinforma.* **2012**, *80* (3), 703–712. https://doi.org/10.1002/prot.23227.

(12) Giera, M.; Ioan-Facsinay, A.; Toes, R.; Gao, F.; Dalli, J.; Deelder, A. M.; Serhan, C. N.; Mayboroda, O. A. Lipid and Lipid Mediator Profiling of Human Synovial Fluid in Rheumatoid Arthritis Patients by Means of LC-MS/MS. *Biochim. Biophys. Acta - Mol. Cell Biol. Lipids* **2012**, *1821* (11), 1415–1424. https://doi.org/10.1016/j.bbalip.2012.07.011.

(13) Snodgrass, R. G.; Brüne, B. Regulation and Functions of 15-Lipoxygenases in Human Macrophages. *Front. Pharmacol.* **2019**, *10* (July), 1–12. https://doi.org/10.3389/fphar.2019.00719.

(14) Perry, S. C.; Kalyanaraman, C.; Tourdot, B. E.; Conrad, W. S.; Akinkugbe, O.; Freedman, J. C.; Holinstat, M.; Jacobson, M. P.; Holman, T. R. 15-Lipoxygenase-1 Biosynthesis of 7S,14S-DiHDHA Implicates 15-Lipoxygenase-2 in Biosynthesis of Resolvin D5. *J. Lipid Res.* **2020**, *61* (7), 1087–1103. https://doi.org/10.1194/JLR.RA120000777.

(15) Serhan, C. N.; Petasis, N. A. Resolvins and Protectins in Inflammation Resolution. *Chemical Reviews*. 2011. https://doi.org/10.1021/cr100396c.

(16) Jameson, J. B.; Kantz, A.; Schultz, L.; Kalyanaraman, C.; Jacobson, M. P.; Maloney, D. J.; Jadhav, A.; Simeonov, A.; Holman, T. R. A High Throughput Screen Identifies Potent and Selective Inhibitors to Human Epithelial 15-Lipoxygenase-2. *PLoS One* **2014**, *9* (8). https://doi.org/10.1371/journal.pone.0104094.

(17) Tsai, W.-C.; Gilbert, N. C.; Ohler, A.; Armstrong, M.; Perry, S.; Kalyanaraman, C.; Yasgar, A.; Rai, G.; Simeonov, A.; Jadhav, A.; et al. Kinetic and Structural Investigations of Novel Inhibitors of Human Epithelial 15-Lipoxygenase-2. *Bioorg. Med. Chem.* **2021**, *46* (August), 116349. https://doi.org/10.1016/j.bmc.2021.116349.

(18) Whittington, C.; Latham, J.; Offenbacher, A. R. Tunneling through the Barriers: Resolving the Origins of the Activation of C-H Bonds Catalyzed by Enzymes. *ACS Symp. Ser.* **2020**, *1357* (January 2020), 139–160. https://doi.org/10.1021/bk-2020-1357.ch007.

(19) Kobe, M. J.; Neau, D. B.; Mitchell, C. E.; Bartlett, S. G.; Newcomer, M. E. The Structure of Human 15-Lipoxygenase-2 with a Substrate Mimic. *J. Biol. Chem.* **2014**. https://doi.org/10.1074/jbc.M113.543777.

(20) Offenbacher, A. R.; Hu, S.; Poss, E. M.; Carr, C. A. M.; Scouras, A. D.; Prigozhin, D. M.; Iavarone, A. T.; Palla, A.; Alber, T.; Fraser, J. S.; et al. Hydrogen-Deuterium Exchange of Lipoxygenase Uncovers a Relationship between Distal, Solvent Exposed Protein Motions and the Thermal Activation Barrier for Catalytic Proton-Coupled Electron Tunneling. ACS Cent. Sci. 2017, 3 (6). https://doi.org/10.1021/acscentsci.7b00142.

CHAPTER 3

INVESTIGATIONS INTO THE THERMAL ACTIVATION NETWORK OF HUMAN 15-LIPOXYGENASE-2

Introduction

Enzymes function as some of the most powerful catalysts in nature, performing many different reactions to convert substrates into the necessary products and releasing those products back into the solvent. An enzyme's structure and active site play a role in helping to make it a proficient catalyst, along with its range of motions. Enzymes are dynamic structures, which promotes sufficient donor-acceptor distances (DAD) and geometries for catalysis.[1] This allows for the residues of the active site to communicate through the enzyme, as well as position the substrate within the active site for the desired reaction to occur. Protein motions are recognized to play an important role in substrate binding, allosteric regulation, and product release.[2] These actions taken on by the enzyme help to lower the thermal activation reaction barrier and achieve rate enhancement.[1] However, enzymatic reactions still exhibit non-zero activation energy barriers (ie. $E_a > 0$) and the physical origins of this activation barrier remain enigmatic.

While local conformations play a role in the chemistry at the active site, global motions also play a role by supporting the structure for a model active site. This local to global communication occurs in the form of heat transfer through the residues of the enzyme. The importance of protein dynamics is highlighted in enzymes that catalyze C-H bond cleavage, or C-H activation.[3] In the case of enzymatic C-H activation, the temperature independent primary KIE ($^{D}k_{cat}$) is very large and the temperature dependent kinetic isotope effect ($\Delta E_a = E_a(D)-E_a(H)$) value is equal to zero, which indicates that tunneling is occurring.[2] The tunneling mechanism implies that the reaction is proceeding through the barrier, in which the hydrogen transfer occurs as a wave.

This process is inherently temperature independent. The observation of an $E_a > 0$ for enzymatic tunneling reactions underscores the importance of the protein (and its thermally-driven dynamics) in modulating the reaction barriers for catalysis to occur. This brings the Marcus-like reorganization energy into consideration.

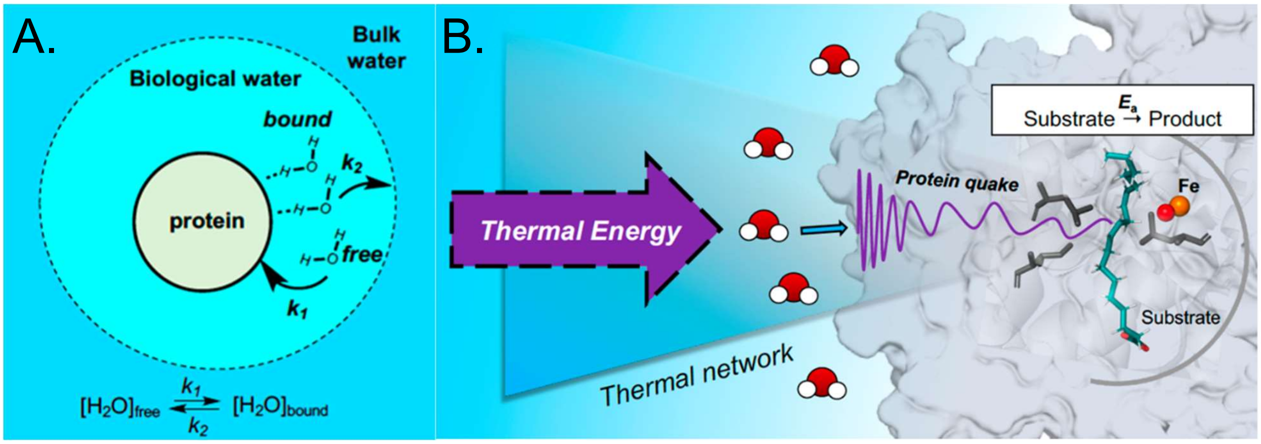
A.
Bulk water
Biological water
bound
protein
k_2
free
k_1
$[H_2O]_{free} \underset{k_2}{\overset{k_1}{\rightleftharpoons}} [H_2O]_{bound}$
B.
Substrate $\xrightarrow{E_a}$ Product
Protein quake
Fe
Thermal Energy
Substrate
Thermal network

Figure 3.1. *(A) Water layers surrounding the protein in which the thermal energy originates from. (B) Representation of the protein motions induced by thermal energy transfer from the surface of the protein to the active site. Figure reproduced from reference (4).*

This leads to the question of how the enzyme uses its conformational flexibility and thermal motions to optimize its role as a catalyst. The motions that promote catalysis span the enzyme much farther than at just the active site. It has been observed that enzymes transfer thermal energy from the surrounding 'biological' solvent through the enzyme into the active site to promote catalytic bond cleavage events (Figure 3.1.A).[4,5] One such network was previously described for the model LOX orthologue from plants, soybean lipoxygenase (SLO) (Figure 3.1.B).[4,5] This network originates at a solvent-exposed loop, 317-334, and has a defined communication network to the local hydrophobic environment in the active site (Figure 3.2).[5] This solved network has been implicated by time, temperature, mutant dependent hydrogen-deuterium exchange (HDX), time resolved fluorescence Stokes shifts, and room temperature X-ray crystallography.[4,5] These studies demonstrate a direct link between protein thermal motions and the activation barrier for catalysis.

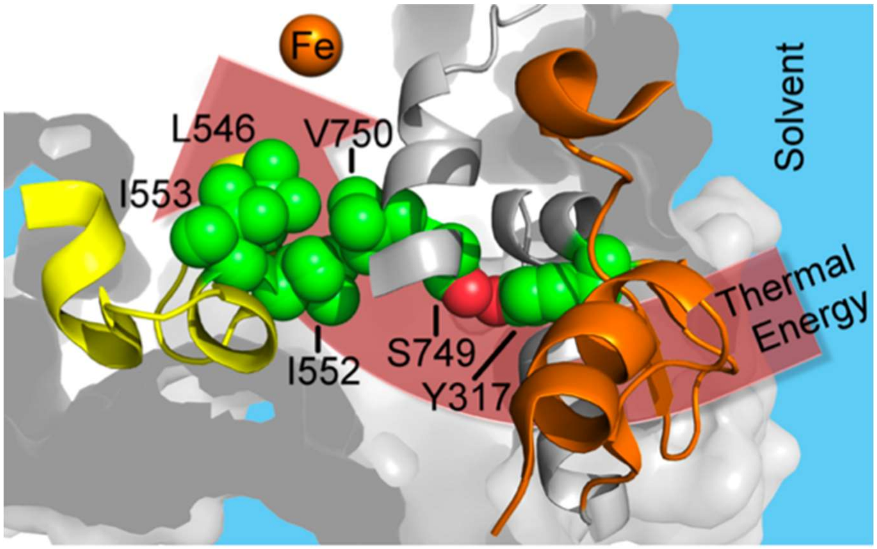

Figure 3.2. *Thermal activation network for SLO. The solvent-exposed loop (orange cartoon) and active site (yellow cartoon) are shown in relation to the residues in the predicted network (green spheres).*

Lipoxygenases (LOXs) are a family of enzymes that span over many organisms, but they all have a low sequence identity between each other. In particular, one of the human 15-lipoxygenases, human epithelial 15-lipoxygenase-2 (15-LOX-2), only has a 28% sequence identity to SLO. Many of the surface loops that are present in SLO are not found in other LOXs, including 15-LOX-2.[1] While these two LOXs are similar in structure, the solvent-exposed thermal activation loop in SLO is not present in 15-LOX-2. Because SLO appears to use this loop to mediate its thermal energy, the transfer of heat through 15-LOX-2 is still in question. 15-LOX-2 appears to have evolved to transfer heat from the solvent to the protein without the loop, but the corresponding network that is relative to that described from the SLO studies has yet to be defined.

Temperature-dependent hydrogen-deuterium exchange (TDHDX-MS) has emerged as a technique to study changes in the flexibility of a protein in relation to changes in time and temperature. These changes can be related to the dynamic motions that are predicted to promote catalysis. This technique has previously been used to study the altered patterns of flexibility due to active site mutations in the enzyme.[5] By determining the differences in flexibility caused by the addition of an active site mutation(s), we can map out the regions of global protein motions that are related to catalysis. Thermal activation networks for adenosine deaminase, enolase, and a family of prokaryotic alcohol dehydrogenases, as well as SLO, have all been identified using the TDHDX-MS approach.[5–7] With each of these enzymes, a single mutation, in which a large hydrophobic residue was mutated to a volume-reducing aliphatic residue (i.e. alanine), was chosen from a location of importance, such as the active site or site of conservation and compared to the wild-type (WT) enzyme to reveal significant regions to catalysis. These cases show the relationship between the active site and the global conformations from the rest of the protein.

Within this chapter we attempt to provide further support for the origins of catalysis and, more specifically, explain the evolution of LOX catalysis by determining the protein motions that are relevant to 15-LOX-2 catalysis. By investigating the thermal activation network of 15-LOX-2, we hope to expand our knowledge of the relationship between enzyme structure and protein dynamics and origins of the empirical E_a in hopes of better understanding enzyme catalysis.

Materials and Methods

Materials

AA and DHA were purchased from Cayman Chemical Company (Ann Arbor, MI) while LA was purchased from Acros Organic, TCI (Palo Alto, CA). Deuterium oxide (D_2O, 99% D), NaOD (99% D), and DCl (99% D) were purchased from Cambridge Isotopes (Tewksbury, MA). Di-deuterated linoleic acid (11,11-D_2-LA) was synthesized as previously described.[8] All bacterial cells, media, salts, and buffers were purchased from Fisher Scientific, Sigma-Aldrich, or VWR at the highest grade available.

Expression and Purification of WT and Variant 15-LOX-2

Wild type and variant 15-LOX-2 encoded in the pET Duet-1 plasmid were transformed into *E.coli* Rosetta 2 cells for protein expression. The cells were transferred into an ampicillin-containing LB media and allowed to shake at 37°C overnight. This overnight starter culture was incubated in large scale (1 L) 2xYT media and ampicillin and expressed using the leaky T7 promoter by incubation at 18°C overnight once the optical density, OD_{600}, reached ~1.0. The cells were harvested in 200 mL fractions in 5-minute intervals at 10000 g and flash frozen in liquid nitrogen until further use. The protein was purified as described, using a Ni-NTA column to capture the His-tagged protein.[9] The cell pellet was resuspended in lysis buffer (50 mM $NaPO_4$, 100 mM NaCl, pH 7.9, 8% glycerol, and 2 mM magnesium sulfate supplemented with lysozyme, DNAse I, and AEBSF) before lysis was performed by sonication. The lysed cells were then centrifuged at 18000 g for 25 minutes. The protein was purified over a linear gradient from buffer A (20 mM Tris-HCl, 20 mM imidazole, 500 mM NaCl, pH 8.0) to buffer B (20 mM Tris-HCl, 200 mM imidazole, 500 mM NaCl, pH 8.0) using a NiNTA column. The presence of protein was confirmed using UV-Vis spectroscopy (280 nm) and SDS-PAGE. The protein was further purified using size exclusion chromatography (SEC) with a Superdex™ 200 increase 10/300 GL column on an ÄKTA™ Prime fast-protein liquid chromatography (FPLC). The protein was eluted with the storage buffer (25 mM Tris, 150 mM NaCl, pH 7.5). Pure protein was flash frozen in liquid nitrogen and stored at -80°C until needed. Typical yields were 20-30 mg/L.

Circular Dichroism (CD) Spectroscopy

The structure of wild-type and variant 15-LOX-2 was assessed using a Jasco model J-815 CD spectrometer at room temperature with bandwidths of 2 nm and with a Starna cell (pathlength of 0.1 cm). The samples were diluted to about 3 μM using 25 mM potassium phosphate, pH 7.0, so that the PMT high voltage (HT) remained ≤ 600V in the range of 190-260 nm. Samples were recorded at 25°C. Measurements for thermal stability of wild-type and variant 15-LOX-2 were carried out at a wavelength of 222 nm over the temperature range of 25-90°C (2°C intervals) with a temperature ramp up rate of 0.6°C/min.

Differential Scanning Calorimetry (DSC)

A NanoDSC microcalorimeter from TA Instruments was used to determine the thermodynamics for the stability of wild-type and variant 15-LOX-2. Protein samples were diluted to be about 30 μM using 25 mM Tris, 150 mM NaCl, pH 7.5. The system was pressurized up to 3 atm and the run was started when the heat was below 75 μW. The temperature range for the run was 30°C-90°C. The raw data was analyzed using NanoAnalyze software from TA instruments. The data was converted to the molar heat capacity using the molecular weight of the protein, the volume of the sample cell, and the concentration (mg/mL). The baseline was integrated using a 4th order polynomial to get a melting temperature (T_m) and ΔH. After integrating the baseline, the data was fit to the Gaussian model.

Temperature Dependent Steady-State Kinetic Measurements

A UV1800 Shimadzu UV-Vis spectrophotometer was used for steady-state kinetic analysis. The enzyme and substrate concentrations were determined enzymatically before being used in the reaction. The reactions were run in 50 mM Hepes buffer, 150 mM NaCl, pH 7.5 at various temperatures (15°C-40°C) over the specified substrate concentrations (5-6 concentrations for each temperature) ranging from 2 μM to 25 μM to ensure that k_{cat} had been reached. The total reaction volume was 1.0 mL, except for reactions with dLA, which had a total reaction volume of 200 μL. The enzyme concentration varied for each enzyme-substrate combination, ranging from 10 μM-30 μM. Each substrate concentration at each temperature was collected and averaged through 3 replicates and reported as the mean ± s.e.m. The substrates used for the substrate proficiency studies were AA, DHA, and LA, but the preferred substrate, AA, was used for the mutant studies.

For isotope effects with dLA, the observed lag phase in the steady-state kinetic traces were too slow to monitor kinetics. Thus, WT 15-LOX-2 was pre-activated to the Fe(III) state using protio substrate and then exchanged with a PD10 column to remove excess substrate and product prior to kinetic analysis. The Fe(III) state of 15-LOX-2 was confirmed by the formation of a 330 nm broad feature in the spectrum and a loss of the kinetic lag phase. Due to the lack of access to deuterated DHA or AA, LA and dLA were used to study the kinetic isotope effects. All kinetic measurements were completed in triplicates. The rates at each substrate concentration were collected and fit to the Michaelis-Menten equation using Igor Pro to calculate the first order (k_{cat}) and second order (k_{cat}/K_M) rate constants. The temperature dependence (E_a) was determined through linear fits of Arrhenius plots.

Hydrogen-Deuterium Exchange (HDX) Sample Preparation

HDX samples were prepared as previously described.[5] Aliquots of 110 μM wild-type, V427L, and V426A 15-LOX-2 stocks were incubated at the desired temperatures (10, 20, 30, 40°C) for 30-60 seconds before diluting 10-fold in D_2O buffer (10 mM Hepes, 250 mM NaCl, pD 7.47). The samples were incubated for 9 time points (10, 20, 45, 60, 180, 600, 1800, 3600, 7200 seconds) for each enzyme and at each temperature. After incubation for the desired time, the samples were cold-quenched (-20°C) and then acid-quenched (to pH 2.4 with 0.32 M citric acid stock solution and 19.6 mM DTT at 0°C) to minimize back-exchange. Guanidine HCl (in citric acid, pH 2.4) was added to the sample to a final concentration of 0.5 M to get the best sequence coverage. Samples were digested with immobilized pepsin for 2.5 minutes. The pepsin was filtered through centrifugation at 7000 g for 10 seconds before being flash-frozen in liquid nitrogen. Samples were stored at -80°C until data collection. The time points were randomly collected over two days for each temperature and mutant to reduce error. The software HDX WorkBench was used to analyze MS data.

Crystallization of 15-LOX-2 V427L

Crystallization screening conditions were followed as previously described.[9] Crystals were grown in sitting drop trays. The conditions that yielded the crystal for diffraction were 16 mM C8E4, 0.7 M NH_4SO_4, 0.1 M Bis-Tris, pH 5.5, 2.5% glycerol at 22°C. Diffraction data was collected at Argonne National Laboratory to a resolution of 2.34 Å. The program, Phenix, was used to analyze the diffraction data. The programs Xtriage, molecular replacement, and Phenix refine were used within the Phenix program. Coot was used to further refine and build the model. This model was compared against the WT 15-LOX-2 model (PDB 4NRE).

Results and Discussion

Protein Expression and Purification

WT 15-LOX-2 and variants were expressed and purified with yields of 20-30 mg/L. An SDS-PAGE was run to determine the presence and purity of protein. The singular band, as well as the migration pattern indicate that the protein is present and has been purified. The 15-LOX-2 variants have the same migration pattern as WT 15-LOX-2, indicating no post-translational modifications (Figure 3.3A). CD and DSC traces were used to determine the thermostability of 15-LOX-2 and the variants. The CD traces show that the secondary structure of WT 15-LOX-2 and the variants are mostly alpha helical with similar T_m values (Figure 3.3B). The DSC traces also showed similar T_m values, which further confirmed the stability between WT 15-LOX-2 and the desired active site variants (Figure 3.3C). The T_m values from DSC are greater than those collected through CD due to the addition of salt that helped to stabilize the proteins.

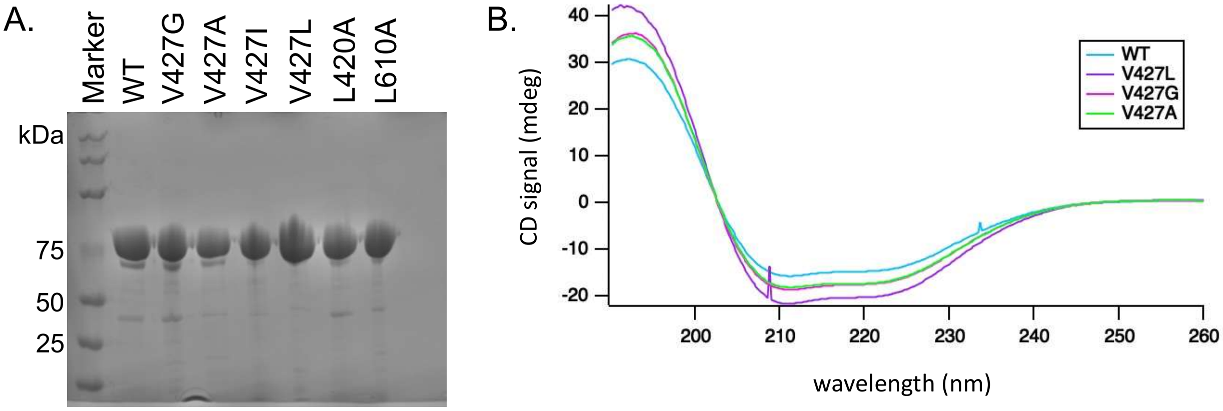

C.

Enzyme Variant	T_m from CD (°C)	T_m from DSC (°C)
WT	51.94	57.08
V426A	-	57.03
V427L	52.95	57.55
V427A	48.43	53.53
V427G	44.05	49.12

Figure 3.3. *Confirmation of protein purification and stability. (A) SDS-PAGE of WT 15-LOX-2 and mutants shows a similar migration pattern for all of the proteins. (B) CD traces of 15-LOX-2 confirms the secondary structure of WT and mutants. (C) Comparison of* T_m *between CD and DSC confirm the stability of each of the proteins.*

Determining the Catalytic Parameters of WT 15-LOX-2 and Variants

The thermal activation network was probed by mutations in the active site. Mutations were chosen based on the proximity of the residue to the substrate, as well as the equivalent active site residues that were previously studied in SLO (Figure 3.4). The chosen hydrophobic residues also played a role in the packing of the active site. By changing the side chain volume of the residues within the active site, the substrate pocket becomes less densely packed, allowing for the substrate to take on a conformation that is not optimal for C-H activation. Mutations of L420A and L620A significantly decreased the k_{cat} of the enzyme and almost entirely killing its activity (Table 3.1). The E_a increased for these two residues as well, with L420A showing a modest increase (E_a = 8.7 ± 1.2 kcal/mol) and L610A showing a much larger increase (E_a = 16.4 ± 0.9 kcal/mol) than WT (Table 3.1). This was expected due to their role in the positioning of the substrate with respect to the catalytic metal, Fe. This impairment within the active site was also shown for SLO through a mutation of equivalent leucine residues (SLO L546A = 15-LOX-2 L420A; SLO L754A = 15-LOX-2 L610A). In SLO, mutating these residues to alanine causes a large decrease in the activity and a large increase in the E_a, from 2 kcal/mol in WT to ~4 kcal/mol in each mutant.[5,10]

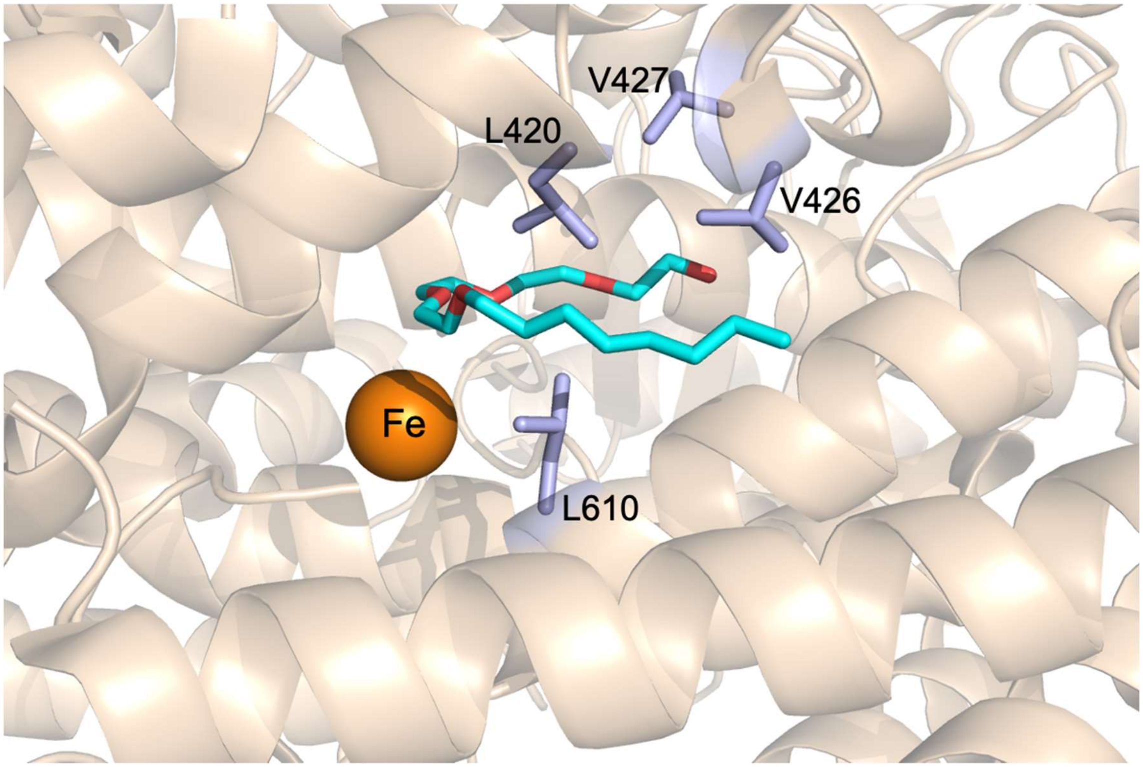

Figure 3.4. *Hydrophobic active site residues of 15-LOX-2 to be studied. The catalytic iron is shown in orange and the substrate mimic, C8E4, is shown in cyan with the residues of interest highlighted in light blue sticks.*

Table 3.1. *Catalytic Parameters for WT 15-LOX-2 and Selected Variants.*[a]

	$k_{cat}{}^{a}$ (s^{-1})	% Decrease from WT	$k_{cat}/K_M{}^{a}$ ($\mu M^{-1}s^{-1}$)	E_a (kcal/mol)
WT	0.93 (0.04)	---	0.29 (0.04)	6.8 (0.2)
L420A	0.012 (0.002)	78	0.00057 (0.00024)	8.7 (1.2)
V426A	0.145 (0.005)	6.4	0.10 (0.02)	11.7 (0.4)
V427L	0.162 (0.008)	5.7	0.13 (0.03)	16.7 (1.6)
V427I	0.67 (0.01)	1.4	0.22 (0.015)	7.5 (0.5)
V427A	0.531 (0.006)	1.75	0.74 (0.07)	8.0 (0.2)
V427G	0.319 (0.007)	2.9	0.39 (0.05)	11.3 (0.3)
L610A	0.072 (0.006)	12.9	0.31 (0.51)	16.4 (0.9)
DM	0.67 (0.03)	1.4	0.079 (0.010)	7.2 (0.3)

[a]The data is averaged from 3 replicates and reported as the mean ± s.e.m. The reactions were run in the prepared buffer with 50 mM Hepes, 150 mM NaCl, pH 7.5 at 25°C with AA.

Residues V426 and V427, which are equivalent to I552 and I553 in SLO, respectively, were also mutated to other hydrophobic residues to impact the packing in the active site. In the evolution of LOXs, the isoleucine residues that are observed in these positions in SLO have become a smaller hydrophobic residue in human 15-LOX-2, which creates a different pattern of packing in the active site for 15-LOX-2 than with SLO. Mutations at V426 and V427 both showed a decrease in activity and increase in E_a (Table 3.1). Residue I553 was studied over a range of side chain volumes in SLO. Previous KIE studies with SLO suggested that mutations at I553 would have a more distinct temperature dependence, therefore we chose to focus on V427 over a range of side chain volumes, as well.[1,5] When comparing hydrophobic residues, valine (WT 15-LOX-2 variant) lands in the middle when it comes to side chain bulk, so we were able to study residues that were both smaller and larger. Mutating to smaller residues would potentially increase DADs within the residues and the substrate while mutating to larger residues would disrupt the specific hydrophobic packing within the active site.[1] In both cases, the communication between the enzyme and the substrate would be disrupted enough to change the catalytic parameters, but the distinction would be between the magnitude of change for each mutation.

V427A showed very modest changes in k_{cat} and E_a compared to WT. Completely taking away the side chain bulk only has a 2.9-fold decrease in k_{cat} from the WT enzyme (Table 3.1). This trend is different than what was observed with SLO, in which the greatest changes to the catalytic parameters were observed with I553G. While leucine and isoleucine have the same side chain volume, the greatest decrease was observed through V427L. This mutant has the smallest k_{cat} value ($0.162 \pm 0.008\ \mathrm{s}^{-1}$) of the V427 series and the largest E_a value (16.7 ± 1.6 kcal/mol).

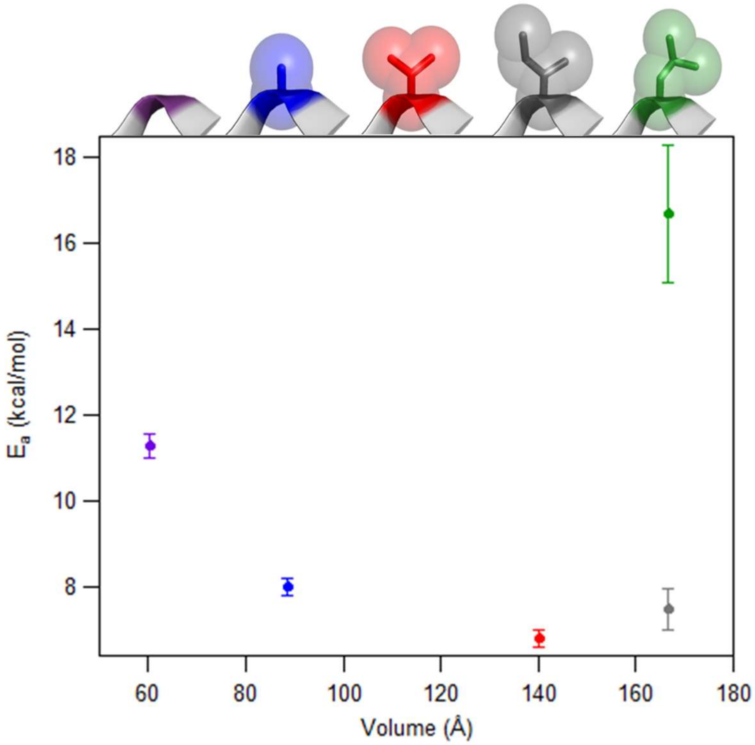

Figure 3.5. *E_a analysis of V427X series over a range of side chain volumes shows a unique non-linear pattern for this residue. The E_a values for each mutant were extrapolated from the linear fits of the Arrhenius plots created through the steady-state kinetic data collected in Table 3.1.*

The difference in catalytic parameters with these residues shows a trend that is unique from that observed in SLO, enolase, and adenine deaminase. In these other proteins, as the side chain volume of the chosen residue increases, so does the E_a. But for residue 427 of 15-LOX-2, as the side chain volume becomes smaller or larger, the E_a increases, with the optimal side chain volume being 140Å, or a valine residue. This creates a V-shaped curve, rather than a linear relationship (Figure 3.5).

V426A, the adjacent residue to V427, showed a 6.4-fold decrease in activity and almost double the E_a value (Table 3.1). These observed changes to the catalytic parameters of V426A were greater than expected, with the catalytic parameters for this residue equivalent not being an emphasized residue in SLO. V426A showed a decrease in k_{cat} (0.145 ± 0.005 s^{-1}) that was similar to the catalytic efficiency of V427L (Table 3.1). Even though the k_{cat} value mirrored that of V427L, the E_a value was not quite as large as the V427L mutant. The E_a of this mutant is higher than the mutation at the V427 position with the same side chain volume (V427A), which would signify the role of this residue in the hydrophobic packing of the active site and the catalysis of 15-LOX-2. Importantly, both V426A and V427L retained comparable protein folding stabilities (T_m and ΔH), whereas smaller volume V427 variants exhibited systematic decreases in their folding stabilities (Figure 3.3C).

The conservation of residues within the active site is similar, but not identical, to all LOXs. While there are some similarities, like the leucine residues at positions 420 and 610 in 15-LOX-2, there are also differences between organisms that have changed the hydrophobic active site packing. But the changes to smaller valine residues at positions 426 and 427 in 15-LOX-2 from larger isoleucine residues in SLO have proven that they are the optimal size for the active site of 15-LOX-2. The compaction that is required in the active site to transfer thermal energy for catalysis is specific for each enzyme. But these mutations can further be used to reveal more about the communication between the local and global environment of the protein.

Kinetic Isotope Effects (KIE) for 15-LOX-2 Variants Remains Unresolved

Determining KIEs for 15-LOX-2 and its variants proved to be more difficult than expected because the only available deuterated substrate is LA, which is a very poor substrate for 15-LOX-2. The latter is validated by the reduced k_{cat} and elevated E_a values for the LA reaction relative to the AA and DHA reactions with 15-LOX-2 (Table 3.2). KIEs were determined for WT and V427A, but the combination of a poor enzyme and a poor substrate made it too difficult to acquire an accurate KIE for V427L (Table 3.3). The ΔE_a value, which represents the temperature dependence of the KIE, shows that both WT and V427A are non-zero, signifying that they are temperature dependent (Table 3.3). While the difference between ΔE_a is small, the value for V427A is slightly larger than WT 15-LOX-2. More KIE data needs to be collected, especially for the mutants of interest from the kinetic analysis (V426A and V427L).

Table 3.2. *Catalytic Parameters for 15-LOX-2 with Various Substrates*

	k_{cat}^{a} (s^{-1})	k_{cat}/K_M^{a} ($\mu M^{-1}s^{-1}$)	E_a (kcal/mol)
AA	0.93 (0.04)	0.29 (0.04)	6.8 (0.2)
DHA	1.1 (0.02)	0.72 (0.07)	7.6 (0.3)
LA	0.18 (0.007)	0.79 (0.57)	12.6 (0.9)

[a]The data is averaged from 3 replicates and reported as the mean ± s.e.m. The reactions were run in the prepared buffer with 50 mM Hepes, 150 mM NaCl, pH 7.5 at 25°C.

Table 3.3. *KIE of 15-LOX-2 and Selected V427 Series Mutants*

	k_{cat}^{a} (s^{-1})	E_a (kcal/mol)	$^{D}k_{cat}^{a}$ (s^{-1})	ΔE_a
WT	0.18 (0.007)	12.6 (0.9)	0.001 (0.0002)	3.6 (0.7)
V427A	0.10 (0.004)	11.9 (0.6)	0.0006 (0.00008)	5.8 (1.7)
V427L	0.06 (0.002)	14.6 (0.6)	-	-

[a]The data is averaged from 3 replicates and reported as the mean ± s.e.m. The reactions were run in the prepared buffer with 50 mM Hepes, 150 mM NaCl, pH 7.5 at 25°C with LA/(11,11-D_2) LA.

Temperature-Dependent Hydrogen Deuterium Exchange Mass Spectrometry (TDHDX-MS) Isolates Regional Changes in Flexibility

Using the same peptide list for 15-LOX-2 from Chapter 2, TDHDX-MS was used to compare WT 15-LOX-2 and the two variants of interest, V426A and V427L. Using TDHDX-MS allows for the comparison of the changes in the protein's flexibility in relation to mutagenesis. The temperatures studied for WT and the mutant 15-LOX-2 proteins include: 10, 20, 30, and 40°C. Note that the highest temperature is at least 10°C below the T_m of these protein variants. From the complete list of peptides (see Appendix A), peptides 193-206 (yellow) and 301-316 (pink) show an altered E_a of HDX upon mutation (Figure 3.6). In peptide 193-206, only V427L shows an altered E_a while V426A mirrors the E_a of WT. For peptide 301-316, a different E_a is shown for each variant, with V427L showing a modest change and V426A showing a larger shift in E_a. Peptide 419-441 (black) shows an increase in the extent of exchange over the site of the mutation (Figure 3.6). This peptide is only present in WT 15-LOX-2 and the V426A variant, but just between these two proteins, there is a notable difference brought upon by this hydrophobic mutation. Together, these sites of changes in flexibility point out a specific region of 15-LOX-2 that changes due to various active site mutations. Changes at peptide 419-441 indicate a local change in dynamics within the active site and around the site of the mutation. But changes observed in additional peptides in 15-LOX-2 indicate a global change throughout the protein as result of the mutation in the active site. There is also a subtle change in extent over peptide 590-602, but this peptide does not fit into the regional flexibility observed throughout the rest of 15-LOX-2. This brings into question the significance of this peptide upon mutations to the active site and its disruption to the hydrophobic packing.

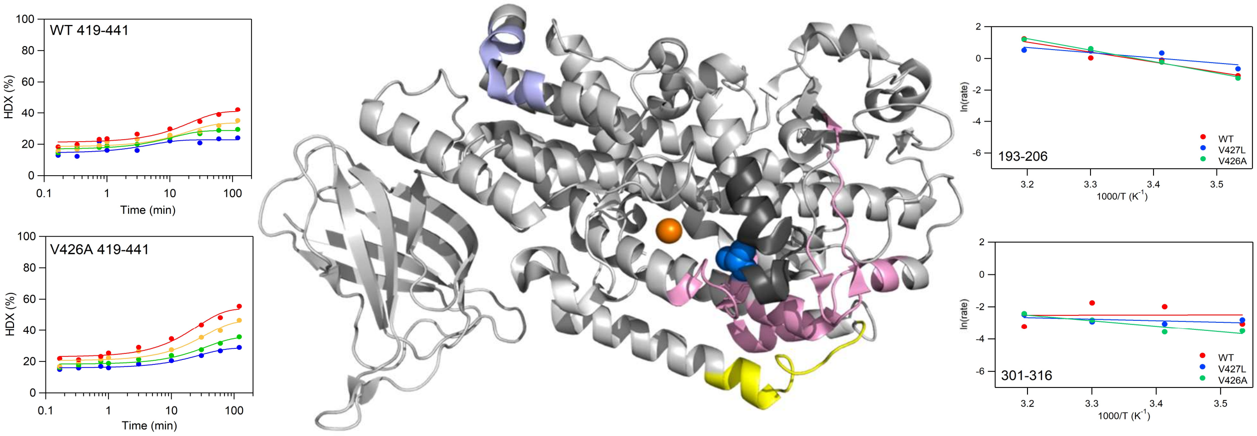

Figure 3.6. *Peptides of significance as shown by TDHDX-MS when WT 15-LOX-2 is compared to V426A and V427L.*

Solving the Crystal Structure of 15-LOX-2 V427L Suggests Influences for Significantly Altered E_a

The crystal structure of 15-LOX-2 V427L was solved to determine if there were any differences within the active site residues or with the substrate positioning upon mutation that would correspond to the greatly enlarged E_a value. The V427L mutant was crystallized and diffracted to 2.34 Å resolution, in collaboration with Dr. Nathan Gilbert (Louisiana State University). It is apparent that this mutant was expressed and crystallized, due to an additional electron density at the 427 position when compared to the X-ray structure of WT 15-LOX-2. The two X-ray structures are almost superimposable, with a nearly identical overlay (RMSD = 2.886) (Figure 3.7A). When looking more closely at the active site, subtle changes are observed with the substrate mimic, C8E4 (Figure 3.7B). The additional side chain volume at V427L also causes a notable rotamer shift at L420, which is an essential residue for the positioning of the substrate (Figure 3.7C). These two changes can help to explain, in part, the significantly altered E_a value that was observed for V427L, relative to WT. These data also support how optimal hydrophobic packing within the active site of 15- LOX-2 is important for enzyme proficiency. With the additional steric bulk in the active site, even the most subtle of changes to occur can significantly alter the thermal activation barrier of the enzyme.

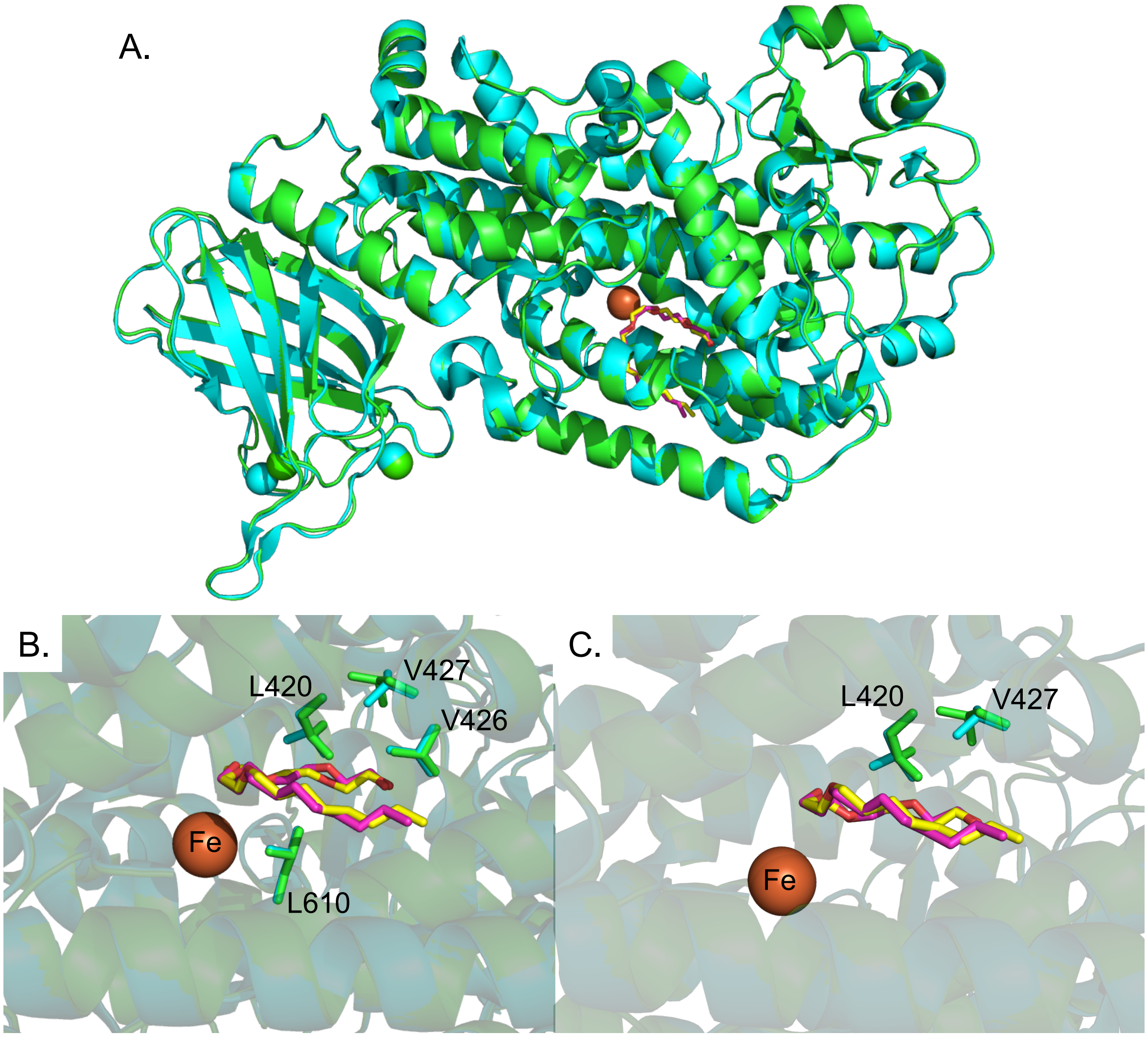

Figure 3.7. *X-ray crystal structure of 15-LOX-2 V427L mutant (green cartoon) overlay with WT 15-LOX-2 (cyan cartoon). (A) shows the identical overlay over the whole protein with the non-heme iron (orange sphere) appearing nearly identical, as well, and the substrate mimic (yellow sticks for WT and magenta sticks for V427L) showing subtle changes. (B) shows the active site of WT 15-LOX-2 and V427L mutant with all of the active site residues present while (C) highlights the site of mutation and L420, which shows a rotamer shift.*

Probing the Solvent Interactions Through Viscosity-Dependence Studies

To further understand the involvement of solvent interactions towards the origins of the E_a of the enzyme’s reaction, we studied the viscosity-dependence of the solvent on kinetic parameters.

This was accomplished by adding the disaccharide, trehalose, at varying concentrations. Trehalose is known to order water, causing perturbed dynamics of the bulk water. From the kinetic analysis, the activation energies (E_a) for the reaction of 15-LOX-2 with AA were seen to increase significantly with trehalose in a dose-dependent fashion, for both pH 7.5 and pH 8.5 (Figure 3.8A) Next, we investigated the dependence on k_{cat}/K_M, which could help us determine if substrate capture is rate-determining. The k_{cat}/K_M values were nearly independent on trehalose, supporting that substrate binding/capture is not rate-limiting in the reaction (Figure 3.8B). Surprisingly, the k_{cat} values were seen to decrease upon the addition of trehalose for pH 7.5 at all temperatures and pH 8.5 at 10°C, but not for pH 8.5 at 25°C (Figure 3.8C). At pH 8.5 and 25°C, the k_{cat} stayed relatively stable; this could be attributed to a change in the rate-determining step(s).

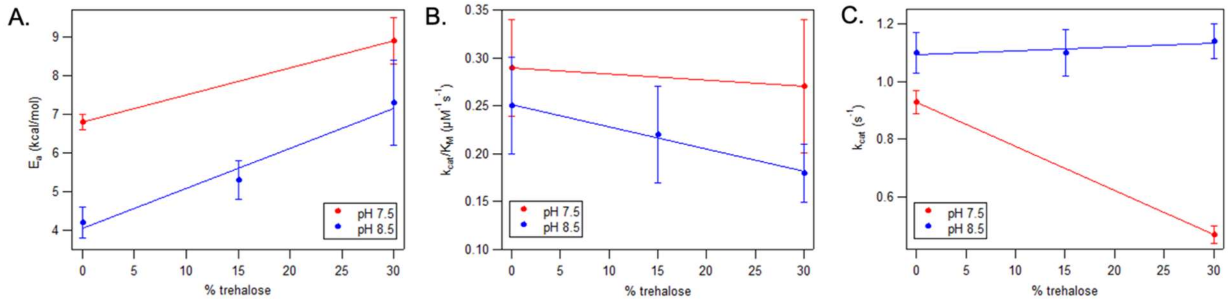

Figure 3.8. *Trehalose effects on the catalytic parameters of 15-LOX-2. Steady-state kinetics were performed in 50 mM Hepes, 150 mM NaCl, pH 7.5 and pH 8.5 with 0%, 15% and 30% w/v trehalose at 25°C with AA. The data was averaged from 3 replicates and reported as the mean ± s.e.m.*

The viscosity dependence observed for k_{cat} and E_a probes the role that the solvent plays in the protein motions of the enzyme. The effect observed on the catalytic parameters of 15-LOX-2 with the increase in viscosity suggests that there are solvent-slaved motions involved in the thermal activation of the enzyme. The observed decrease in k_{cat} with increasing viscosity suggests that under these conditions, there is an internal reorganization/isomerization of the ES complex to a catalytically productive ES' complex, which attributes the thermal activation of the protein to the bulk water. As discussed above, there are two shells of water: the bulk water shell is a secondary solvent shell, with the biological water layer immediately surrounding and reaching the solvent exposed areas of the protein. The viscosity effects reveal that the E_a originates from two levels of motions of 15-LOX-2, with the bulk water controlling the internal isomerization linked to the viscosity dependence on k_{cat}. This behavior contrasts that of SLO, where the k_{cat} and E_a values are intendent of viscosity, but is similar to the motions observed with the hydride tunneling reaction of human glycolate oxidase (hGOX), in which tunneling is thermally activated (not ground state tunneling).[11] With hGOX, similar trends are observed for k_{cat} over a range of solvent viscosities at constant temperature that are attributed to solvent-slaved motions.[11]

Conclusion

The thermal activation network, as well as the optimization of catalysis, of 15-LOX-2 has been probed herein using steady-state kinetics, TDHDX-MS, and X-ray crystallography combined with site-directed mutagenesis. The thermal energy that drives the protein motions for catalysis were also traced using viscosity studies.

Future studies will be aimed at labeling the protein site-selectively with fluorophores to carry out time-resolved experiments in an effort to provide kinetic information regarding the thermal heat transfer in 15-LOX-2. The altered substrate binding will also be further studied by a high-resolution ENDOR technique that was previously developed to study the SLO-LA complex structure.[12] This will allow the subtle shifts within the active site of 15-LOX-2 as a function of mutation to be studied further.

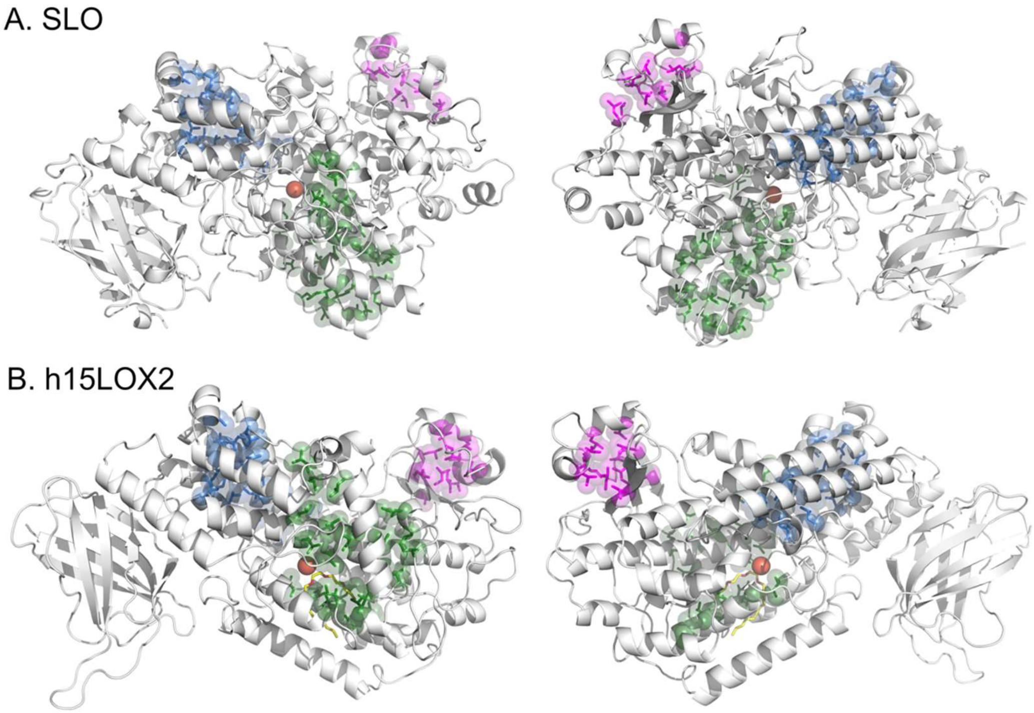

__Figure 3.9.__ Hydrophobic isoleucine-leucine-valine islands present in SLO (A) and 15-LOX-2 (B).

The thermal activation network was initially predicted to lie within one of the isoleucine-leucine-valine (ILV) islands observed within SLO and 15-LOX-2. From our accumulated data, the 15-LOX-2 network is much more confined to the active site than SLO, consistent with this ILV model. Note that the previously identified thermal activation loop, along with the defined thermal activation network for SLO, are all located within the green ILV island (Figure 3.9A). Overall, these studies have shown the importance of active site packing, as well as protein motions, to the origins of the activation barrier for catalysis.

References

(1) Klinman, J. P.; Offenbacher, A. R.; Hu, S. Origins of Enzyme Catalysis: Experimental Findings for C-H Activation, New Models, and Their Relevance to Prevailing Theoretical Constructs. *Journal of the American Chemical Society*. 2017. https://doi.org/10.1021/jacs.7b08418.

(2) Whittington, C.; Latham, J.; Offenbacher, A. R. Tunneling through the Barriers: Resolving the Origins of the Activation of C-H Bonds Catalyzed by Enzymes. *ACS Symp. Ser.* **2020**, *1357* (January 2020), 139–160. https://doi.org/10.1021/bk-2020-1357.ch007.

(3) Klinman, J. P.; Kohen, A. Hydrogen Tunneling Links Protein Dynamics to Enzyme Catalysis. *Annu. Rev. Biochem.* **2013**, *82*, 471–496. https://doi.org/10.1146/annurev-biochem-051710-133623.

(4) Zaragoza, J. P. T.; Nguy, A.; Minnetian, N.; Deng, Z.; Iavarone, A. T.; Offenbacher, A. R.; Klinman, J. P. Detecting and Characterizing the Kinetic Activation of Thermal Networks in Proteins: Thermal Transfer from a Distal, Solvent-Exposed Loop to the Active Site in Soybean Lipoxygenase. *J. Phys. Chem. B* **2019**, *123* (41). https://doi.org/10.1021/acs.jpcb.9b07228.

(5) Offenbacher, A. R.; Hu, S.; Poss, E. M.; Carr, C. A. M.; Scouras, A. D.; Prigozhin, D. M.; Iavarone, A. T.; Palla, A.; Alber, T.; Fraser, J. S.; et al. Hydrogen-Deuterium Exchange of Lipoxygenase Uncovers a Relationship between Distal, Solvent Exposed Protein Motions and the Thermal Activation Barrier for Catalytic Proton-Coupled Electron Tunneling. *ACS Cent. Sci.* **2017**. https://doi.org/10.1021/acscentsci.7b00142.

(6) Gao, S.; Thompson, E. J.; Barrow, S. L.; Zhang, W.; Iavarone, A. T.; Klinman, J. P. Hydrogen-Deuterium Exchange within Adenosine Deaminase, a TIM Barrel Hydrolase,

Identifies Networks for Thermal Activation of Catalysis. *J. Am. Chem. Soc.* **2020**, *142* (47), 19936–19949. https://doi.org/10.1021/jacs.0c07866.

(7) Thompson, E. J.; Paul, A.; Iavarone, A. T.; Klinman, J. P. Identification of Thermal Conduits That Link the Protein-Water Interface to the Active Site Loop and Catalytic Base in Enolase. *J. Am. Chem. Soc.* **2021**, *143* (2). https://doi.org/10.1021/jacs.0c09423.

(8) Offenbacher, A. R.; Zhu, H.; Klinman, J. P. Synthesis of Site-Specifically13C Labeled Linoleic Acids. *Tetrahedron Lett.* **2016**, *57* (41). https://doi.org/10.1016/j.tetlet.2016.08.071.

(9) Kobe, M. J.; Neau, D. B.; Mitchell, C. E.; Bartlett, S. G.; Newcomer, M. E. The Structure of Human 15-Lipoxygenase-2 with a Substrate Mimic. *J. Biol. Chem.* **2014**. https://doi.org/10.1074/jbc.M113.543777.

(10) Hu, S.; Offenbacher, A. R.; Thompson, E. M.; Gee, C. L.; Wilcoxen, J.; Carr, C. A. M.; Prigozhin, D. M.; Yang, V.; Alber, T.; Britt, R. D.; et al. Biophysical Characterization of a Disabled Double Mutant of Soybean Lipoxygenase: The “Undoing” of Precise Substrate Positioning Relative to Metal Cofactor and an Identified Dynamical Network. *J. Am. Chem. Soc.* **2019**. https://doi.org/10.1021/jacs.8b10992.

(11) Romero, E.; Ladani, S. T.; Hamelberg, D.; Gadda, G. Solvent-Slaved Motions in the Hydride Tunneling Reaction Catalyzed by Human Glycolate Oxidase. *ACS Catal.* **2016**, *6* (3), 2113–2120. https://doi.org/10.1021/acscatal.5b02889.

(12) Horitani, M.; Offenbacher, A. R.; Marcus Carr, C. A.; Yu, T.; Hoeke, V.; Cutsail, G. E.; Hammes-Schiffer, S.; Klinman, J. P.; Hoffman, B. M. 13C ENDOR Spectroscopy of Lipoxygenase-Substrate Complexes Reveals the Structural Basis for C-H Activation by Tunneling. *J. Am. Chem. Soc.* **2017**, *139* (5), 1984–1997.

https://doi.org/10.1021/jacs.6b11856.

APPENDIX A

HDX-MS TRACES FOR WT, V427L, V426A 15-LOX-2

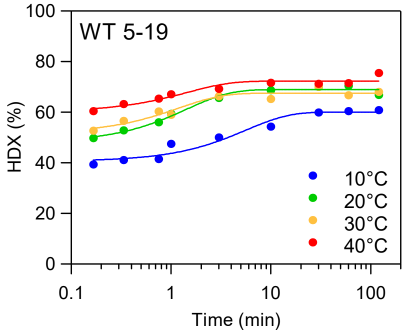

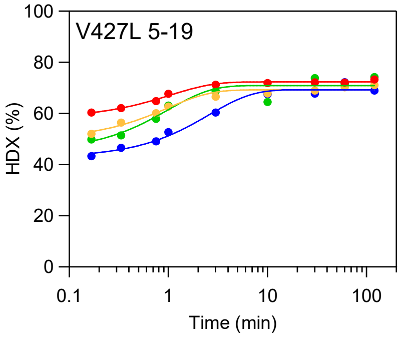

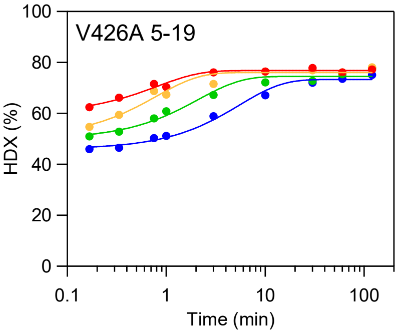

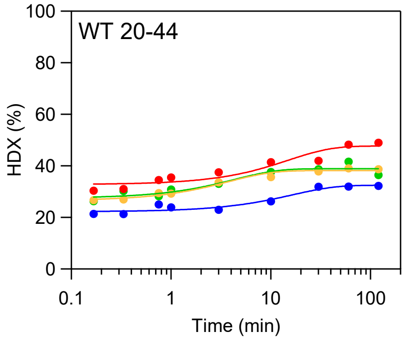

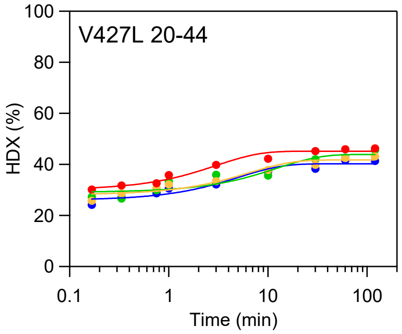

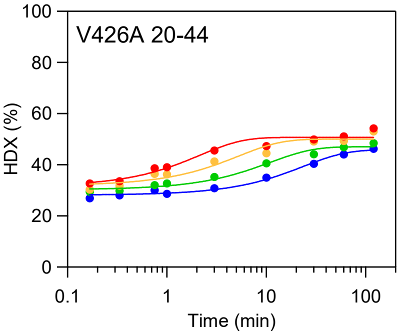

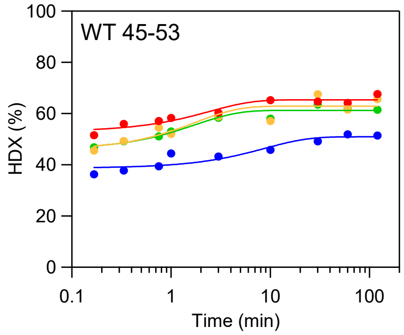

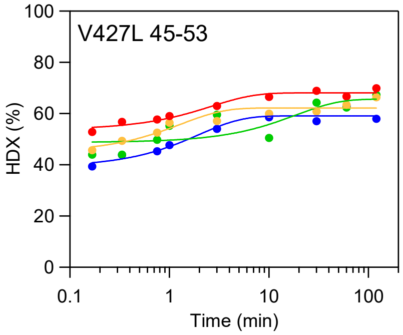

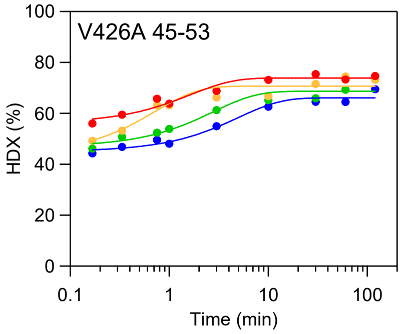

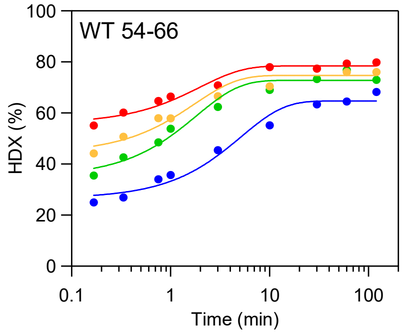

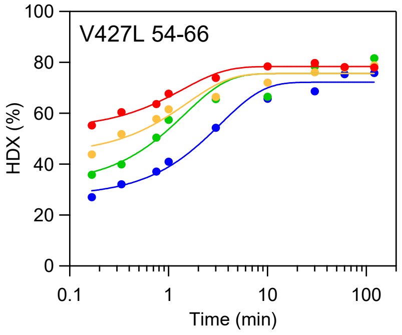

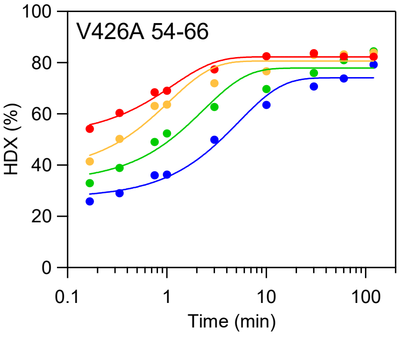

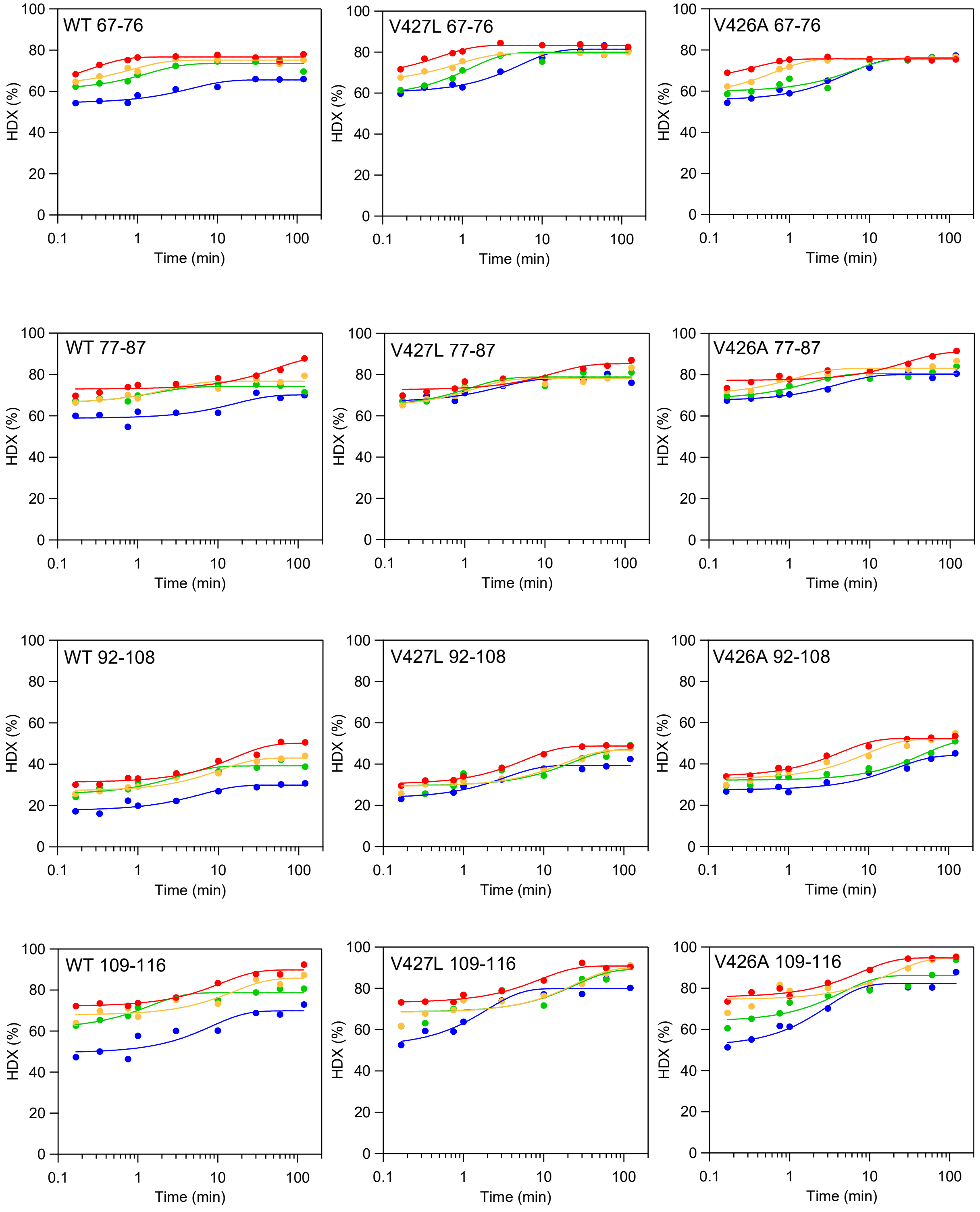
WT 67-76
V427L 67-76
V426A 67-76
WT 77-87
V427L 77-87
V426A 77-87
WT 92-108
V427L 92-108
V426A 92-108
WT 109-116
V427L 109-116
V426A 109-116
HDX (%)
0
20
40
60
80
100
Time (min)
0.1
1
10
100

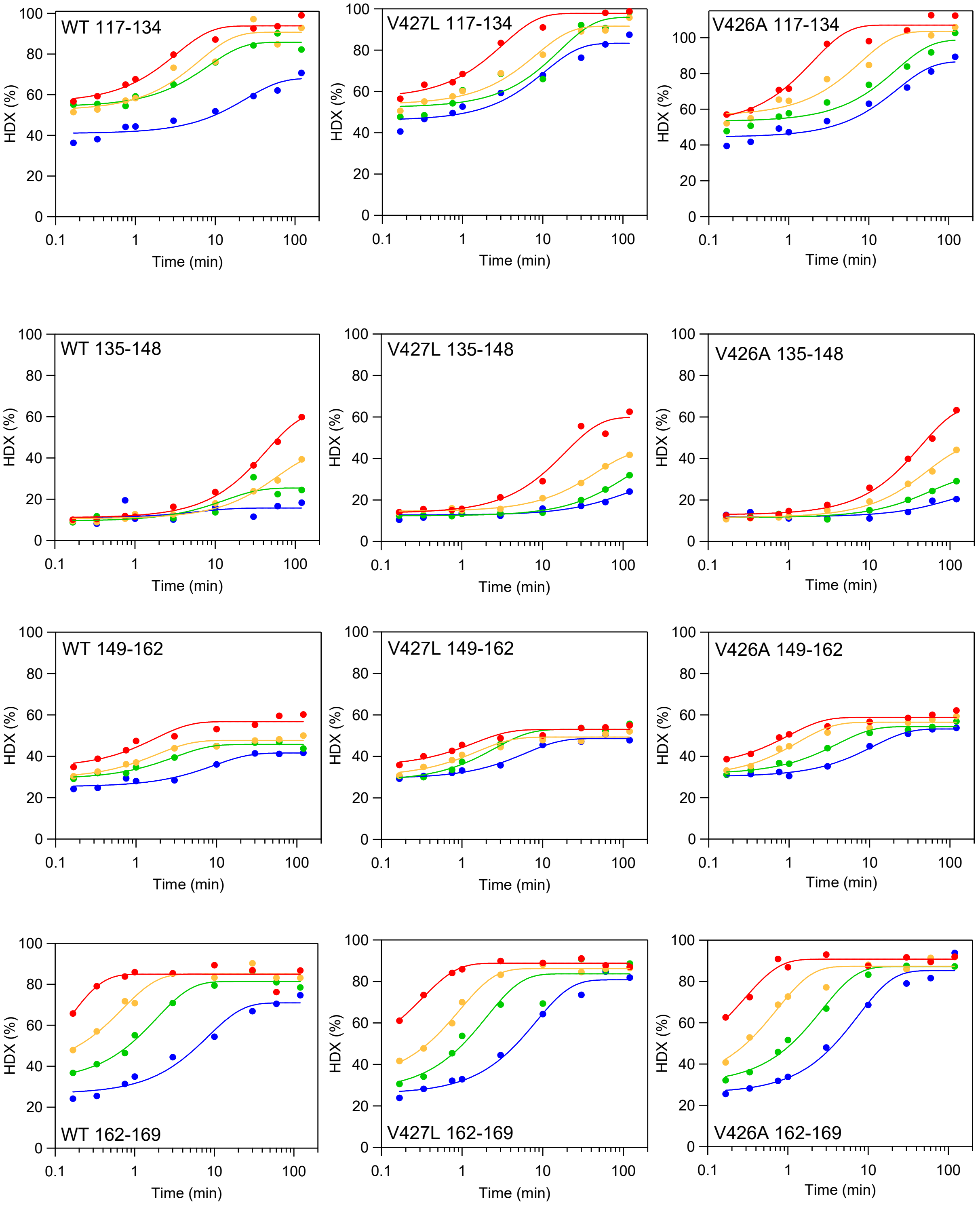
WT 117-134
V427L 117-134
V426A 117-134
WT 135-148
V427L 135-148
V426A 135-148
WT 149-162
V427L 149-162
V426A 149-162
WT 162-169
V427L 162-169
V426A 162-169
HDX (%)
Time (min)
0
20
40
60
80
100
0.1
1
10
100

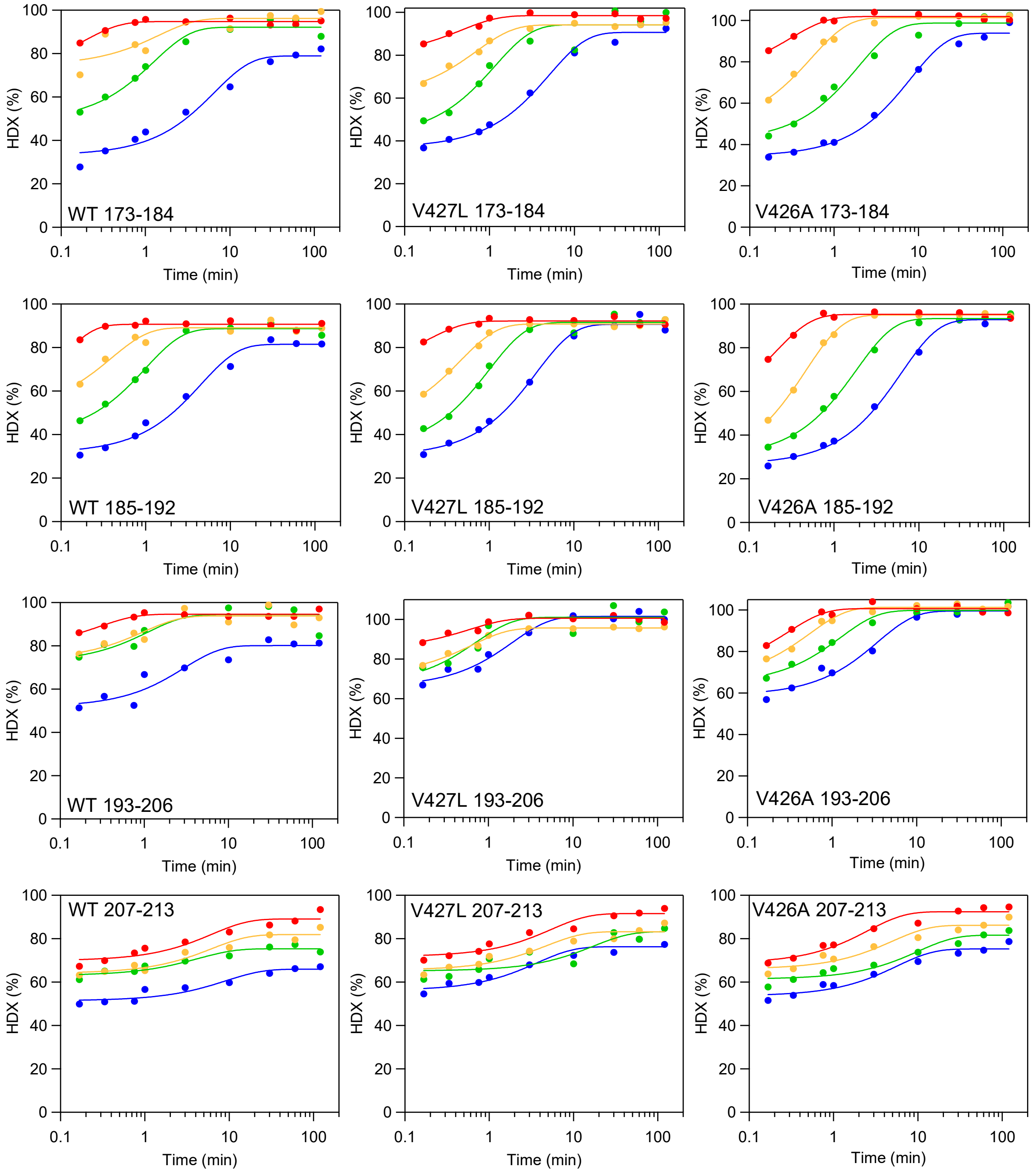
WT 173-184
V427L 173-184
V426A 173-184
WT 185-192
V427L 185-192
V426A 185-192
WT 193-206
V427L 193-206
V426A 193-206
WT 207-213
V427L 207-213
V426A 207-213
HDX (%)
Time (min)
0
20
40
60
80
100
0.1
1
10
100

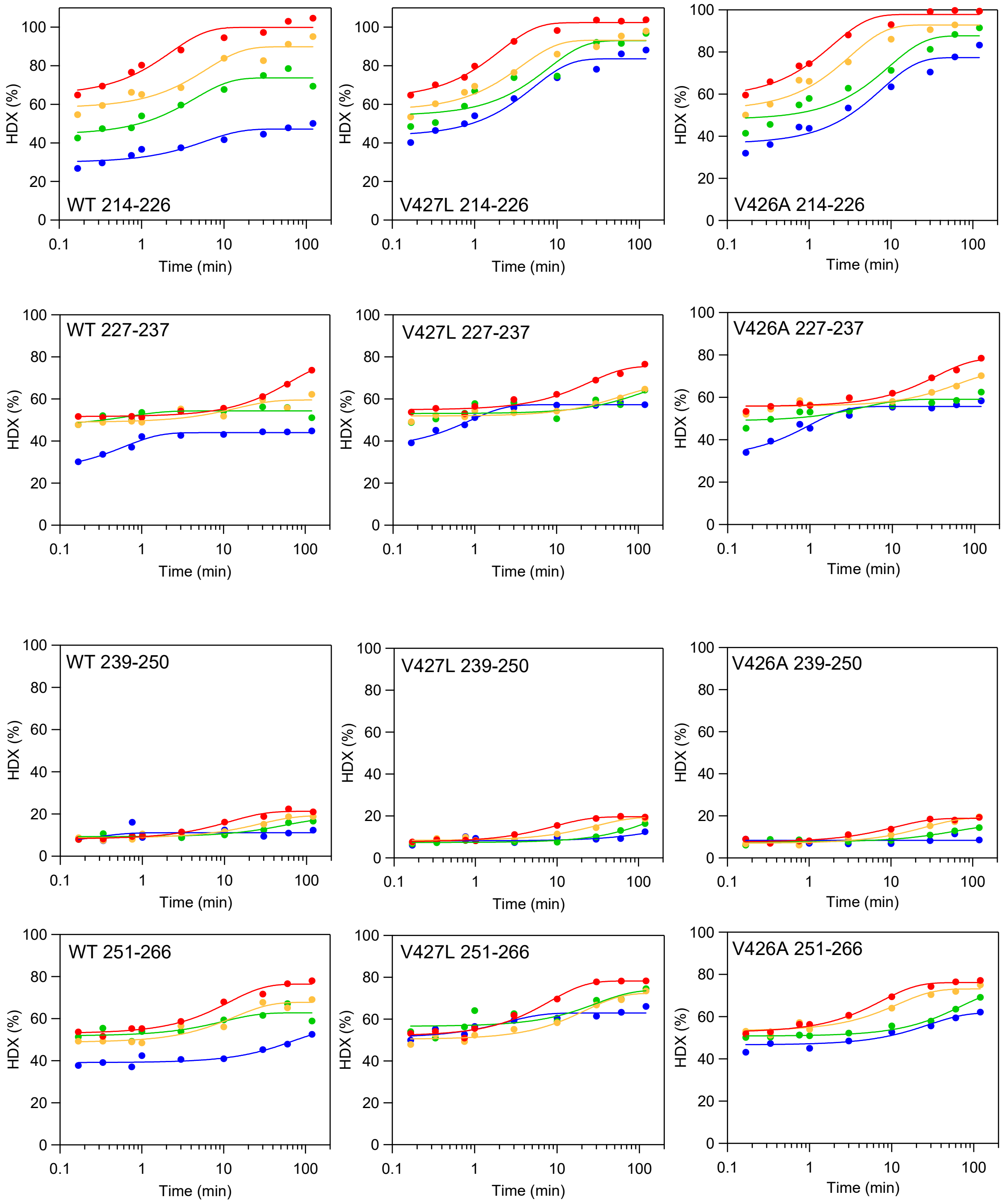
WT 214-226
V427L 214-226
V426A 214-226
WT 227-237
V427L 227-237
V426A 227-237
WT 239-250
V427L 239-250
V426A 239-250
WT 251-266
V427L 251-266
V426A 251-266
HDX (%)
0
20
40
60
80
100
Time (min)
0.1
1
10
100

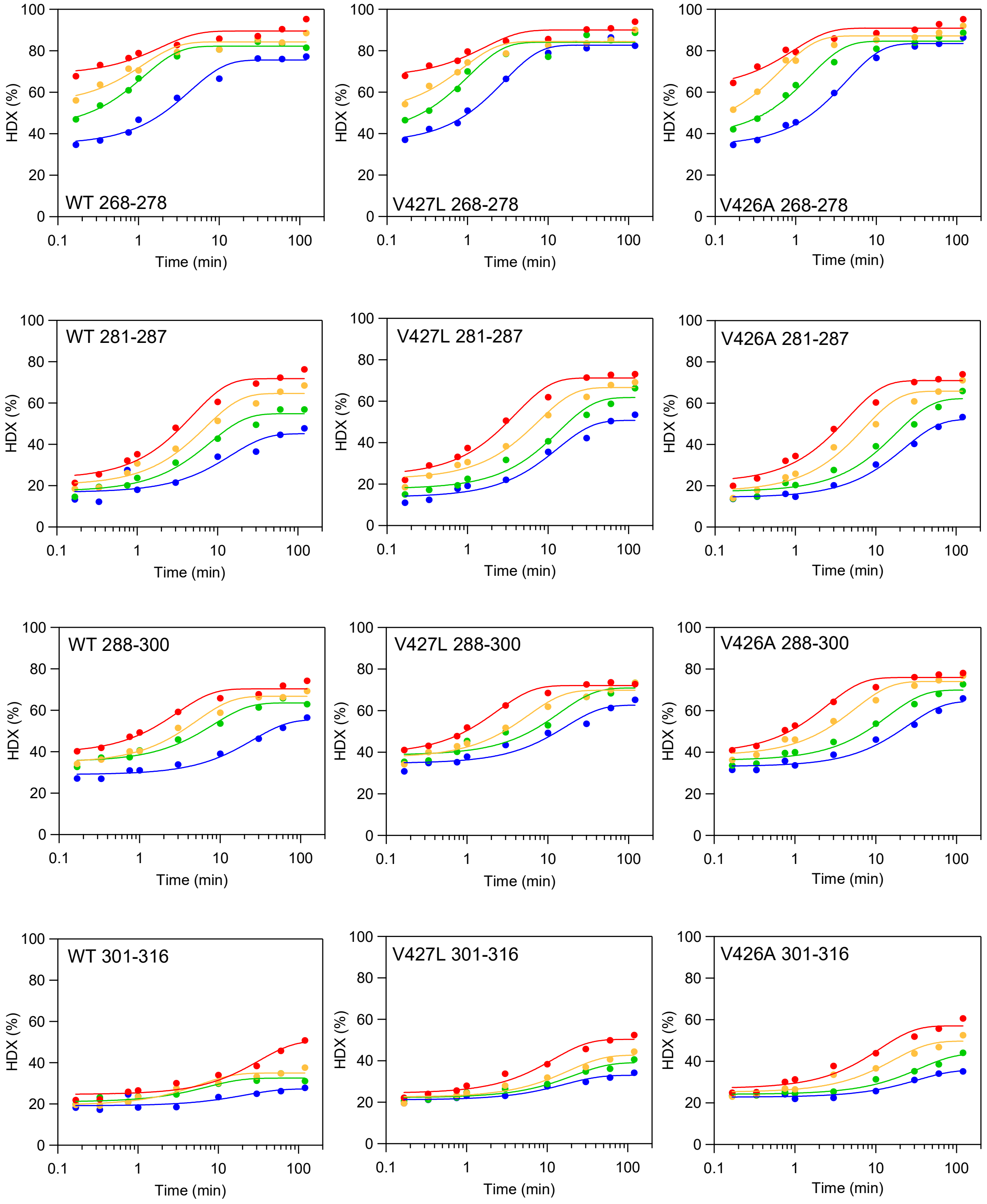
WT 268-278
V427L 268-278
V426A 268-278
WT 281-287
V427L 281-287
V426A 281-287
WT 288-300
V427L 288-300
V426A 288-300
WT 301-316
V427L 301-316
V426A 301-316
HDX (%)
Time (min)
0
20
40
60
80
100
0.1
1
10
100

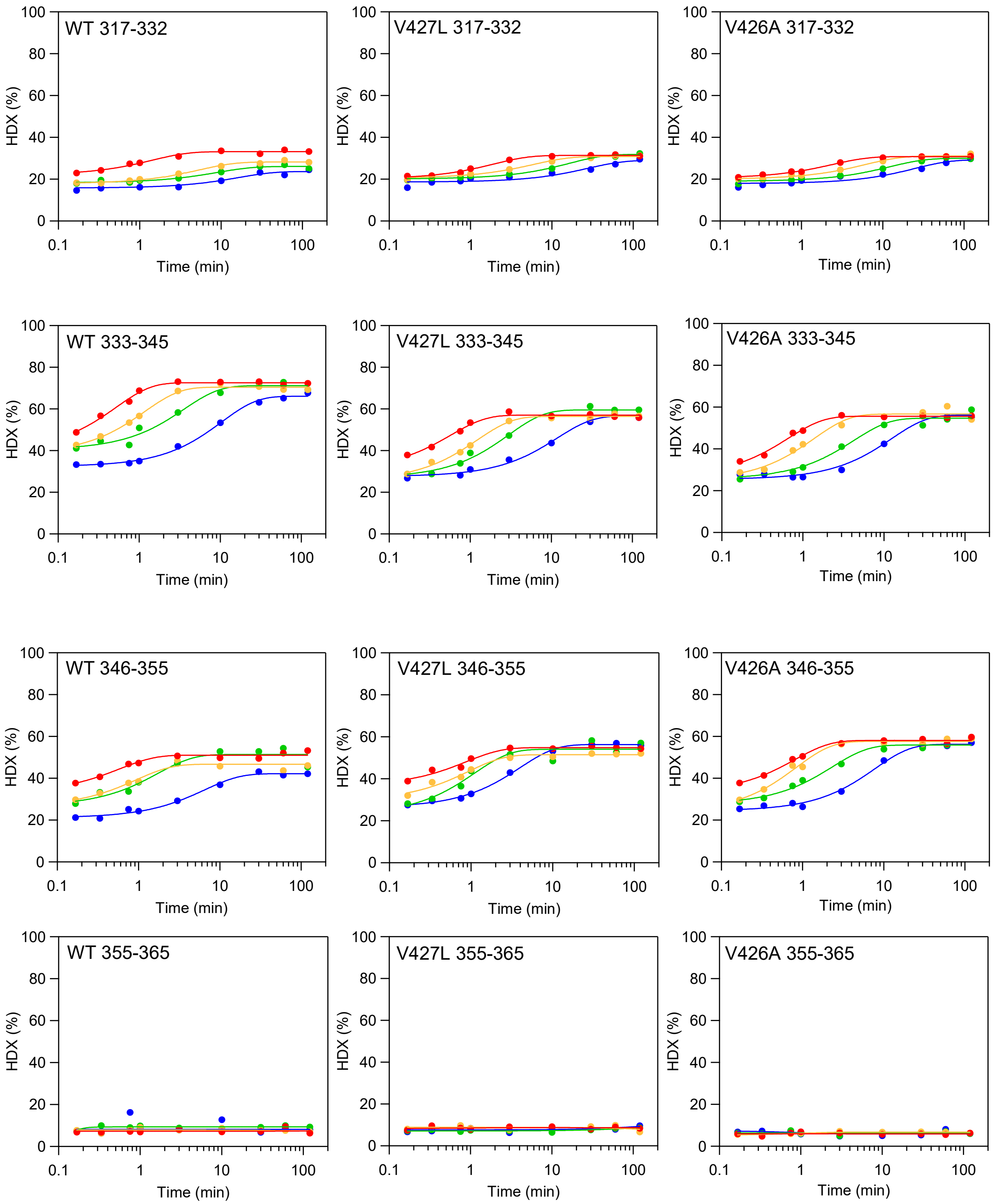
WT 317-332
V427L 317-332
V426A 317-332
WT 333-345
V427L 333-345
V426A 333-345
WT 346-355
V427L 346-355
V426A 346-355
WT 355-365
V427L 355-365
V426A 355-365
HDX (%)
Time (min)
0
20
40
60
80
100
0.1
1
10
100

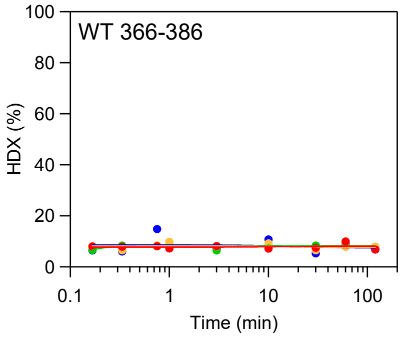
WT 366-386
HDX (%)
100
80
60
40
20
0
0.1
1
10
100
Time (min)

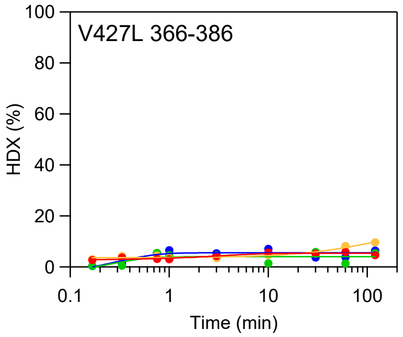
V427L 366-386
HDX (%)
100
80
60
40
20
0
0.1
1
10
100
Time (min)

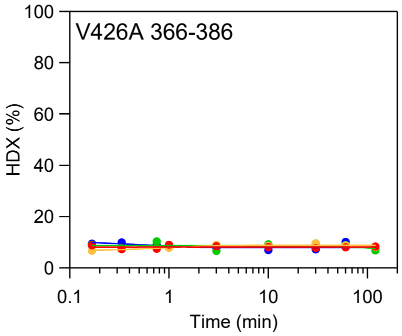
V426A 366-386
HDX (%)
100
80
60
40
20
0
0.1
1
10
100
Time (min)

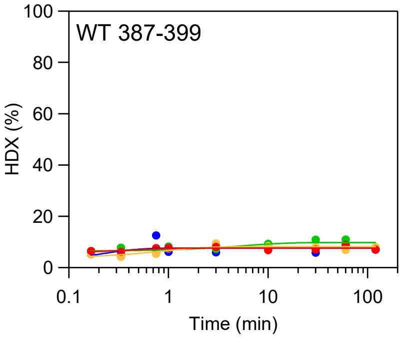
WT 387-399
HDX (%)
100
80
60
40
20
0
0.1
1
10
100
Time (min)

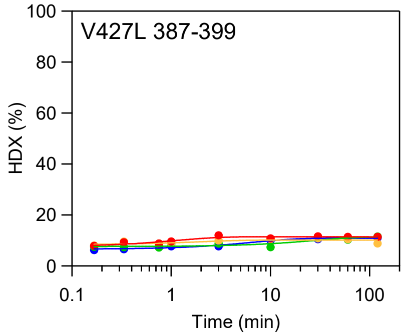
V427L 387-399
HDX (%)
100
80
60
40
20
0
0.1
1
10
100
Time (min)

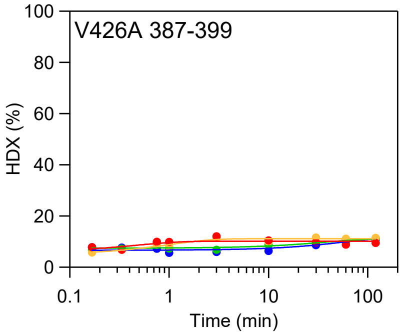
V426A 387-399
HDX (%)
100
80
60
40
20
0
0.1
1
10
100
Time (min)

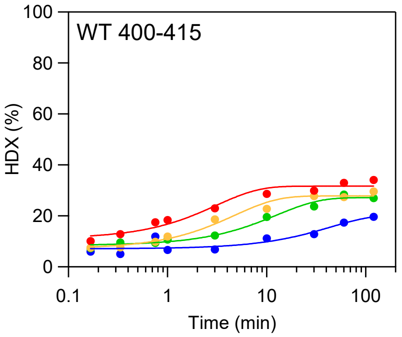
WT 400-415
HDX (%)
100
80
60
40
20
0
0.1
1
10
100
Time (min)

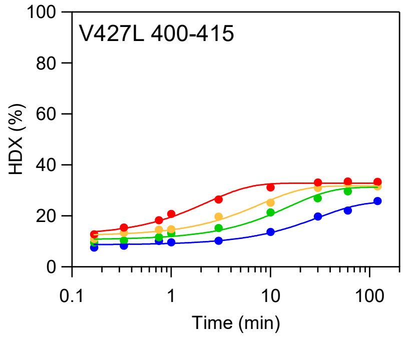
V427L 400-415
HDX (%)
100
80
60
40
20
0
0.1
1
10
100
Time (min)

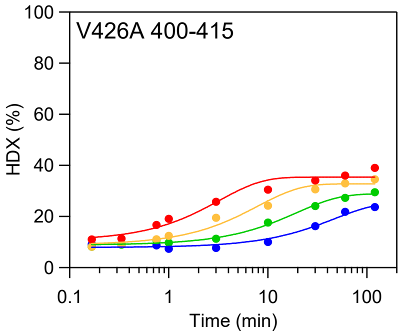
V426A 400-415
HDX (%)
100
80
60
40
20
0
0.1
1
10
100
Time (min)

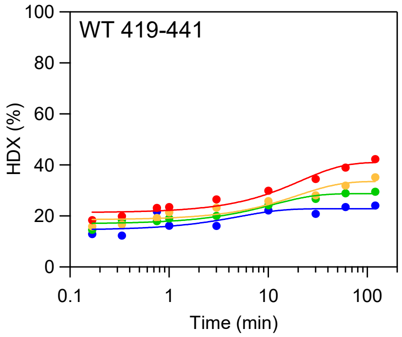
WT 419-441
HDX (%)
100
80
60
40
20
0
0.1
1
10
100
Time (min)

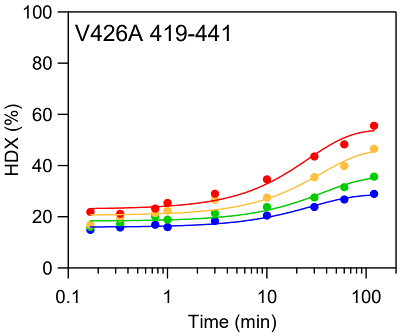
V426A 419-441
HDX (%)
100
80
60
40
20
0
0.1
1
10
100
Time (min)

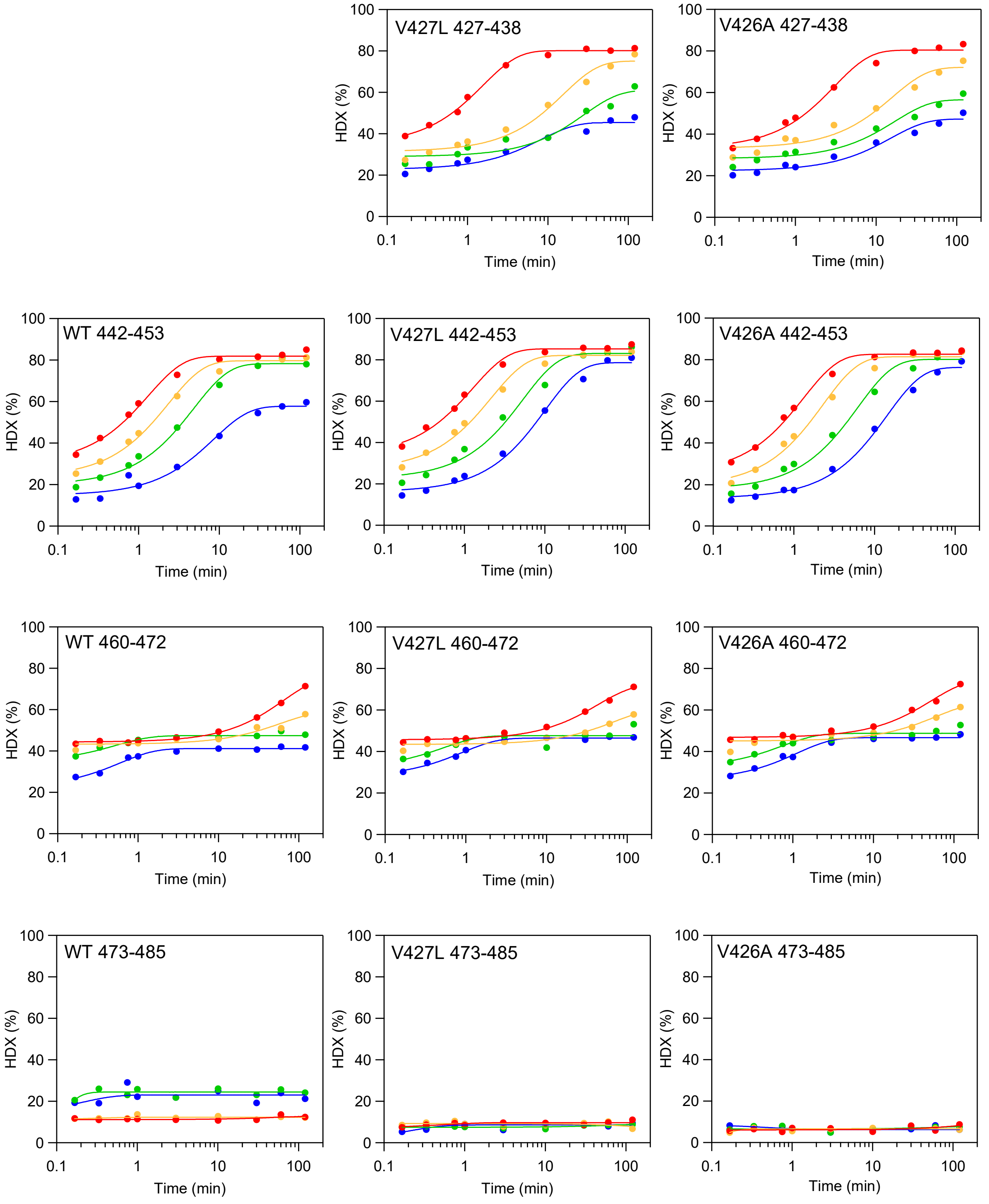
V427L 427-438
V426A 427-438
WT 442-453
V427L 442-453
V426A 442-453
WT 460-472
V427L 460-472
V426A 460-472
WT 473-485
V427L 473-485
V426A 473-485
HDX (%)
Time (min)
0
20
40
60
80
100
0.1
1
10
100

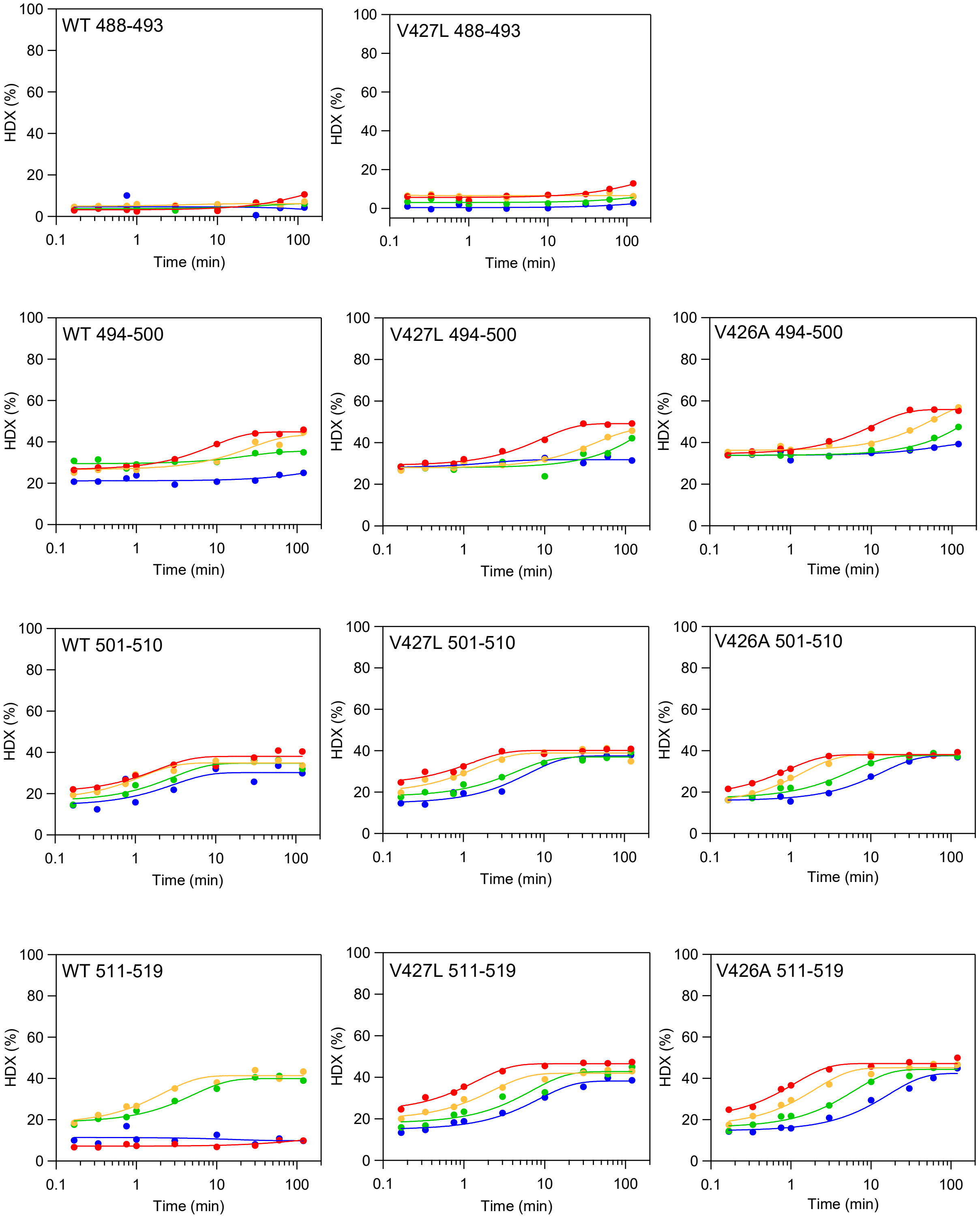
WT 488-493
V427L 488-493
WT 494-500
V427L 494-500
V426A 494-500
WT 501-510
V427L 501-510
V426A 501-510
WT 511-519
V427L 511-519
V426A 511-519
HDX (%)
0
20
40
60
80
100
Time (min)
0.1
1
10
100

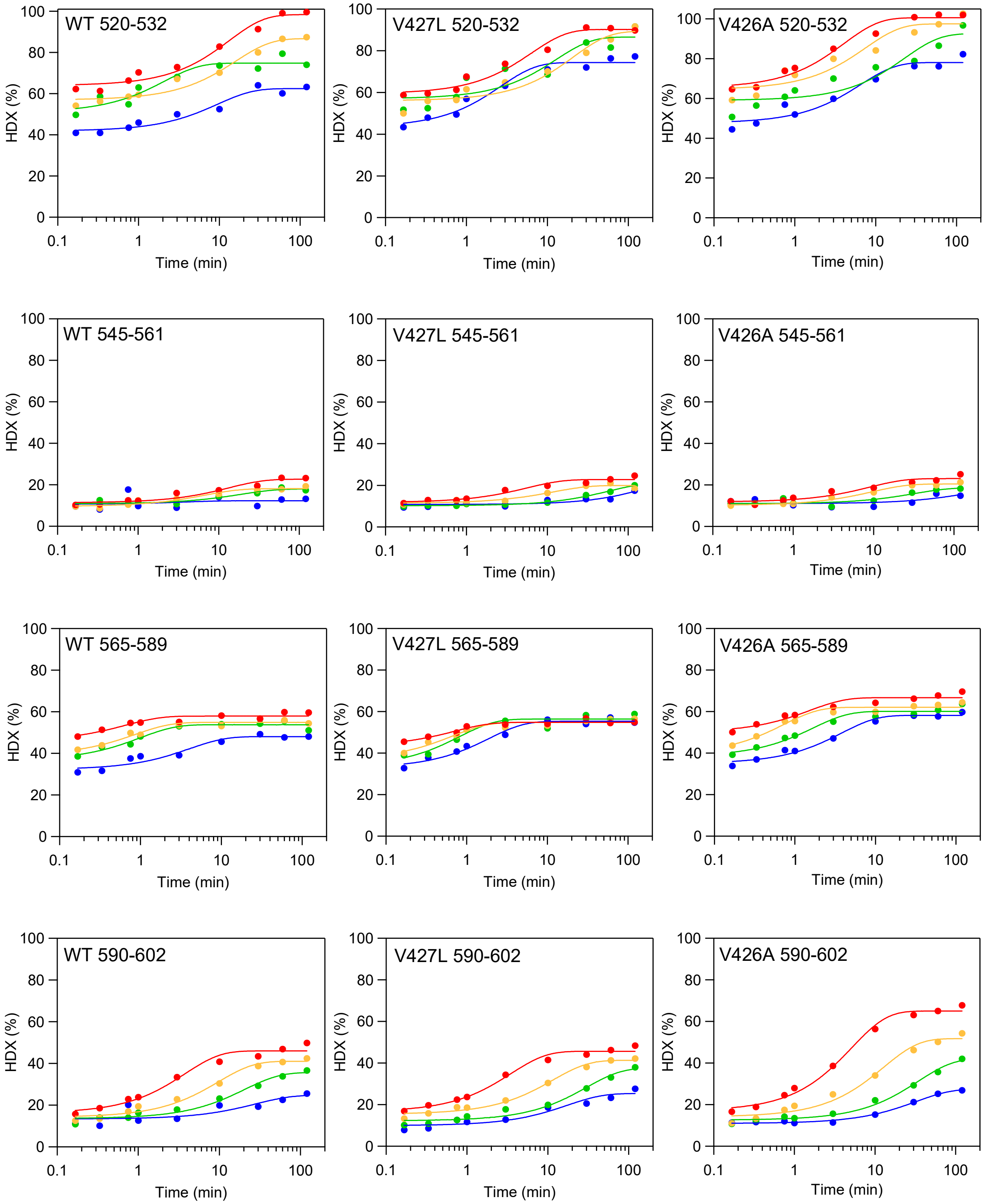
WT 520-532
V427L 520-532
V426A 520-532
WT 545-561
V427L 545-561
V426A 545-561
WT 565-589
V427L 565-589
V426A 565-589
WT 590-602
V427L 590-602
V426A 590-602
HDX (%)
Time (min)
0
20
40
60
80
100
0.1
1
10
100

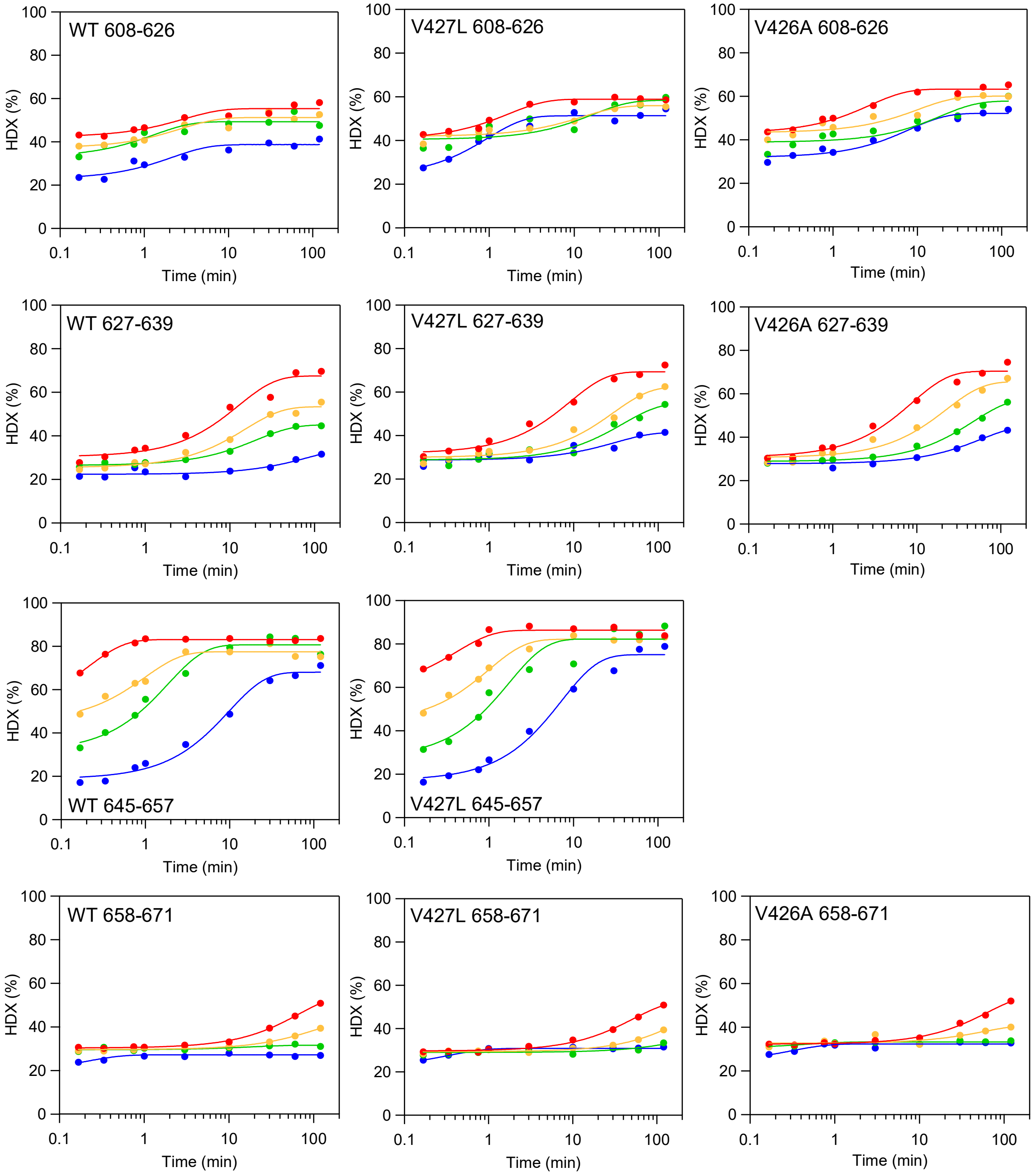
WT 608-626
V427L 608-626
V426A 608-626
WT 627-639
V427L 627-639
V426A 627-639
WT 645-657
V427L 645-657
WT 658-671
V427L 658-671
V426A 658-671
HDX (%)
0
20
40
60
80
100
Time (min)
0.1
1
10
100